AD-A113 812 SPERRY RESEARCH CENTER SUDBURY MA F/G 20/6
DESIGN AND FABRICATION OF MULTIMODE OPTICAL SWITCHES.(U)
MAR 82 R A SOREF F19628-80-C-0147
UNCLASSIFIED SRC-CR-81-54 RADC-TR-82-22 NL

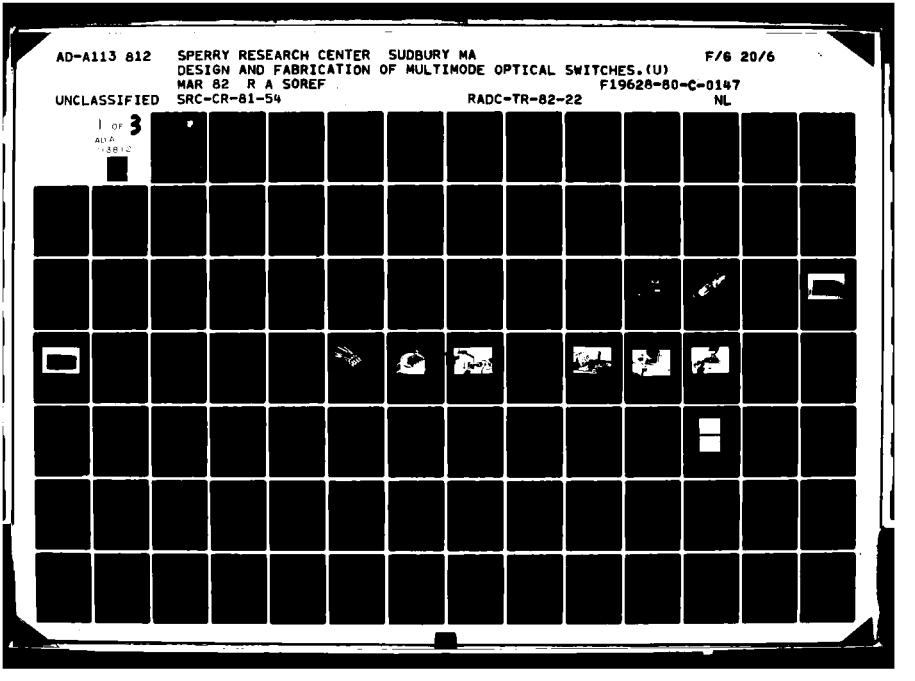

(12)

RADC-TR-82-22
Final Technical Report
March 1982

DESIGN AND FABRICATION OF MULTIMODE OPTICAL SWITCHES

Sperry Research Center

Richard A. Soref

ROME AIR DEVELOPMENT CENTER
Air Force Systems Command
Griffiss Air Force Base, New York 13441

This report has been reviewed by the RADC Public Affairs Office (PA) and is releasable to the National Technical Information Service (NTIS). At NTIS it will be releasable to the general public, including foreign nations.

RADC-TR-82-22 has been reviewed and is approved for publication.

APPROVED: Rudolph A Bradbury

RUDOLPH BRADBURY
Project Engineer

APPROVED: Harold Roth

HAROLD ROTH
Director, Solid State Sciences Division

FOR THE COMMANDER: John P. Huss

JOHN P. HUSS
Acting Chief, Plans Office

If your address has changed or if you wish to be removed from the RADC mailing list, or if the addressee is no longer employed by your organization, please notify RADC (ESO) Hanscom AFB MA 01731. This will assist us in maintaining a current mailing list.

Do not return copies of this report unless contractual obligations or notices on a specific document requires that it be returned.

UNCLASSIFIED

SECURITY CLASSIFICATION OF THIS PAGE (When Data Entered)

REPORT DOCUMENTATION PAGE	READ INSTRUCTIONS BEFORE COMPLETING FORM
1. REPORT NUMBER: RADC-TR-82-22	2. GOVT ACCESSION NO.: AD-A113 812
3. RECIPIENT'S CATALOG NUMBER:	
4. TITLE (and Subtitle): DESIGN AND FABRICATION OF MULTIMODE OPTICAL SWITCHES	5. TYPE OF REPORT & PERIOD COVERED: Final Technical Report 5 June 80 - 5 September 81
	6. PERFORMING ORG. REPORT NUMBER: SRC-CR-81-54
7. AUTHOR(s): Richard A. Soref	8. CONTRACT OR GRANT NUMBER(s): F19628-80-C-0147
9. PERFORMING ORGANIZATION NAME AND ADDRESS: Sperry Research Center, 100 North Road, Sudbury MA 01776	10. PROGRAM ELEMENT, PROJECT, TASK AREA & WORK UNIT NUMBERS: 61102F, 2305J240
11. CONTROLLING OFFICE NAME AND ADDRESS: Deputy for Electronic Technology (RADC/ESO), Hanscom AFB MA 01731	12. REPORT DATE: March 1982
	13. NUMBER OF PAGES: 154
14. MONITORING AGENCY NAME & ADDRESS (if different from Controlling Office): Same	15. SECURITY CLASS. (of this report): UNCLASSIFIED
	15a. DECLASSIFICATION/DOWNGRADING SCHEDULE: N/A

16. DISTRIBUTION STATEMENT (of this Report)

Approved for public release; distribution unlimited

17. DISTRIBUTION STATEMENT (of the abstract entered in Block 20, if different from Report)

Same

18. SUPPLEMENTARY NOTES

RADC Project Engineer: Rudolph Bradbury (ESO)

19. KEY WORDS (Continue on reverse side if necessary and identify by block number)

Fiber Optics
Optical Switching
Liquid Crystals
Matrix Switch
Electro-Optical Devices
Multimode Fibers
Optical Communications
Frustrated Total Internal Reflection (over)

20. ABSTRACT (Continue on reverse side if necessary and identify by block number)

A new optical switching component for multimode fiber-optic networks has been developed. This voltage-controlled switch is an 8-port device coupled by GRINrod lenses to four input fibers and to four output fibers (graded index, 50-μm core diameter). The device switchs light from any input fiber to any output fiber in a simultaneous 4-fold input/output pairing, and there are 24 such states in this nonblocking matrix switch. Switching is accomplished via controlled reflection from two 6-μm (over)

DD FORM 1 JAN 73 1473 EDITION OF 1 NOV 65 IS OBSOLETE

UNCLASSIFIED

SECURITY CLASSIFICATION OF THIS PAGE (When Data Entered)

layers of nematic liquid crystal. This switch is the first multimode, electro-optic, fiber-optic matrix. Construction is simple and compact; only four glass prisms and two liquid layers are used in the switch. The matrix architecture is based on a new dual-switching-array concept, a two-stage interconnection that provides very low levels of optical crosstalk; more than 53 dB below the optical input level. The 5-ms on/off response time is faster than that of electro-mechanical matrices, although the 40 Vrms addressing voltage is higher. The optical insertion loss had a minimum value of 6 dB and an average value of 15 dB. The latter is due to misalignment of fibers during attachment to the switch, which can be remedied. Because the present switch does not use moving parts, it is quite reliable.

TABLE OF CONTENTS

TABLE OF CONTENTS (Continued)

LIST OF ILLUSTRATIONS

LIST OF ILLUSTRATIONS (cont.)

SECTION I

INTRODUCTION

This is the Final Report under Contract No. F19628-80-C-0147

Light from multimode fibers has been switched by means of electro-mechanical [1-8], mechanical [9-11], electro-optic [12-16], magneto-optic [17,18], and acousto-optic techniques. Currently, the electro-mechanical and electro-optic techniques are the most practical, but, over the longer term, we feel that the electro-optic approach will prove to be more reliable because it does not use moving parts. The electro-optic liquid crystal technique [19-25] offers low-voltage, low-power control and is attractive in applications where millisecond response is acceptable.

Prior work on liquid crystal switches has been confined to simple functions such as binary state 2 x 2 switching [21,24,25]. More elaborate liquid crystal switching functions are investigated in this work.

As fiber optic networks grow more complex, centralized network-control switches will be needed to route optical signals. The "optical switchboards" would function in the same manner as an electronic PBX in a metal-wire telephone system.

The goal of this work is to create structures for an N x N optical matrix switch with N! distinct configurations. For implementation of our ideas, the N = 4 example was chosen as being large enough to demonstrate switching complexity, yet small enough to keep assembly costs low.

We have conceived, built, and tested a voltage-controlled 4 x 4 fiber optical switching component with 24 different states. This switch is based on a new "dual array" concept. The structure is simple, compact, and uses only four glass prisms, together with two layers of nematic liquid crystal. To our knowledge, this is the first low-voltage, electro optic,

matrix switch for multimode fibers.

This report describes the design, construction, and operation of the matrix. The observed performance is good, especially in the area of optical crosstalk where more than 40 dB of isolation between switched signals is obtained. Control voltages are about 40 V rms. Only one polarization component in the unpolarized fiber light is switched, so the optical insertion loss is higher than in the unpolarized 2 x 2 switch [21,24,25].

SECTION II

PRIOR WORK

Only a small amount of work has been done on multimode fiber optical matrices. There were three recent studies of electro-mechanical devices [5,6,7] and one effort in the electro optic area [10]; a 3 x 2 structure based on the Pockel's effect in $LiTaO_3$. The latter switch required 130 V for operation. An order-of-magnitude reduction in voltage is reported in the present work.

SECTION III
MATRIX SWITCHING FUNCTION

The N x N matrix has N multimode fiber inputs, N multimode fiber outputs, and is capable of connecting any input to any output: thus, the matrix provides a means of routing N simultaneous wideband optical signals among 2N terminals in a fiber optic telecommunications network, or in a fiber-linked distributed computer. Optical paths in the matrix are short, so the N x N switch does not in any way compromise the high information bandwidth of the fiber system. The matrices discussed here are electro-optic, that is, the flow pattern of optical signals is governed by a set of electronic commands (voltage inputs to the matrix). This addressing is discussed below.

We are concerned here mainly with one-to-one mappings of inputs to outputs. At any instant of time, there is an N-fold in/out pairing in the matrix; in other words, N "optical conversations" are going on simultaneously. Each N-fold pairing is called a "configuration" or "state" of the matrix, and permutation theory shows that there are N! such states. Voltage addressing takes the matrix from state to state.

To facilitate measurements, and to minimize fabrication costs, we decided to implement the optical matrix in a 4 x 4 version. Figure 1 illustrates the 24 states of this 4 x 4 switch. The eight fibers are numbered and the solid lines represent optical paths.

We do not envision the matrix being used for "party line calls" in which several inputs are connected to one output, or vice versa, although this can be done on a limited basis. Rather, our intention is to create a nonblocking optical network in which a given 4-fold pairing does not prevent any other from being made, as in Fig. 1. The dual-array technique discussed below, allowed us to implement the Fig. 1 functions in an efficient, low-crosstalk structure.

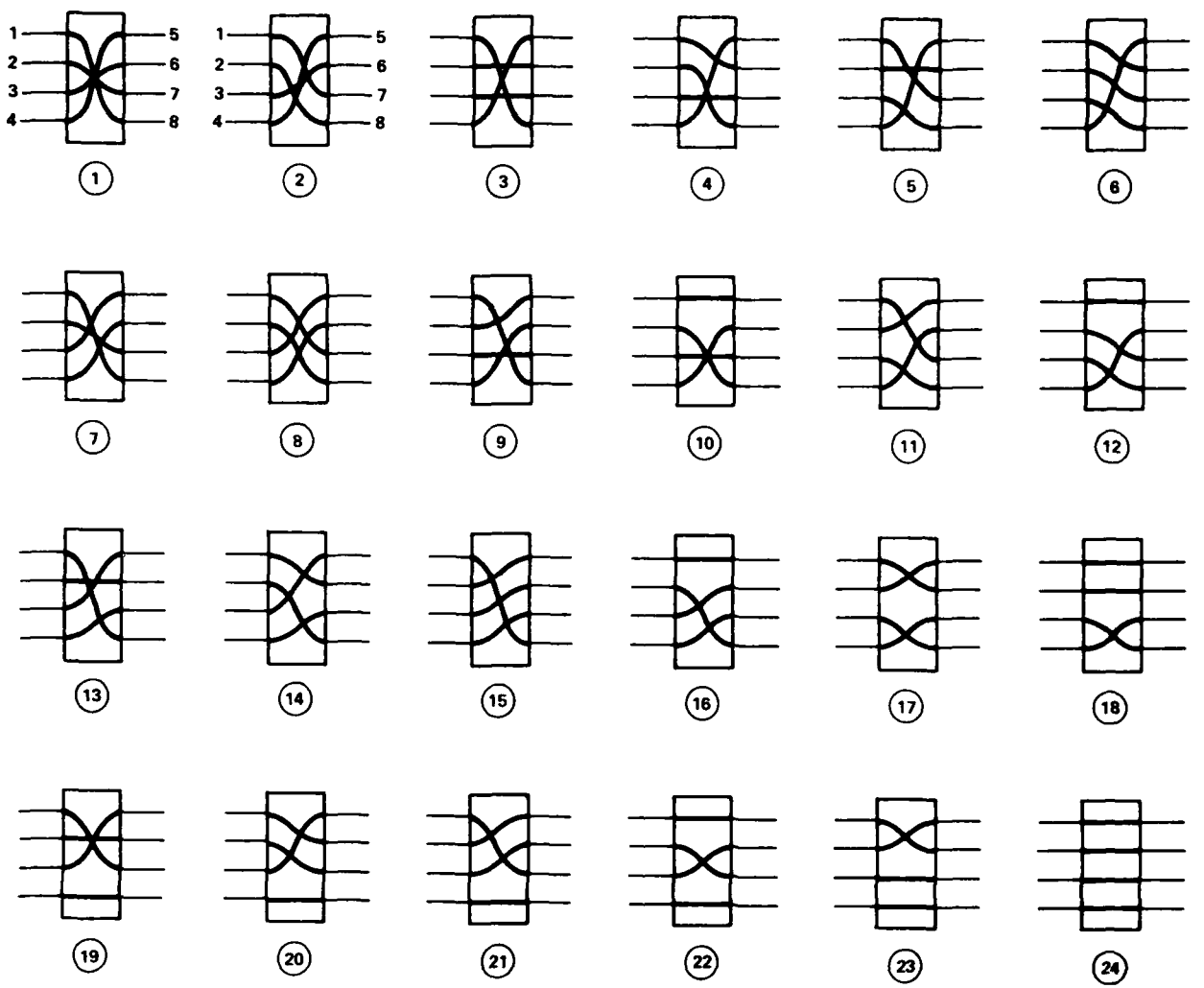

FIG. 1 Twenty four states of nonblocking 4 x 4 optical switch. Heavy lines represent optical paths within switch. Thin lines represent optical fibers.

81-884

SECTION IV

DUAL-ARRAY CONCEPT

We showed recently how two-stage switching led to low-crosstalk in a 2 x 2 device [25] and we felt that the same crosstalk benefits could be realized in an N x N with the two-stage approach. It seemed at first that two N^2 crossbars would be needed, but further study showed that pairs of simpler switches (1 x N multi-pole devices) would give favorable results. The 1 x N "building blocks" are especially convenient in the liquid crystal approach as discussed below.

The dual-array method for making a general M x N matrix is best elucidated with a concrete example; that of the 3 x 4 matrix switch shown in Fig. 2. Here, we have a "first array" consisting of three 1 x 4 switches: a_1, a_2, a_3, and a "second array" of four 3 x 1 switches, b_1, b_2, b_3, b_4. The a-switches are grouped side-by-side in parallel planes, as are the b-switches. If we look at the first array, we see that it produces a 3 x 4 array of possible output positions (as shown by the black dots) equally spaced in a rectangular grouping with three rows and four columns. Similarly, the second array has a 4 x 3 grouping of possible input positions.

The first array (#1) can "feed" the second array (#2) in a meaningful way if the output rows of the first array are connected optically to the input columns of the second array (and the columns of #1 are mapped into the rows of #2). To do this, we simply rotate switching-array #2 by 90° with respect to #1. In other words, we orient the parallel planes of #1 at right angles to the planes of #2 as shown. In this row-column mapping, it is assumed that the x- and y-spacing of the output/input beam positions is identical in the two arrays (which can be arranged easily).

The row-column mapping gives the desired matrix switching because any output switch (b_1 or b_2, etc) can select light from any matrix

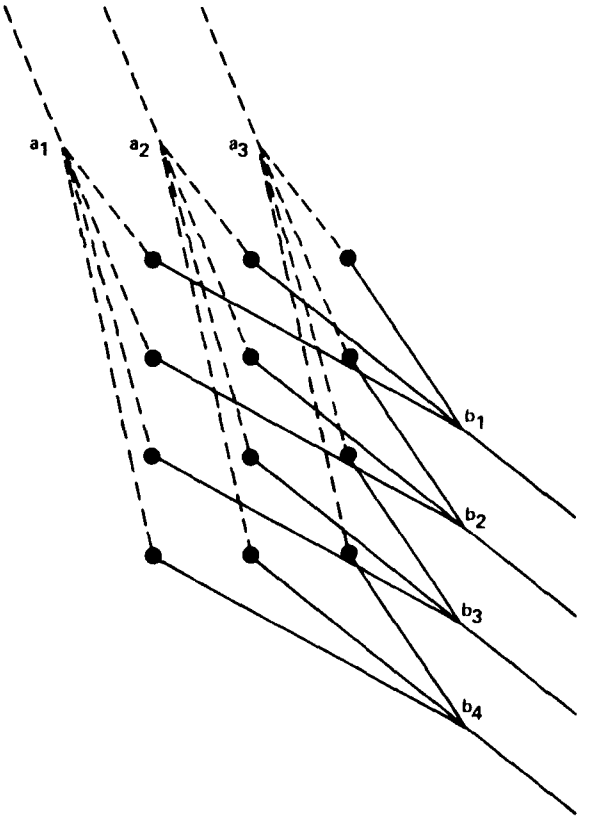

81-883

FIG. 2 Dual switching arrays for making an M x N matrix switch. The 3 x 4 example is illustrated. Dashed lines show first array. Solid lines show second array. Lines represent optical paths.

input. In the symmetric N x N case, we get nonblocking switching, because each successive output switch b_i, can select a matrix input that has not been chosen by the preceeding output switches, b_1, b_2, ...b_{i-1}. Because the leakage light passes through two successive stages in the dual-array matrix, the optical crosstalk is reduced significantly with respect to the single-stage properties. For the N x N matrix, the first switching array can be expressed as a 1 x N switch, replicated N times, and the second array is an N x 1, replicated N times; in other words, the arrays are N(1 x N) and (N x 1)N.

SECTION V

THE 1 x N AND N x 1 LIQUID CRYSTAL SWITCHES

The 1 x 4 switching effect used in the 4 x 4 matrix is based on the electro optic effect shown in Fig. 3 (see [19]). Here, an unpolarized light beam (resolved into its s- and p-polarization components) is incident obliquely on a thin layer of nematic liquid crystal (the type of liquid that aligns along an external E field). At zero field, the liquid crystal molecules are parallel to the electroded glass "walls". At V = 0, Fig. 3A, the optical incidence angle is greater than the optical critical angle; thus, both components are totally reflected. In Fig. 3B, the applied voltage is well above threshold, and the molecular order approaches the perpendicular alignment as shown. Here, the optical p-component is almost completely transmitted, while the s-light remains totally reflected. This means that 50% of the unpolarized beam is switched through the liquid. Similar results are given by other electro-optic effects in liquid crystals ([23], Fig. 1), but to keep the discussion simple, we shall not refer to those effects.

The 1 x 4 and 4 x 1 switches use a succession of controlled reflections of the sort shown in Fig. 3. Figure 4 presents our designs for these multi-way switches. The Figures illustrate side views. Before tracing the optical ray paths, let us consider the structural features. Each device uses only one layer of liquid crystal held between two high-index glass prisms, a layer whose order is everywhere parallel to the walls at zero field. Both prism surfaces in contact with the liquid are coated with a thin film of transparent conductive material. The thin trapezoidal prism (top prism) has its electrode divided into four local areas for independent voltage control, while a uniform electrode (common ground) covers the surface of the triangular prism (bottom prism). The independent voltage sources V_1, V_2,....V_4 that reorder the liquid locally are not shown in Fig. 4 to simplify those drawings.

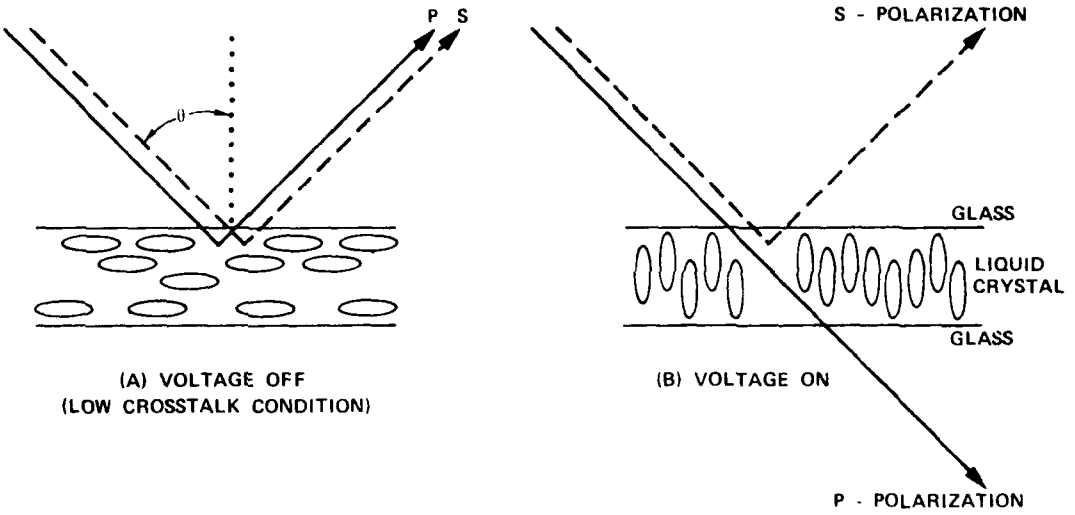

FIG. 3 Total or partial reflection of light by field-ordered liquid crystal layer. Reflection of p-component is "frustratable". 81-872

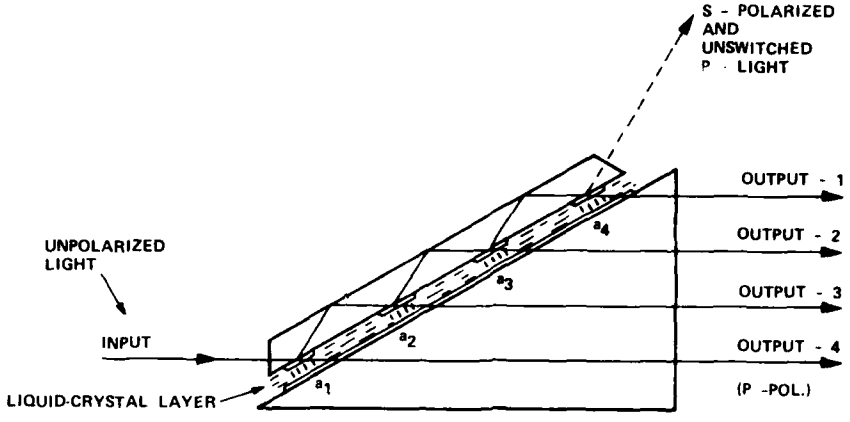

(A) 1-TO-4 SWITCH,
AND BEAM DIVIDER

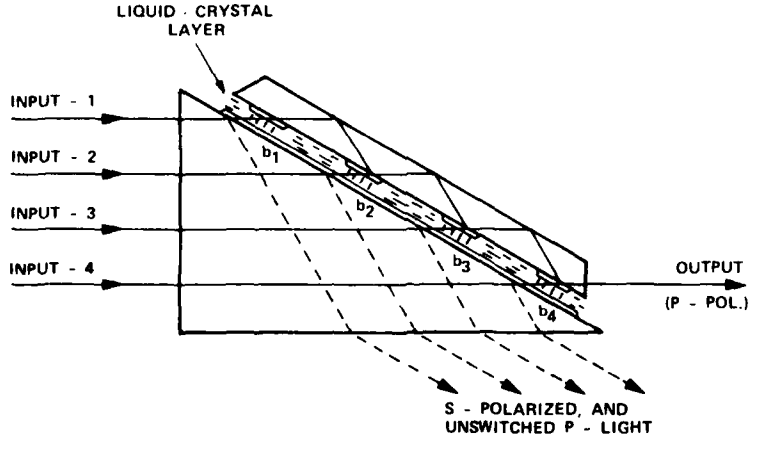

(B) 4-TO-1 SWITCH,
AND BEAM COMBINER

81 8 79

FIG. 4 New designs for electro-optical 1 x 4 and 4 x 1 liquid crystal switches.

Let us consider the rays in Fig. 4A. Because the top prism has polished, parallel faces, the incoming light beam makes a series of regular "bounces", up to three total internal reflections at the glass/air interfaces and as many as three partial-or-total reflections at the glass/liquid interfaces, depending upon the V_1, V_2,...V_4 voltage values. Each successive interaction with the liquid crystal is an electro-optic "decision point" where the p-light can be totally switched to a bottom prism output, or sent to the next location after traveling in the top prism. Note that the s-component is unswitched, and travels to the top prism output via multiple reflections. Also, if the applied voltages are only slightly above threshold, we can have partial switching at any of the four locations. Therefore, this device has the ability to send p-light to any of the four outputs, or to all four outputs simultaneously (or to two or three outputs simultaneously) in any desired fractional distribution.

In Fig. 4B, the input and output ports have been reversed by rotating the Fig. 4A structure 180°. Now we can combine four beams, or can "admit" one of four beams in the switch while "rejecting" the other three. To illustrate this, assume four parallel, independent, unpolarized optical inputs as in Fig. 4B. As per Fig. 3, by proper choice of the values V_1,...V_4, we can transmit 100% of the p-component into the top prism at the first LC interaction location and send that switched light to the top prism output by a series of internal reflections. Or, we could transmit all of the p-light at the second location only (or at the third or fourth location only), making a 4 x 1 device. The s-light, which is always unswitched, is reflected out of the bottom prism as shown, along with the unselected p-beams. Summarizing, the Fig. 4B device can give four-port switching of p-light, or it can mix two, three, or four independent p-beams in any desired proportions by adjustment of V_1,...V_4. Those combined beams emerge collinearly from the top prism port. Each switch uses only two pieces of glass, yet functions in a complex manner due to the multiple internal reflections.

Note that the 1 x 4 and 4 x 1 operations have been carried out within a plane (all beams are coplanar). This opens up the possibility of combining several optical switches within a monolithic structure. If the glass prisms in Figs. 4A and 4B are extended uniformly in a direction normal to the switching plane, while retaining the same LC layer, and if additional sets of independent electrodes are provided in those parallel planes, then we can contain four 1 x 4 switches, for example, in two pieces of glass, with just one LC film "servicing" all four 1 x 4 switches. This is illustrated in Fig. 5. In other words, it is easy to "replicate" the multipole switches side-by-side in parallel planes within the same simple glass structure as shown. This makes it easy to build a dual-array structure as discussed below in Section VI.

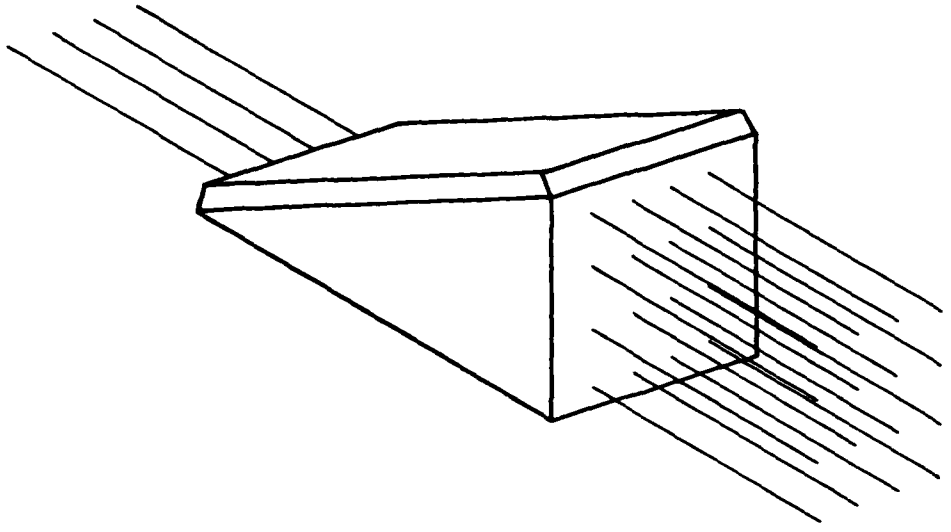

81-882

FIG. 5 Replication of four, independent 1 x 4 switches in a simple structure (two prisms, one LC).

SECTION VI

THE "HALF MATRIX" SWITCH

Our goal is to make a 4 x 4 matrix by the dual-array technique. Because the N x M matrix is symmetric, N = M = 4, the first and second arrays are identical; that is, the 4(1 x 4) and (4 x 1)4 devices are structurally the same; only the labeling of the input and output ports has been interchanged. For convenience, we shall refer to each array as a "half-matrix" switch. The appearance of each half-matrix is shown in Fig. 5.

SECTION VII

THE COMPLETE 4 X 4 MATRIX SWITCH

A. Fiber Coupling

Lens-coupling to the optical fibers is needed for each half-matrix in the final matrix. The lenses serve two purposes: collimating the divergent light from the input fiber, and recapturing the beam for efficient insertion into the output fiber core. Although the optical switch can process "mildly divergent" light, it works best for collimated light beams. With a divergent beam, the device would not switch wide-angle off-axis rays and the optical crosstalk would increase. Collimation minimizes loss and crosstalk.

Conventional bi-convex lenses would work with air gaps between the switch and the fibers. Spherical rod lenses could also perform the fiber-coupling task, but we prefer graded index rod lenses (GRINrods) for this application because they can accomplish the necessary collimation/decollimation without air gaps; that is, each GRINrod is in direct contact with a fiber-end and with the switch's input surface (locked in place with thin films of optical cement). These waveguide lenses have a length of 0.25 pitch at the wavelength of interest, and are purchased typically from the Nippon Sheet Glass Company under the trade name Selfoc Microlenses. The numerical aperture of the microlens is chosen equal to, or slightly larger than that of the fiber.

Because the input fiber core is not an ideal optical point-source, there is inevitable beam-spreading within the switch after the first Selfoc. If the second Selfoc is sufficiently far from the first, the second will collect only the central region of the light beam. Then, there is extra fiber-fiber coupling loss introduced by the fiber/Selfoc-Selfoc/fiber pairs.

The lens/lens coupling loss can contribute more than 1 dB to the optical insertion loss of the 4 x 4 matrix, and if the size of the N x N matrix is expanded to larger N, coupling loss can become a limiting factor, so these coupling considerations enter into matrix design (Appendix A discusses the tradeoffs).

B. The Structure

The 4 x 4 structure is a 4(1 x 4) half-matrix (designated #1) joined to a (4 x 1)4 half-matrix (designated #2) in such a way that the 16 possible output beams from #1 are coaxial with the 16 possible input beams of #2. Before the structures are joined, #2 is rotated 90° with respect to #1 about its main symmetry axis to give the aforementioned row-column mapping. As stated earlier, #1 switches only p-polarized light into its bottom prism, and only the light polarized in the incidence plane of #2 goes through switch #2 into its top prism as per Fig. 4. Because of the orthogonal #1-#2 orientation, the optical outputs of #1 will have the "wrong" polarization for #2 unless a retardation plate intervenes to rotate the plane of polarization by 90°. This 90° rotation is done in our 4 x 4 structure as illustrated in Fig. 6, a view orthogonal to the 16 beam axes at the midplane where #1 joins #2. Here, an optical half-wave plate is interposed with its axes at 45° to the polarization plane of #1 to produce the desired 90° rotation of #1 outputs for #2 input. The HWP can be a thin transparent sheet of mica or plastic having negligible optical loss. The $\lambda/2$ plate is cemented with transparent index-matching adhesive to both #1 and #2. Similarly, the eight p/4-GRINrod lenses and the eight multimode fiber strands are joined to #1 and #2 (four on each) with clear, index matching cement. This completes the assembly of the dual-array 4 x 4 matrix, and we arrive at the final structure shown in Fig. 7 where the optical beam paths are indicated by dashed lines. We see the four glass prisms, the two layers of initially parallel liquid crystal, the HWP, the microlenses, the fibers, and the two sets of 16 independent control electrodes (shown as rectangles) for the two half-matrices. Although not shown here, the actual electrode pattern includes lead-in paths shown in the photomask of

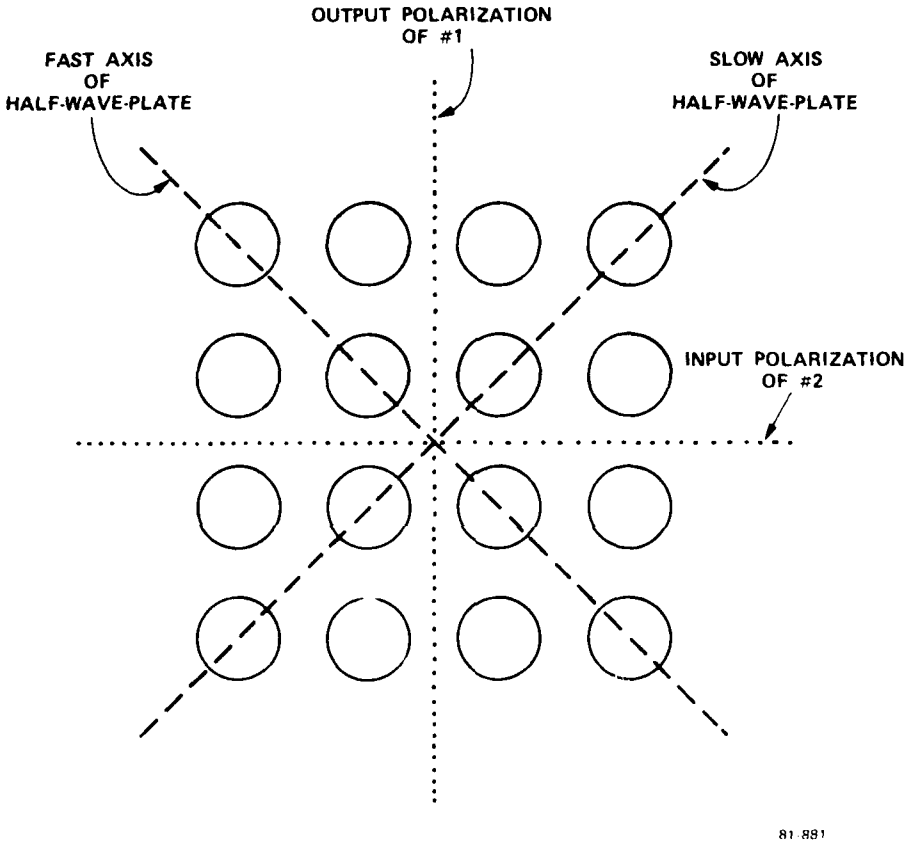

FIG. 6 Cross-section view of optical beams at midplane of matrix, showing effect of HWP on optical polarization states.

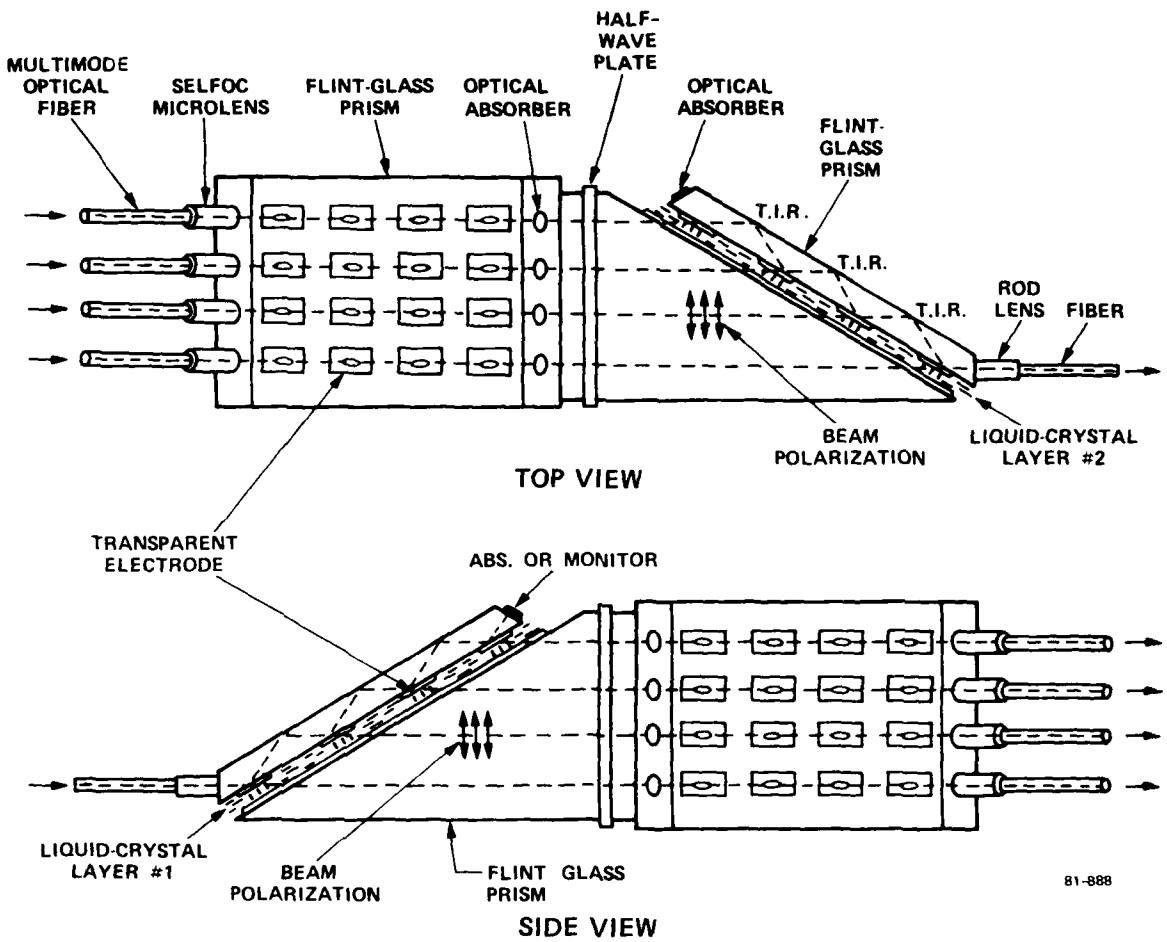

FIG. 7 Structure of our new 4 x 4 fiber optical matrix switch.

QSR-1, (Fig. 15, Appendix B). At the eight unused optical ports in Fig. 7 (four on #1 and four on #2 on the thin prisms), we place optically absorptive material, although the four extra ports on #1 can be used to monitor the input light signals if desired.

The structure is compact and rugged since all parts are permanently cemented together. A perspective view of the final optical matrix is shown in Fig. 8. The size is 2.3 cm x 2.3 cm x 12.0 cm including lenses. This drawing does not include the 17 wires that fan out from each half-matrix, nor does it show the electrical control logic chips attached thereto (see QSR-1, Fig. 4).

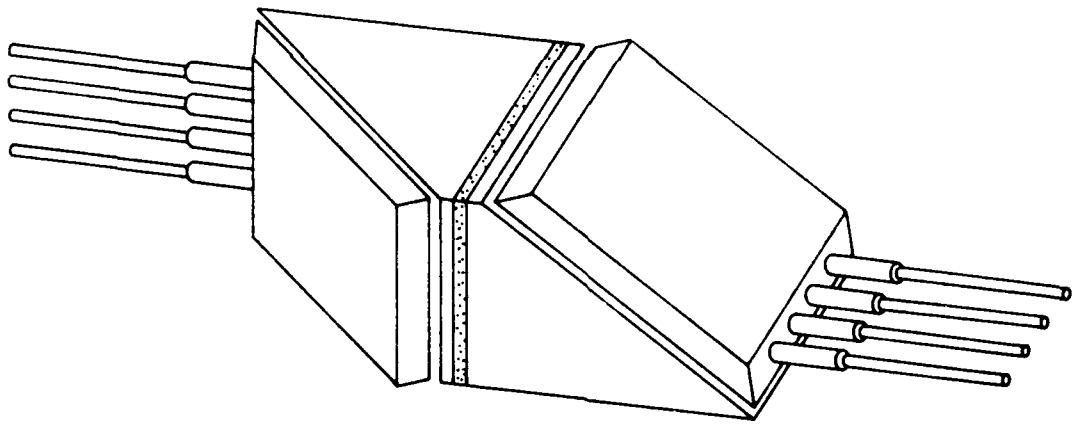

PERSPECTIVE VIEW

81-880

FIG. 8 Another view of the Figure-7 4 x 4 switch.

SECTION VIII

ADDRESSING PROCEDURE

To clarify the voltage-addressing procedure, let us denote an electrode in the first half-matrix switch as a_{ij}, while in the second half-matrix, the electrodes are b_{ij}. Here, i = 1,2,3,4 and j = 1,2,3,4, with i and j representing row and column indices, respectively. Recall from Fig. 1 that the four input fibers are mapped in one-to-one fashion onto the four output fibers. To accomplish that mapping, it is necessary to apply full voltage to only four of the 16 a_{ij} and to four of the 16 b_{ij}, with the remaining 24 electrodes being grounded. In each 16 element array, only one element per row and one per column is turned ON at any instant. To keep track of the optical fibers with the a_{ij} and b_{ij} electrode terminology, we note that the first subscript in a_{ij} also stands for the input fiber index, while the second subscript in b_{ij} also corresponds to the output fiber index.

We pointed out in Section IV that it is essential to map the rows of the first half-matrix output array onto the columns of the second half-matrix input array. This is done spatially (by rotating the second half-matrix 90°) and electronically (by turning ON the appropriate elements of the second array to capture light beams "emitted" by the first array). The addressing condition can be stated simply: When element a_{ij} is turned ON in the first array to transmit a beam, we turn ON element b_{ji} to accept that beam in the second array. In other words, we apply voltage simultaneously to a_{ij} and b_{ji} (four dual elements) and keep the others at zero potential. An example will clarify this. If we wish to send light from input fiber-1 to output fiber-4, together with 2→3, 3→1, and 4→2, then we would apply switching voltage to the following eight elements in the complete matrix: $(a_{14} + b_{41})$, $(a_{23} + b_{32})$, $(a_{31} + b_{13})$ and $(a_{42} + b_{24})$.

As a final note, we should mention that the optical continuity between the input and output fibers is interrupted when all addressing voltages are turned OFF. To state this in another way, if the electrical power fails by accident in the control circuit, the four optical "links" through the switch are broken. At V = 0, all the light comes out of the four monitor ports in the first half-matrix. The link blockage at V = 0 would be advantageous if "secure transmission" were desired.

SECTION IX
MATRIX THEORY AND DESIGN

A. Choice of Materials and Prism Angles

The uniform layers of nematic liquid crystal are about 6 μm thick as spelled out in Part B-2 below. Properties of representative nematic liquid crystal mixtures (a June 1980 sampling of commercial products) are listed in Tables 1A and 1B of QSR-1. The birefringence, or difference between the ordinary and extraordinary refractive indices $n_e - n_o$, ranges from +0.12 to +0.26. For voltage-tuned internal reflection ("frustratable TIR"), we require:

$$n_g \approx n_e \tag{1}$$

$$n_g > n_o \tag{2}$$

where n_g is the glass prism index. Inequality (2) follows automatically from the LC birefringence, and a more precise statement of requirement (1) is that

$$n_e - n_g = +0.01 \tag{3}$$

as discussed in QSR-1 (page 16, Appendix B). Having identified Schott Optical Glass materials F1, F2,...SF13, SF14 as being likely candidates for the 4 x 4 switch, we find in Table 4 of QSR-1 eight combinations of glass and liquid crystal materials that most nearly satisfy (3) above. From that list, we chose the glass/LC combination that had the smallest critical angle (arc $\sin[n_o/n_g]$) because that choice permits the smallest prism angle in the optical switch (beneficial for short optical paths and low insertion loss). The resulting pair is: Schott SF14 flint glass and nematic mixture E9 sold

by EM Industries. The liquid crystal is usable from +7°C to +84°C. The refractive index of the flint glass material is: n_g (589 nm) = 1.7618, while for the liquid crystal, n_o (589 nm) = 1.520, and n_e (589 nm) = 1.775. The prism angle $\theta_p = 66^\circ$ was selected as being a good compromise between insertion loss and speed requirements. The optical incidence angle on the LC is thereby 66°. In designing the glass prisms (QSR-1), one needs to allow overlap between the top and bottom prisms so that external contact to the transparent conductive coatings may be made in the overhang area. We used an x-overlap of 4.3 mm and a y-overlap of 12.0 mm. Following the QSR-1 design procedure, the final dimensions of the prisms were: 45.3 mm x 27.6 mm x 2.8 mm, and 52.3 mm x 23.3 mm x 23.3 mm.

B. Performance

1. Insertion loss. In theory, there are five contributions to the optical insertion loss: 1) switching loss, 2) internal reflection loss, 3) lens-lens coupling loss, 4) input/output reflection losses at fiber/lens and lens/switch interfaces, and 5) electrode absorption loss. Taking these in turn, the first loss is, in principle, 3.0 dB because one polarization component is totally switched in the first half-matrix and the second half-matrix accepts (transmits) all of that light without loss. In the worst case, there are twelve total internal (oblique) reflections within the 4 x 4, each of which has an efficiency of about 98%, which leads to a 1.0 dB total loss. As discussed below, the predicted coupling loss for 2 mm Selfoc SLS rods separated by 9 cm in flint glass is ~1.0 dB. In the fourth area, due to the beneficial effects of optical index-matching cement at all external interfaces, those Fresnel losses are negligible. Also negligible are the electrode losses, estimated at 1% to 2% per ITO film. Adding these factors, the predicted optical insertion loss of the 4 x 4 matrix switch is 5.0 dB.

2. Required voltage and LC thickness. For any addressed element, the electric field within the liquid crystal is approximately uniform and

given by V/δ, where V is the applied voltage and δ the LC layer thickness. What voltages and thicknesses are required?

Prior experiments have shown that the nematic director comes close to its "ultimate" perpendicular orientation at E fields greater than six volts per micron. Thus, the ON voltage is $(6V/\mu m)\delta$. By decreasing the LC film thickness, one decreases the required addressing voltage; generally, the thinner the LC, the better. There are, however, theoretical and practical limits on how small δ can be made. Note first that there are liquid crystal boundary layers at both prism surfaces where the LC order does not change irrespective of V (although the transition-layer thickness is V^{-1} dependent). The boundary layers take up a greater fraction of the volume as $\delta \to 0$, and these layers do not contribute to switching. In addition, as $\delta \to 0$, the optical switching becomes "thwarted" because light will "tunnel" through a sufficiently thin LC, irrespective of its order. Tunneling theory indicates that the LC should be thicker than ~5 optical wavelengths in order for electro-optical switching to occur. This imposes a lower limit of $\delta \sim 3$ μm for visible light and $\delta \sim 5$ μm for near infrared radiation, $\lambda \sim 1$ μm.

However, the practical construction limits on δ would come into play sooner than the theoretical limits. To attain very thin but uniform LC layers, the optical flatness requirements for the prism surfaces become very stringent and the prism spacing procedures become difficult. With "conventional specifications" on optical components, it is unlikely that $\delta = 3$ μm can be achieved without excessive cost, whereas $\delta = 6$ μm is eminently feasible.

SECTION X

EXPERIMENTAL WORK

A. Matrix Construction

Some details of our technical procedure are given in QSR-3 (Appendix D). That information will be summarized and updated here. We shall examine eight aspects of the construction and assembly procedure.

1. Electrodes. The electrode film thickness should be less than a quarter wave; otherwise, the electrode's refractive index would affect the switching process. During the construction, a transparent conductive film of indium-tin oxide (ITO) was deposited on the appropriate prism surface with an rf sputtering system. After briefly sputter-etching the glass, the ITO was put down in a pure argon atmosphere (0.020 Torr partial pressure) from a mixed oxide sputtering target: 88% In_2O_3 and 12% SnO_2. The resulting ITO film, about 1000Å thick, had a faint interference color and was "highly transparent" (although the absolute value of its optical transmission was not measured). No "post-bake" oxidation/reduction operation was performed. After being exposed to room atmosphere for a day, the ITO electrical resistance increased ~2x and stabilized, with its transparency unchanged.

We performed photolithography on the top prism ITO film to define the electrode pattern. When photoresist is spun on the prism surface, the resist always becomes thicker in a band around the perimeter of the surface, an effect known as "edge buildup". For the first few switches, where positive resist was used, the edge-resist could not be exposed sufficiently to UV without undercutting the rest of the pattern. Therefore, we changed to negative resist, Kodak KPR, for the final switching devices. Here, the edge buildup is washed away during development. The KPR was spun on at 5000 rpm, then baked at 60°C for 45 minutes. After exposure to UV through the electrode mask for 40 seconds, the development was carried out, followed

by a 100°C bake for 120 min. To etch away unwanted ITO areas, the prism was then immersed in undiluted hydrochloric acid for 20 seconds.

2. Surface Preparation. The liquid crystal alignment is determined by whatever treatment is given to the ITO surfaces. At first, we tried the standard "oblique SiO" surface treatment, where ~250Å of SiO is put atop the ITO layer at 60° incidence, deposited via vacuum evaporation. However, in the first test-switches, the initial liquid crystal order was permanently altered by high electric fields: 50 Vrms applied across 6 μm (see QSR-3). As an alternative, we then tested the surface-rubbing procedure, familiar from the early days of liquid crystal technology. Here, we found that the liquid crystal order cycled in a repeatable fashion when the 8 V/μm fields were turned on and off. Consequently, this surface treatment was selected for the final switching devices.

The clean ITO film on each prism was rubbed unidirectionally with a cotton swab (Q-tip) for 20 seconds, using a total of three swabs per prism, 60 seconds of stroking in a raster scan. This led to a uniform, well-ordered liquid crystal film, relatively free from defects and thread-disclinations. After voltage removal, this liquid crystal film always reverted to its homogeneous order. The reasons why the high fields destroyed the LC anchoring forces at the SiO surface but not at the rubbed surface are not clear at the present time.

3. Prism Spacing and LC Filling Procedure. For each half-matrix, a plastic fixture was used to press the top and bottom prisms together firmly during assembly so that the prisms would seat properly on the plastic spacers, thereby assuring a uniform gap between them. After placing the surface-treated bottom prism in the pressure jig, two pieces of clean ½-mil teflon tape, 3 cm x 0.1 cm, cut from a ½-inch ribbon with a razor blade, were placed on opposite sides of the surface, while making sure that the tape was not wrinkled. Then the surface-treated top prism, properly aligned, was placed atop the teflon spacers, after which the jig was tightened. Six dots

of Varian Associates Torr-Seal Epoxy were placed along the exposed 6.3 μm air gap between the prisms, after which this assembly was put in a 55° oven where the epoxy cured for 80 minutes.

After the epoxy cured, the empty half-matrix was placed on a 95°C hotplate for 30 minutes, so that it reached a temperature sufficient to melt the E9 liquid crystal. A bottle of E9 was also heated on the same hotplate. With clean glass pipettes, molten LC was transferred to the slit between the prisms where LC flowed in along the surface-order direction to fill the 6 μm cavity in about 2 minutes. Then the hotplate was turned off and the switch cooled slowly to room temperature.

The top prism overhangs the bottom prism by 4.3 mm in one direction, revealing 16 parallel bars of ITO, the fanned-out electrical leads. Here, we attached short lengths of tinned #26-gauge copper wire, one wire per bar, with strips of Tracon type 2902 silver conductive epoxy, which provided electrical access to the switch. Similarly, for a common ground, a wire was attached to the bottom prism sheet electrode in the region where it extended 6 mm beyond the top prism. The 17 wires were soldered to a male quick-disconnect ribbon-conductor-connector that plugged into a female ribbon-socket from the control box. Those connectors made it easy to change switches during our electro-optic checkout procedure.

The completed half-matrix switches (without fibers) are shown in Figs. 9 and 10. On the bottom of each switch, we cemented a brass plate to act as a mounting pedestal and as a strain-reliever for the four optical fibers that are subsequently attached to the half-matrix. In these photographs, we have positioned the half-matrices in the approximate spatial relationship that they will have in the final matrix; namely, in-line but mutually oriented at 90° (a rotation about the main axis).

4. LC Thickness Variations. Maintaining a uniform liquid crystal layer thickness (δ) over a large area has always been a fairly difficult technological problem. This difficulty has come up in the LC

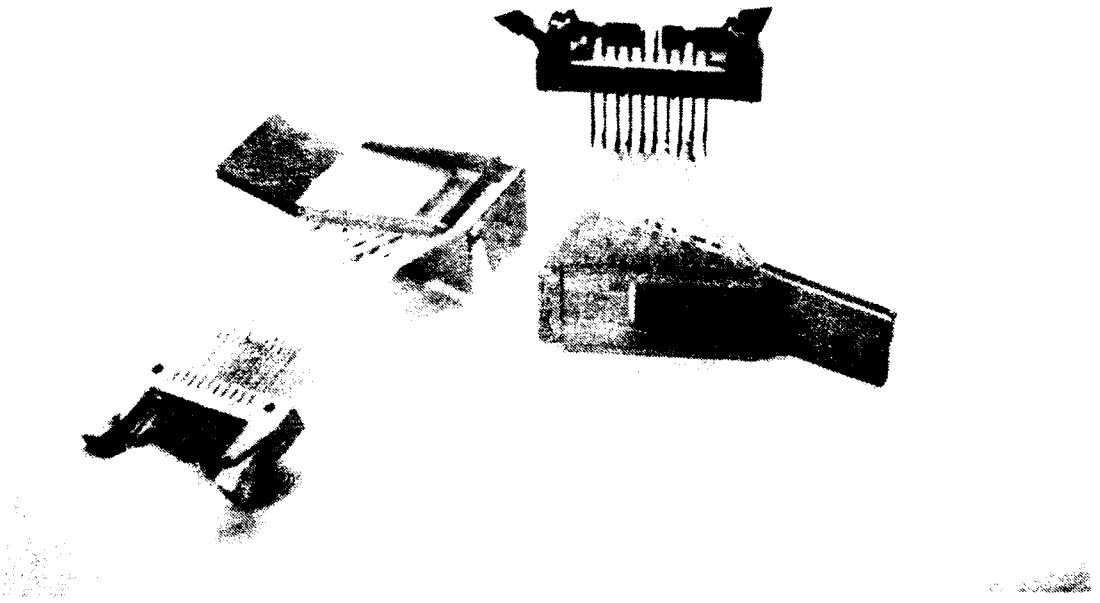

81 91

FIG. 9 Two identical 4 x 4 half-matrix switches as they appear prior to being assembled into the final matrix. Demountable electrical connectors for 17-conductor ribbon cable are shown. Each brass plate provides strain relief for 4-fiber assemblies (not shown).

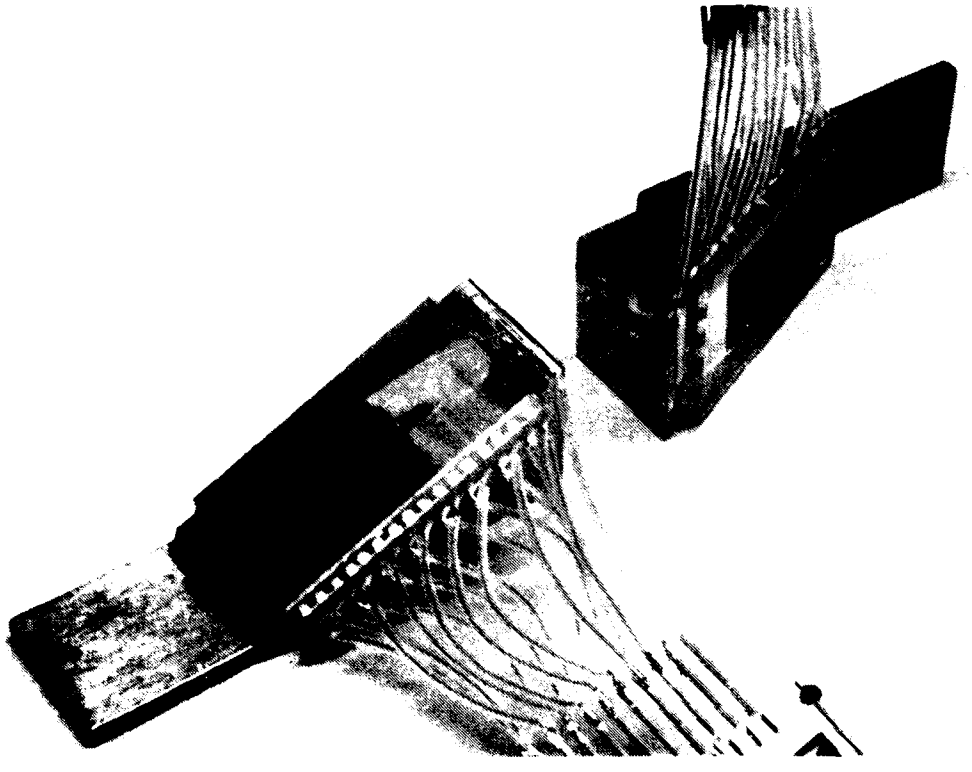

FIG. 10 Close-up view of Figure 9. The half-wave plate will be mounted in the space between the half-matrices.

display industry and is also evident in our optical switching application because here we require an LC thickness of about 50% of that for displays (6 μm vs. 12 μm). In fact, we would prefer $\delta \sim 4$ μm for low voltage operation (Sec. IX-B2) but have set aside that goal as being "overly ambitious" for the present time/money constraints.

The half-matrix has a 5.7 cm x 2.3 cm active LC area. Any changes in δ over this area show up immediately in the electro-optic response (Sec. B-1), so it is advantageous to monitor δ over a wide area for each half-matrix in order to know what progress (or lack thereof) has been made in holding δ constant. We set up apparatus for doing this during the Third Quarter (QSR-3, pages 11-16) and the equipment proved a valuable tool during the checkout and test procedures. The method is to examine the optical interference colors transmitted by the birefringent LC layer (illuminated with white light) through the large, polished faces of the prisms (not the faces where fiber light comes in). Thickness changes show up as color changes.

Two representative results for 4 x 4 half-matrix switches (shown here in black and white) are presented in Figs. 11 and 12. For the Fig. 11 device, the color is the same (red) over 3/4 of the entire area, shading to green at either end; so a reasonably good thickness result has been attained. The result is less favorable in Fig. 12 where the color shifts from red in the right 1/3 area, to green in the midregion, to purple in the left 1/3 area.

The theory of white light transmission through a planar birefringent layer gives correlations between layer thickness and output color. From theory, and from the Fig. 11 and 12 data, we estimate that the LC thickness shifts by 1 to 2 μm in localized regions of our experimental devices. Most of this variation is due to local, unwanted curvature of the prism surfaces. At a higher cost, the vendor (Optics for Research) could have polished those surfaces flatter, so we could have obtained a better δ-uniformity than observed. Nevertheless, the present thickness changes were not large

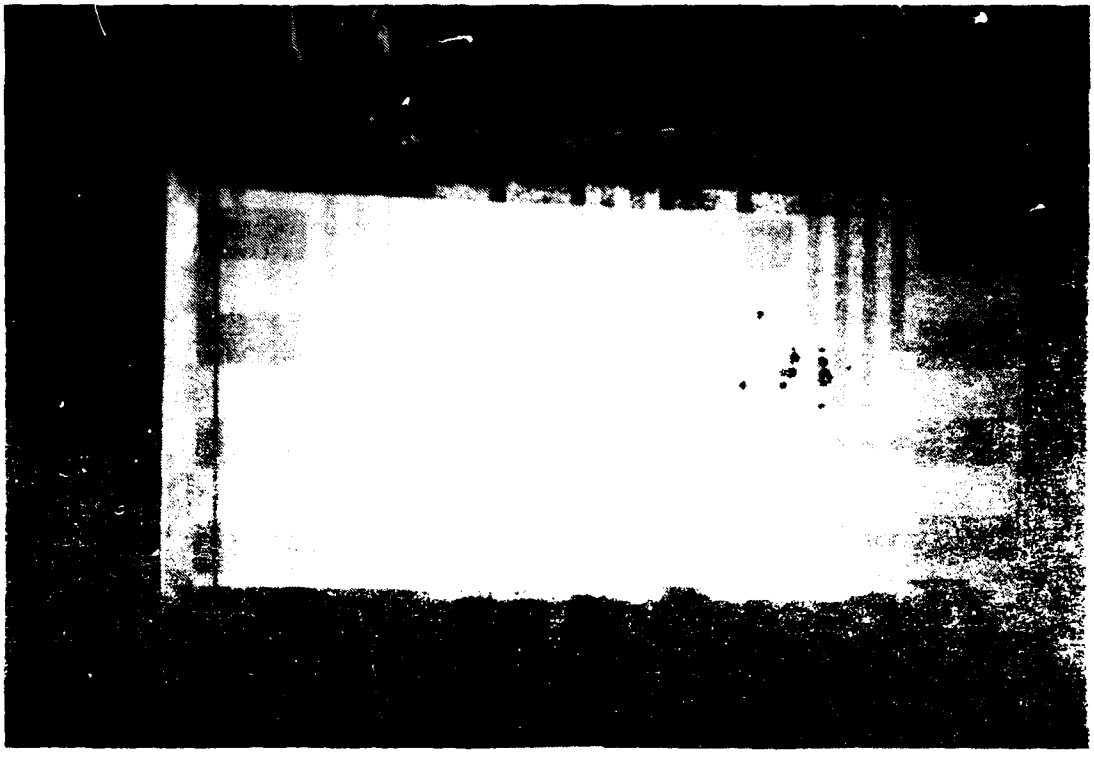

FIG. 11 Optical interference color photograph of ordered 6 μm liquid crystal layer in 4 x 4 half matrix switch "A" viewed normal to the layer.

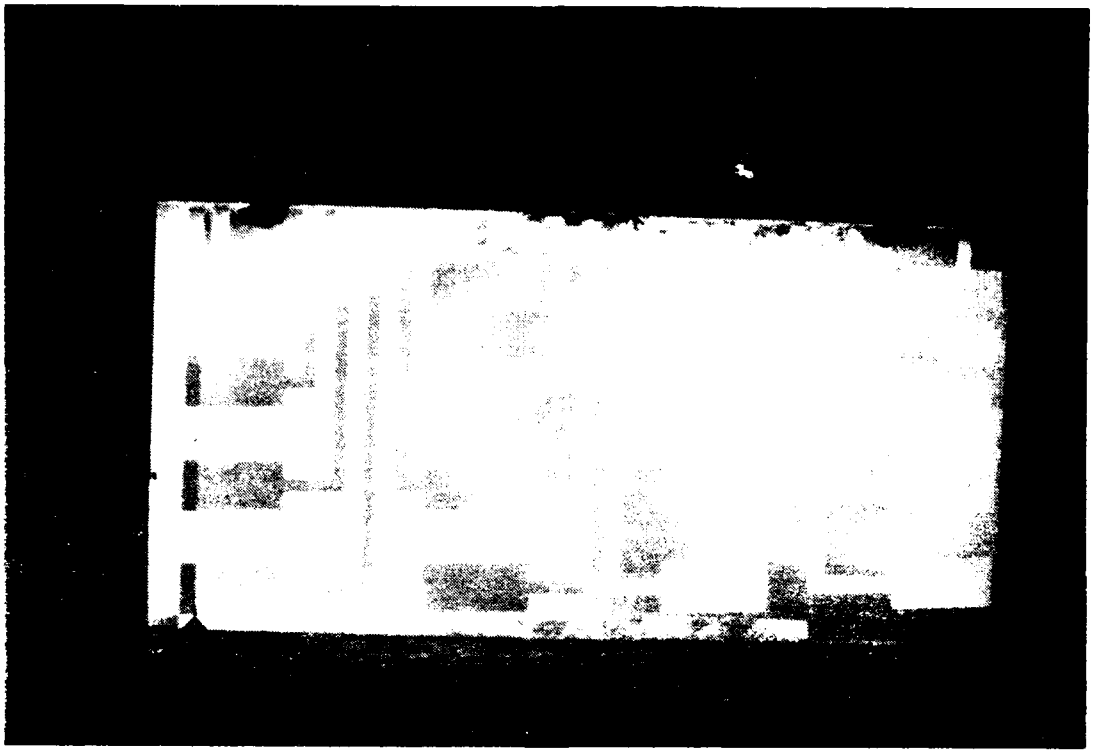

61-914

FIG. 12 Same as Figure 11 for half-matrix "B"

enough to overly degrade the electro-optic response (Section B-1) and the observed response was acceptable.

5. Matrix Control Box. Manual selection of any matrix state was accomplished with a control box built in our electronics shop. Figure 13 shows the circuit diagram of this controller that has 16 miniature toggle switches for applying voltage to any element in either half-matrix. By making the toggle switches SPDT, we can automatically ground any element that is not turned on. A high-resistance potentiometer is shunted across each element so that it can receive partial addressing-voltage rather than full voltage, if desired. The voltage source for the 4 x 4 controller is an audio-frequency square-wave generator with 0-40 Vrms output.

The output leads from the controller consist of two 17-wire ribbons, one for each half-matrix. As we mentioned earlier, our addressing scheme supplies voltage to the $a_{ij} + b_{ji}$ electrode pairs; therefore, the ribbons in Fig. 13 are internally wired so that toggle switch 1-1 sends voltage to elements a_{11} and b_{11}, with toggle 1-2 controlling $a_{12} + b_{21}$, toggle 1-3 addressing $a_{13} + b_{31}$, etc.

6. Four-Fiber Arrays. The fibers selected here are communications grade Corguide 1515 all silica, slightly graded, multimode waveguides. These have a core diameter of 50 μm, an outside diameter of 125 μm. and an NA of 0.21. Their attenuation is 4.7 dB/km, with a -3 dB bandwidth of 350 MHz-km. This core size was chosen to give an optical $\pm 0.5^{\circ}$ output beam divergence with SLS lenses.

Eight 1-meter strands were prepared, each strand being placed in a protective plastic jacket, with the fiber ends then cemented into 1/8"-D brass ferrules. Machine polishing of each ferrule produced smooth, flat ends on each fiber. Next, one fiber end was butt-coupled to a Seltoc type SLS microlens, 2 mm diameter, 0.25 pitch at 633 nm (0.35 NA, 0.9 mm length). The fiber end was centered in the rod lens while the resulting

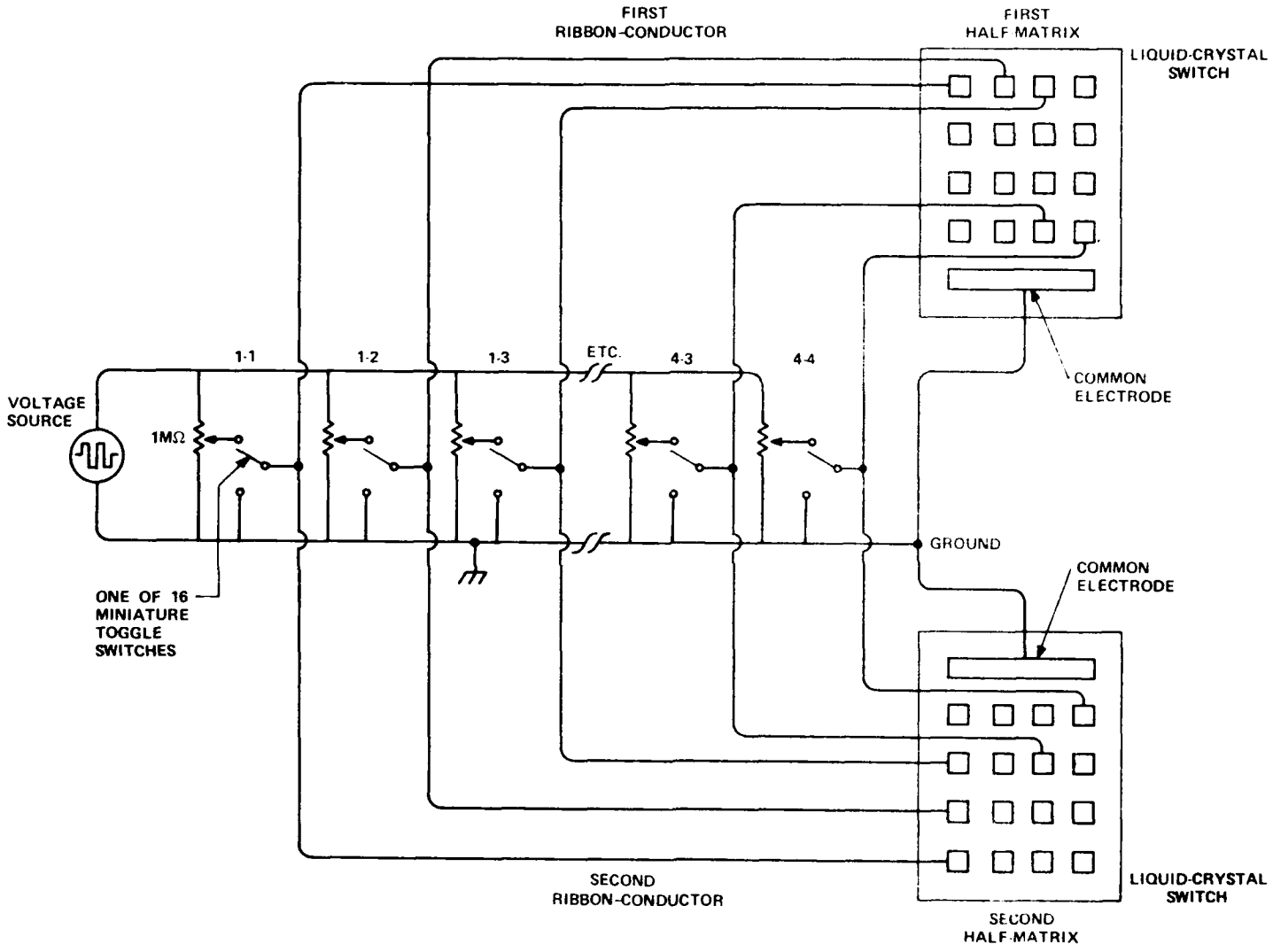

FIG. 13 Circuit of manual control box for 4 x 4 matrix.

81-877

far-field radiation pattern was observed on a screen. Upon reaching the minimum beam divergence condition, visually determined, a small drop of transparent Devcon 5-minute epoxy was inserted between fiber and lens to join those two permanently. This lens-to-fiber "pigtailing" process was repeated eight times.

Having made the collimated beam pigtails, we decided to group them into prealigned quartets to simplify the fiber-to-switch alignment process in the 4 x 4 matrix. Alternatively, the pigtails could have been attached one-at-a-time to the matrix, but we felt that this would have prolonged and complicated the alignment process.

By examining the 16-electrode pattern, we found that the center-to-center spacing of the electrode rows was 5.1 mm. This means that the optical beams entering the matrix should be parallel to one another, should be coplanar, and should be spaced 5.1 mm on centers. To obtain the precise beam spacing and to assure beam parallelism, we designed a brass mounting fixture to hold four fiber/lens pigtails in the desired spatial relationship. This one-piece brass jig had four parallel holes for the GRINrod lenses (2 mm-D; loose, sliding fit) and four coaxial holes for the fiber ferrules (4.5 mm-D; loose fit, so that cement could be added after the ferrule had been suitably "manipulated").

The optical far-field pattern from the 4-fiber array fell on a white viewing screen or "target" 65 cm from the fiber output ends. The alignment procedure was to line up the far-field spots within black circles drawn on the target; specifically, we drew four overlapping 10 mm-D circles on the target, a linear array spaced exactly 5.1 mm center-to-center. First, the empty jig was oriented with its axes on-target via black illumination. Next, the pigtails were laser-excited (20x objective, core modes only) and were placed one-by-one in the jig. Mechanically, we micro-manipulated each pigtail until its output spot overlapped the target circle exactly. The pigtail was temporarily held there with Apiezon wax, then cemented

permanently into the brass jig with clear epoxy. The process was repeated three more times. The resulting four-fiber array is shown in Figs. 14 and 15. The mutual alignment attained is judged "fair to good". Looking at the final four 10 mm-D light spots as they appear on the target, we found position discrepancies of ±0.5 mm relative to the target circles. The alignment described here was limited by our ability to move the lens/fiber pigtails through small x-y-ϕ_1-ϕ_2 increments, and by the nonroundness of the output spots (due to fiber modal distributions, laser speckle, and fiber-end polishing errors). Having completed the first array, we built an identical 4-fiber array in the same way.

7. Optical Alignment and Matrix Assembly. We completed assembly of the 4 x 4 matrix in the following ten steps: 1) Cement the half-wave plate onto the output surface of the first half-matrix, 2) optically excite all fibers in the first 4-fiber array, 3) apply partial addressing voltage to all 16 electrodes in the first half-matrix, 4) move the first fiber array into precise alignment with the first half-matrix, 5) join those fibers to the first half-matrix, 6) apply partial addressing voltage to all 16 elements in the second half-matrix, while keeping partial voltage on the first half-matrix, 7) manipulate the second half-matrix into the exact required alignment with respect to the first half-matrix, 8) cement the second half-matrix to the first along the HWP surface, 9) manipulate the second 4-fiber array into the desired alignment with respect to the output surface of the full 4 x 4 matrix, and 10) attach those second four fibers to the full matrix at the second-half end. This procedure took several days. We shall provide details of the process.

The 2.3 cm x 2.3 cm half-wave plate (axes along the diagonals) was a Polaroid 0.030" plastic sheet having half-wave retardation at 560 nm (the commercial product that came closest to $\lambda/2$ retardation at 633 nm). It was cemented with a bubble-free film of clear epoxy. Figure 16 illustrates the first optical alignment process. The first 4-fiber array is attached with double-stick tape to an aluminum arm that is bolted to an

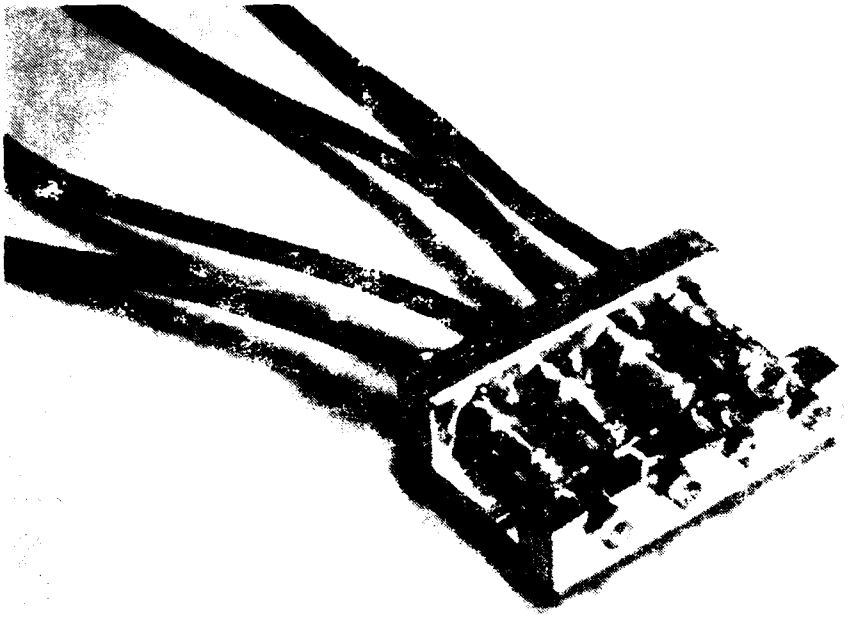

. 3. 14 Linear array of four multimode fibers and four Selfoc lenses used in matrix. Brass jig provides precise spacing between lenses.

81-915

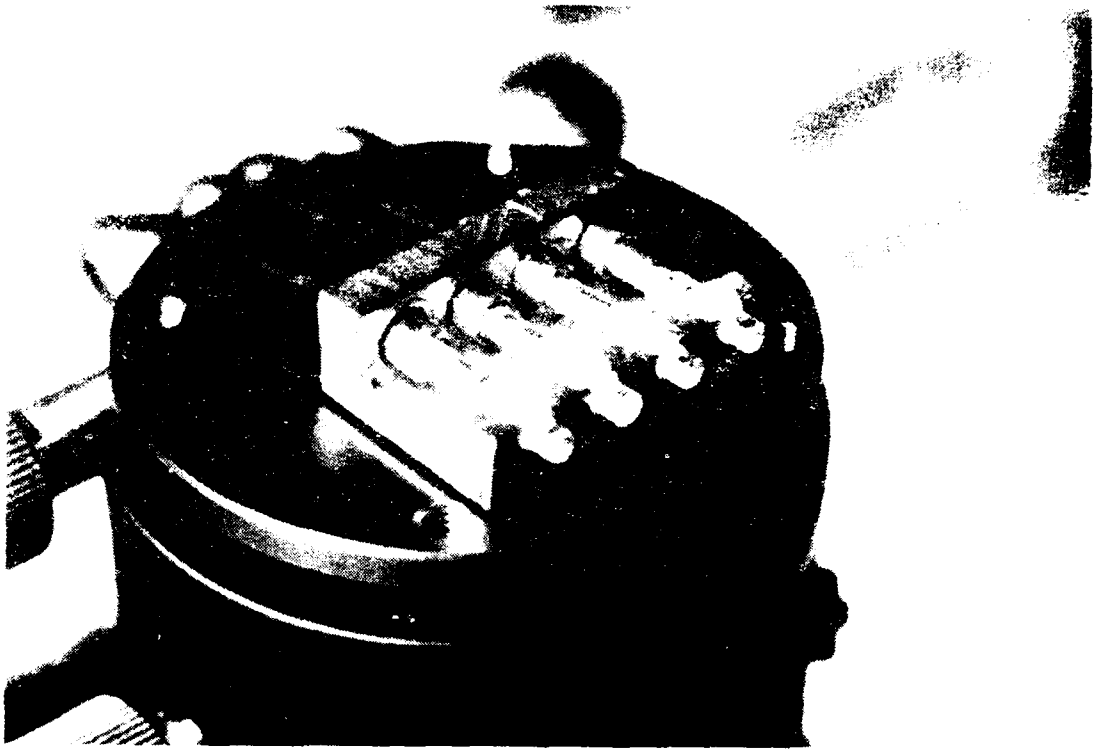

FIG. 15 View of Figure 14 assembly mounted on $\phi_1 - \phi_2$ micropositioner table

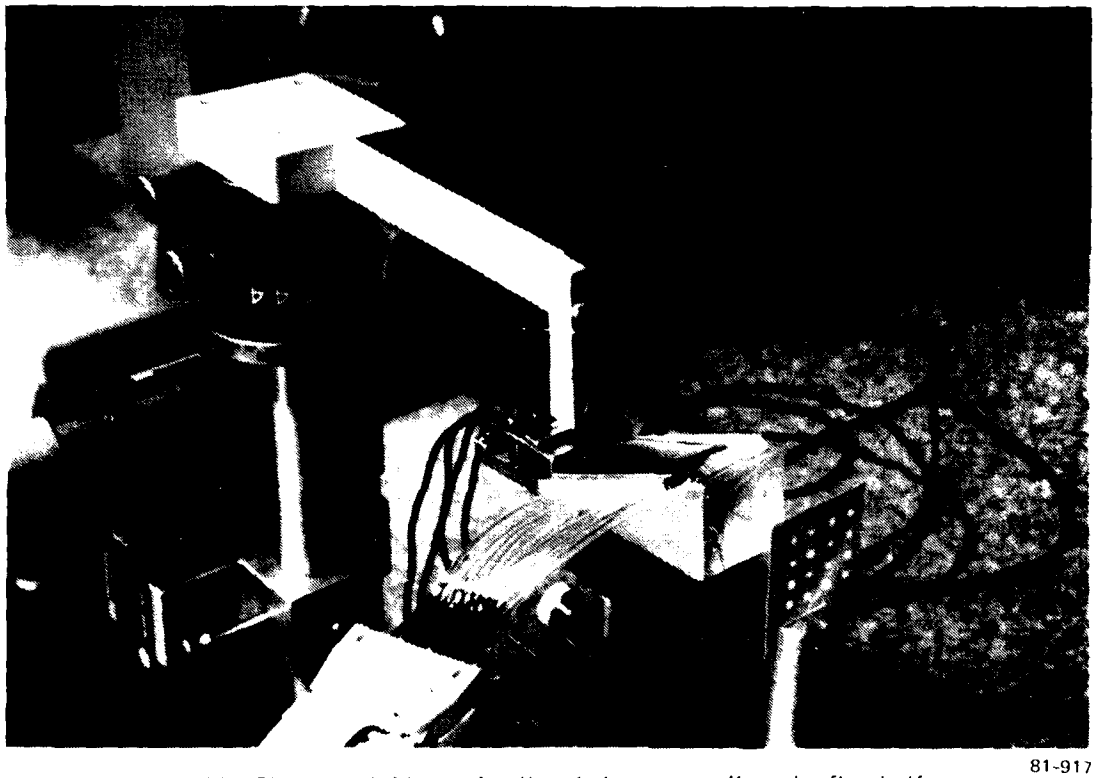

81-917

FIG. 16 Photograph illustrating "work-in-progress" on the first half-matrix switch. Micropositioner arm for the first 4-fiber array is seen, together with optical 16-beam output that results from partial switching at all electrodes.

x-y-z-ϕ_1-ϕ_2 micropositioner. The four red light beams entering the partially addressed (15 Vrms) half-matrix result in 16 simultaneous switched outputs as shown. The position of each incoming light beam within an ITO electrode-rectangle is noted by looking at the faint scattered light from the liquid crystal film. So, we moved the fiber array until the beams were centered in the rectangles and until the 4 x 4 beam pattern of Fig. 16 was equi-spaced in both x- and y-directions. Then a tiny drop of clear epoxy bonded each SLS lens to the small face of the prism. The adhesive filled the 2-mil lens/prism air gap. Extra adhesive was then added to the fiber mounting; then the micropositioner arm was removed. Next, we applied 15 Vrms to all elements of the second half-matrix while bringing it quite near the first half-matrix with a micropositioner. (The first half is excited as in Fig. 16). After going through the second half, the 16 switched light beams now merged into four somewhat fuzzy output beams at the 0.28 cm x 23.3 cm output face. Before cementing the second half-matrix to the first with transparent epoxy, we again looked for symmetry of the 16 beams within the ITO rectangles, and for symmetry of the 4 output beams.

The last two steps are an optimization process: the maximized capture of light by fibers 5,6,7,8. This optimization proved difficult because the output beam positions moved by a fraction of a millimeter when we went from matrix-state to matrix-state (motion relative to the central positions with 15 V on all 32 elements - See Section X-B2). Starting with the second 4-fiber array attached to the micropositioner arm as in Fig. 16 we selected three quite different matrix states (per Fig. 1) with 40 V applied to 8 elements. We then did a simultaneous maximization of the fiber optical throughput for those three states, after which the fibers were attached as above.

8. The Final 4 x 4 Matrix. Three views of the final matrix as it appears in our laboratory are shown in the photographs of Figs. 17, 18, and 19. In Fig. 17, most of the equipment is visible, including the control box, the electrical connections, the four-part laser excitation of

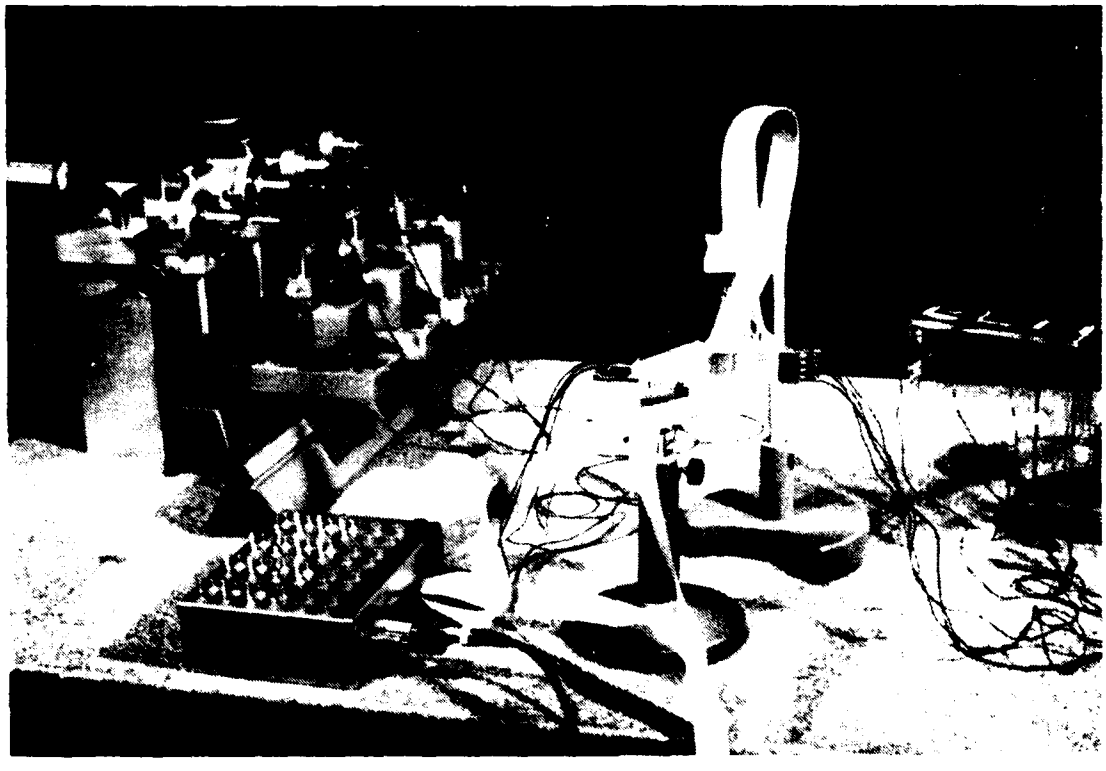

FIG. 17 The final 8-fiber electro-optical 4 x 4 matrix switch and associated equipment, including matrix control box (foreground), both electrical ribbons, and simultaneous gas-laser excitation of four input fibers.

81 920

FIG. 18 Medium range view of Figure 17 switch.

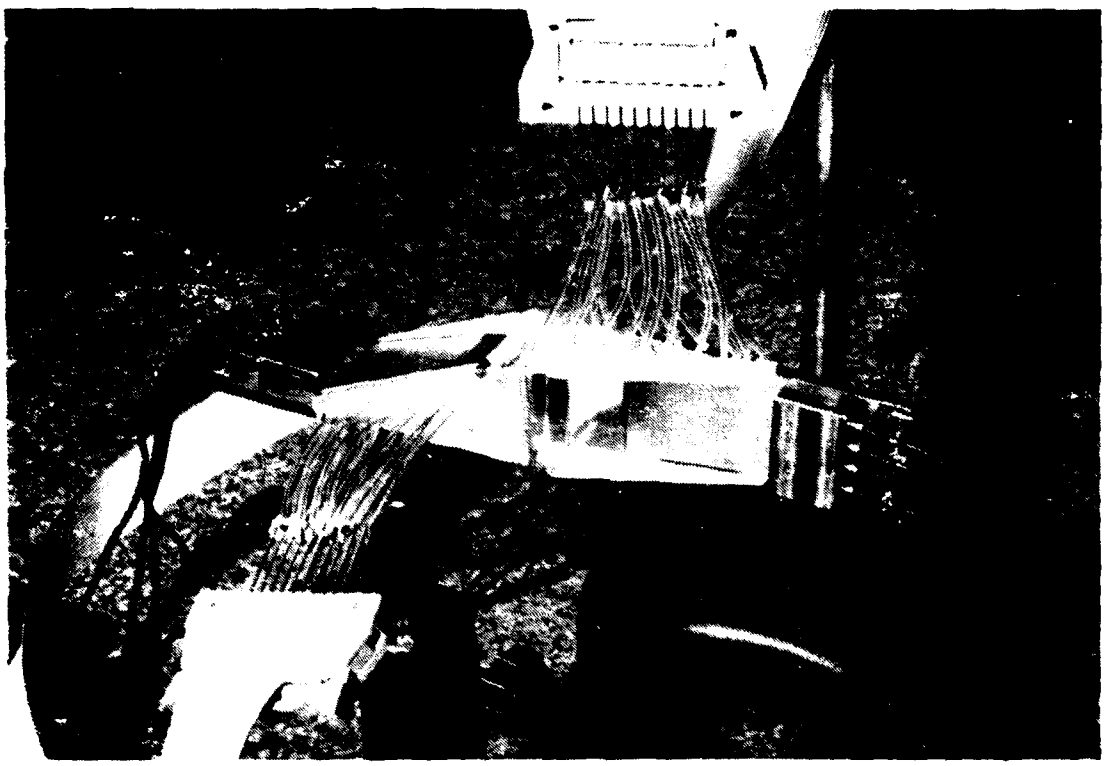

81-922

FIG. 19 Close-up view of Figure 17 switch.

the input fibers via beamsplitters (Section B-1) and the four output fibers arrayed on a plastic box for easy access by the photo-detector. The second and third photos show close-up views of the switch. Because the eight 1-m fibers are covered with 1-mm-D plastic tubes, they look like "black wires" in the photos. To facilitate photographing the 4 x 4 switch, we mounted it atop an 8" laboratory stand with a small square of double-sided adhesive tape, but the switch is inherently a portable, free-standing, self-contained device. No air gaps remain in the switch after cement has been applied, and the switch becomes a rugged, monolithic "package". Adequate strain relief for the fibers is provided by epoxy dots attached to the metal base plates and one can, for example, pull on the fibers without changing the switch's performance. The switch "body" is also quite strong because of the epoxy that holds all parts together, and the switch should be relatively immune to damage. The two sets of 17 leads seen in Figs. 18-19 could be wired in parallel nearer to the switch body, thereby miniaturizing the electrical input region. Other commercial packaging steps could be taken; for example, connectorization. Although technically difficult, it is conceivable that the fiber pigtails could be replaced by AMP-type connectors that provide detachable fiber connections to the matrix. Here, a Selfoc rod lens would be mounted in the center of each female connector.

B. Results

1. Electro-Optic Turn-On. Liquid crystal cells are capable of operating reliably and repeatably for many millions of on/off cycles. Lifetimes of several years are attainable if the liquid crystal regions are actuated by ac drive. But, under dc drive, the lifetime is limited; thus we chose ac control signals for the present experiments.

The liquid crystal orientation responds to the rms value of the applied voltage. We found that sine-wave and square-wave drive produced similar reuslts, although the turn-on was slightly faster with square waves. A square-wave source was used here.

If the drive frequency is in the low audio frequency range, there will be some "ripple modulation" on the switched light because the present liquid crystal cells are fast (see Part 4 below). We used control frequencies in the 1 to 2 kHz range, which kept the ripple quite small. Although control frequencies from 2 to 40 kHz will work, the higher frequencies accentuate the capacitive coupling effects between electrodes (discussed in Part 3 below), whereas the 1 kHz control voltage minimized the unwanted electrical cross coupling.

The first experiments were done on half-matrix switches, before the fibers were attached. Six devices were built, and the two devices with the most uniform turn-on characteristics were selected for use in the final 4 x 4 matrix. A 633 nm laser beam, totally p-polarized, was incident normally on the small face of the top prism along one row of the 16-electrode pattern. Of the four electrodes in that row, one was connected to a cw 1200 Hz square wave source and the other three were grounded. A photodetector recorded the intensity of light switched into the lower prism as a function of applied rms voltage. Then, this measurement was carried out for the other three row-elements, after which the remaining three rows were optically tested in the same way.

Figures 20 and 21 display the observed electro-optic turn-on curves for the best two half-matrices. Initially, the transmission rises and falls rapidly before increasing towards its final value. These narrow peaks and valleys occur between zero and 10 Vrms. The optical throughput for most of the 16 elements has a voltage dependence of approximately $\{1-\exp(-V/V_o)\}$, which is an envelope-function fitted to the curves. The throughput saturates above 15 Vrms, approaching its high-field asymptote closely in the 30 to 40 Vrms range. Reflection losses at the two glass/air interfaces permit a theoretical maximum switched transmission of 86% for the p-light. Experimental values of 80 to 83% compare favorably with this. There are, however, a few "weak" elements in each switch where the turn-on is incomplete at 40 Vrms. This is attributed to a local variation in the

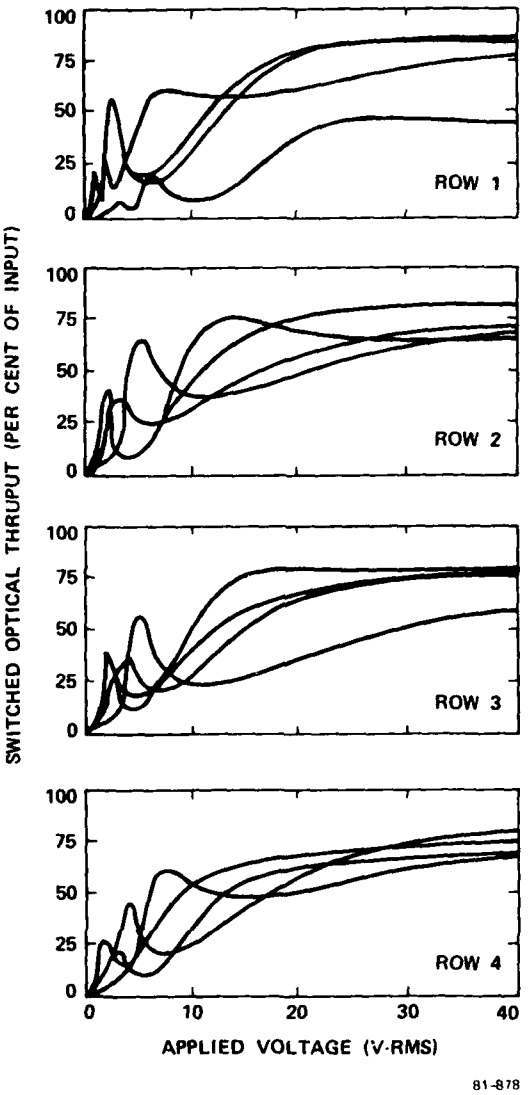

FIG. 20 Measured dependence of switched light intensity upon applied voltage for the first half-matrix switch.

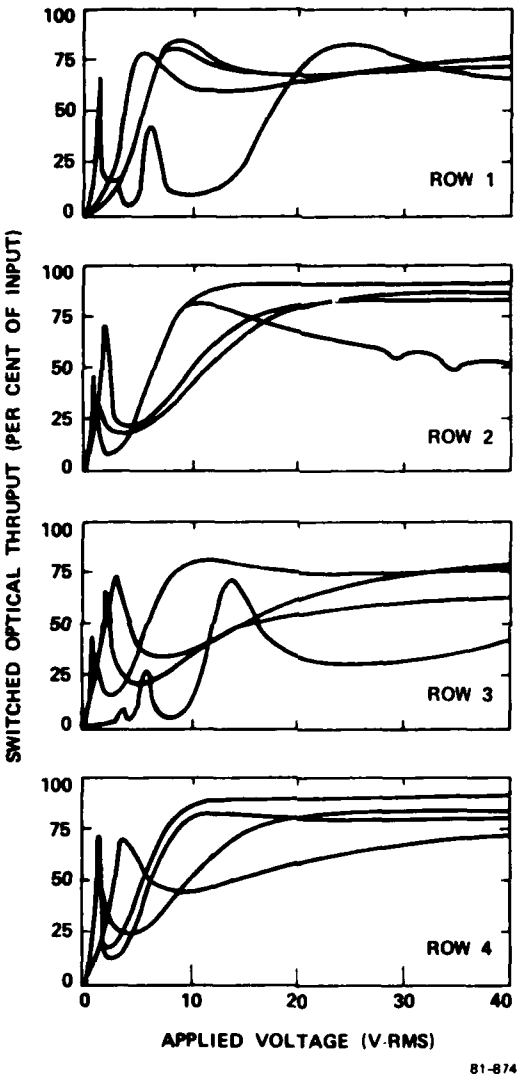

FIG. 21 Same as Figure 20 for the second half-matrix.

LC layer thickness: at those locations, the LC film is 1 to 2 μm thicker than the nominal 6 μm value. Weak elements can cause excess loss in the final matrix, although in most addressing situations, two weak elements will not be in cascade. In most cases, a strong element will feed a strong element, while in a few instances, a weak element will face a strong element. The latter situation does show up in the insertion-loss statistics discussed below (Part 2).

After having combined the switches of Figs. 20 and 21 (per Section X), the electro-optic curves of the resulting fiber-coupled 4 x 4 matrix were measured in various states. Figure 22 illustrates the measurement set-up which was also used for loss and crosstalk measurements. A 633 nm laser beam was divided into four quarter-strength beams with pairs of beamsplitting prisms. After securing each of four input fibers in a Newport FP-5 micropositioner, we focused an optical beam into each fiber core with a 20x microscope objective. Any of the four simultaneous fiber excitations (or any combination) could be blocked by shutters as desired. At the output fibers, a movable detector detector recorded the intensity of light switched through the matrix. For configuring the switch, the matrix control box described above was used. It was actuated by a cw 1200 Hz square-wave generator whose voltage amplitude was adjustable.

The measured electro-optic turn-on characteristics of a representative state of the complete fiber optical matrix are presented in Fig. 23. The general shape of the curves is the same as in Figs. 20 and 21, but some differences have appeared. Here, there is a larger variation in the final values of optical transmission in the 30 to 40 Vrms range. As discussed in Part 3 below, this is due, predominantly, to geometric factors such as fiber misalignments, nonparallel prism faces, and "unequal" elements in the half-matrices. Also, the low voltage oscillatory behavior of Figs. 20 and 21 has been smoothed out, and there is now a ~5 Vrms threshold in the matrix, somewhat higher than the thresholds of the half matrices.

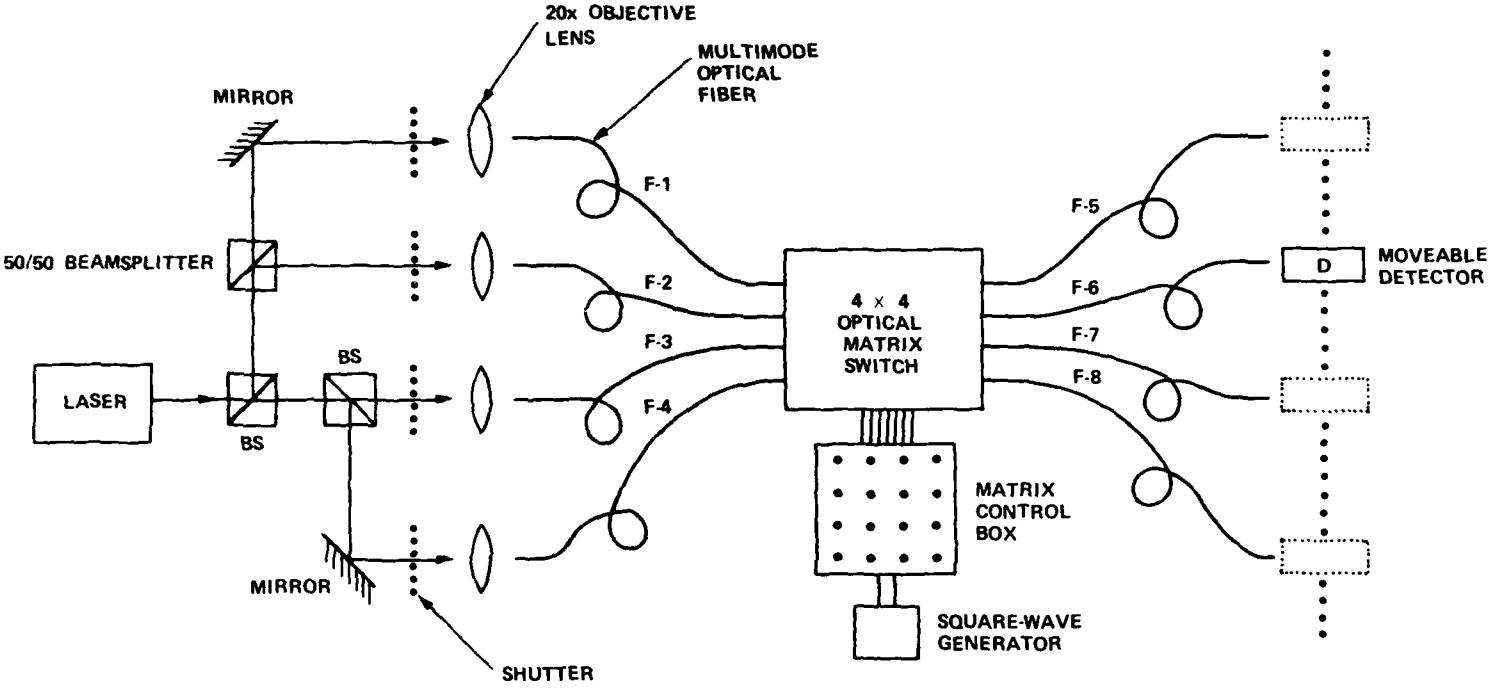

FIG. 22 Experimental system for measuring electro-optic turn-on of 4 x 4 matrix, as well as optical insertion loss, optical crosstalk, and transient response (with pulsed source).

81-875

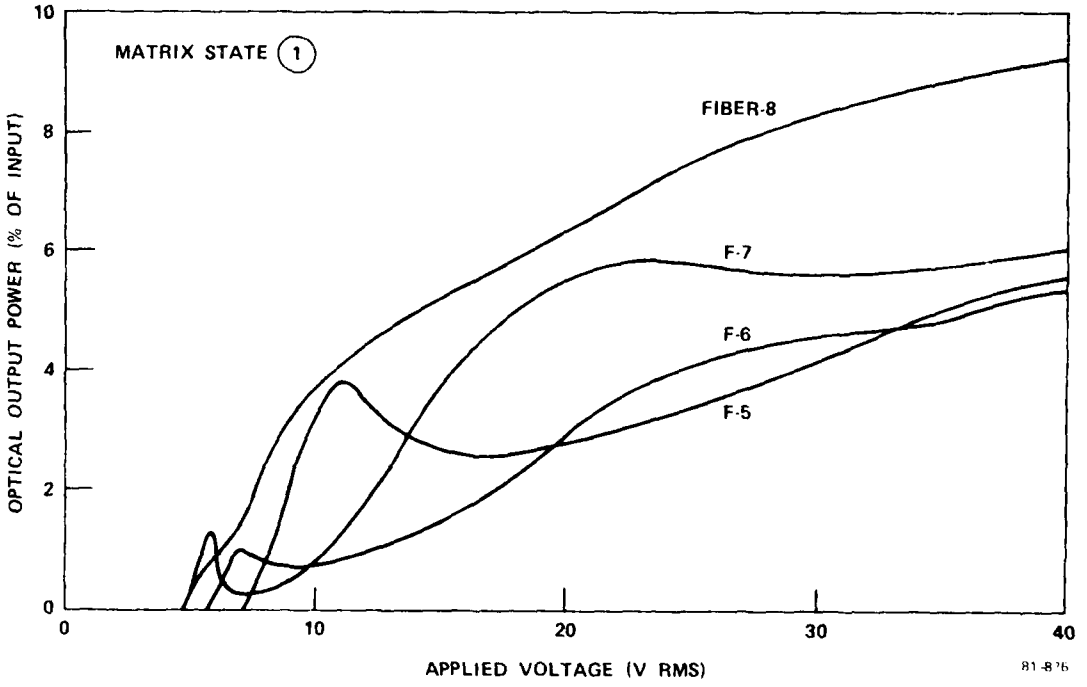

FIG. 23 Measured dependence of switched light intensity upon applied voltage in one state of the final 4 x 4 fiber optic matrix.

2. Optical Insertion Loss. A convenient way to monitor the optical power entering the matrix is to record the intensity emerging from the upper port of the first half-matrix (the dashed line in Fig. 4A) with zero voltage applied to the matrix. In the V=0 condition, all of the unpolarized input fiber light is totally internally reflected (seven times) in the top prism and exits from the second small face. At each internal reflection, the loss is very small, less than 0.09 dB, and the input fiber loss is negligible because the fiber is short and because no cladding modes were excited. Therefore, we made less than 0.7 dB error in determining the optical input power from the "monitor ports".

The optical insertion loss of the matrix in dB is 10 log P/P', where P is an output fiber power, and P' an input fiber power. (This does not include splice- or connection-loss to the fiber). The power P' is measured as discussed above, and P is found by butt-coupling a silicon photodiode detector to an output fiber. We measured the optical throughput on fibers 5,6,7,8 for each of 24 switching states, a total of 96 data points. During each measurement, the state was selected with 40 Vrms applied in our usual 4 + 4 crosspoint addressing scheme.

The results are presented in Fig. 24. The switched optical transmission for the four output fibers has been plotted as a function of the matrix state-number (per Fig.1). The minimum observed optical insertion loss was 6 dB (states 1 and 10) which is not far from the theoretical limit of 5 dB (Sec. XI). Averaged over 24 states, the mean value of insertion loss was 15 dB. Unfortunately, the loss ranged as high as 24 dB in some states.

The scatter in optical throughput values from state-to-state is probably the most serious problem encountered in this work. However, the problems are mechanical rather than fundamental in nature and are amenable to solution by improved mechanical procedures.

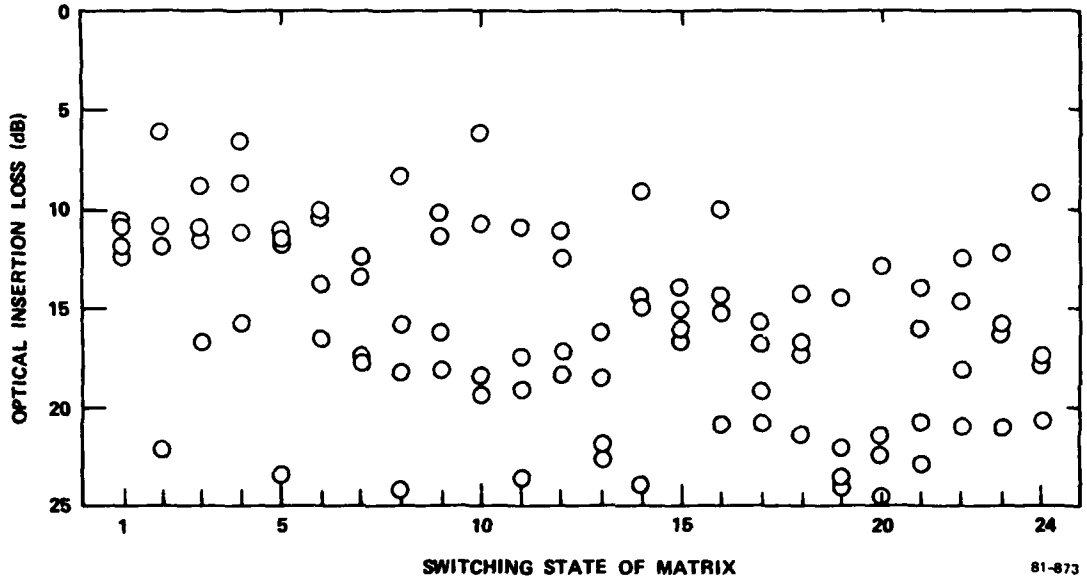

FIG. 24 Complete set of optical insertion loss measurements for the final 4 x 4 fiber optic matrix.

Three causes of variation in the optical insertion loss were found: 1) mechanical misalignment of fiber axes relative to the switch's principal axes, 2) nonparallelism of the major faces of the top prism in each half-matrix, and 3) transfer of light from a liquid crystal element having low transmission in the first half-matrix to a "normal" element in the second half, or vice versa. The misalignment was the most important factor. This was determined by examining the optical beam pattern at the matrix output before the second array of four fiber+lenses was attached. As the matrix was reconfigured from state to state, the collimated beam positions shifted laterally by about ±0.1 diameters. Thus, no fixed array of four lenses could capture efficiently the spatially varying beams in all 24 cases. Factors 2 and 3 above were less decisive in the loss. The nonparallelism was judged "small" and the weak/strong combinations affected only a few states.

There are two reasons why the four output beams moved laterally as the matrix state was changed: 1) angular errors exist in the four input light-beam positions because the Selfoc lenses are canted slightly with respect to those beams, as per Section XI-E, and 2) the optical path lengths within the matrix are different for the different states because light travels in "staircase" fashion in each half-matrix. The number of steps taken in the x- and y-staircases depends upon which state was chosen. Because the resulting path lengths differ, the "walk-off" or excursion of the output beam from its central position will differ.

3. Optical Crosstalk. Crosstalk was measured in each of 24 matrix states, with four measurements per state being made. A particular state was addressed by putting 40 Vrms on eight crosspoint elements (the four $a_{ij} + b_{ji}$ discussed above). Equal strength light was launched into three of the four input fibers; thus, one of the four output fibers was nominally "dark". We recorded the optical crosstalk strength at the dark fiber, and then repeated the measurement for the other three input possibilities in that state. The simultaneous 3-fold optical excitation

gives a rigorous test of the crosstalk properties of the matrix. During this test, it is important to shield the detector from scattered light emanating from the glass "body" of the matrix. We determined the light levels with a UDT model-122 Laser Power Meter, that had a 10^{-3} μW scale.

In 19 out of the 24 states, we found that the crosstalk at 40 Vrms was more than 53 dB below the optical input level. The above determination was limited by the optical source power available (1 mW laser) and by the minimum detectable power. The < -53 dB crosstalk is indeed a low crosstalk level. In the remaining 5 states, the optical crosstalk was somewhat higher due to unwanted electrical crosstalk (discussed below). Here, the optical crosstalk was voltage-dependent and rose above the -53 dB minimum-detection level, starting at 32 Vrms. The 40 V optical crosstalk was observed to range from 53 to 44 dB below the optical input level.

Returning to the < -53 dB crosstalk result, if we use the 15-dB average optical-insertion-loss result, we can express the crosstalk in terms of the signal-to-noise ratios at the output fibers of the matrix. Thus, on average, the output signal-to-crosstalk is more than 38 dB for 19 states, and 29 to 38 dB for the others.

Optical crosstalk is sometimes caused by electrical crosstalk. Electrical crosstalk may be defined as the unwanted electrical coupling between the nominally independent electrode elements. In the matrix, this electrical effect will show up optically because elements nominally OFF would be partially ON. Thus, even if the liquid-crystal effect functions perfectly with zero optical crosstalk, one could, nevertheless, observe optical crosstalk traceable to electrical effects.

Our electrical model for each half-matrix is a 3-dimensional ladder network of RC elements with 17 external leads. Here, electrical crosstalk comes about in two ways: capacitive coupling between elements, and imperfect grounding of nominally OFF elements. The capacitive effect

is, to a large extent, unavoidable because the dielectric liquid crystal material will fill the spaces between electrodes in a simple, noncompartmentalized construction.

Imperfect grounding arises from the finite sheet resistance of the transparent conductive material (ITO). The ITO films that we deposited had a sheet resistance of approximately 3000 Ohms per square on the top prism. This produced a resistance of 30 to 50 kOhm for the ITO lead-in path to each element. In addition, the sheet resistance of the common electrode (bottom prism) varied form 2000 Ohms per square to 6000 Ohms per square across the surface because the ITO was sputter-deposited at 24^{o} off-normal on the prism hypotenuse. This "distributed ground sheet" led to unwanted voltage appearing on elements that were allegedly grounded at zero potential. We found that the larger the addressing voltage applied to ON elements, the larger the leakage voltage appearing on OFF elements (and the greater the crosstalk), a result consistent with the above electrical model.

To a great extent, the inter-element coupling is a procedural problem, one that would be solvable in future versions of the switch. For example, improved ITO films could be developed with the same high degree of optical transmission, but with lower resistivity, say 200 Ohms per square. The ITO lead-in paths could be coated with gold, or other low-resistance metal film. Also, one could replace the sheet electrode on the bottom prism with a 16-element array, identical to that on the top prism. All three measures would give better electrical isolation of elements. For these reasons, we believe that it is possible to obtain less than -53 dB crosstalk for all elements in all 24 states at 40 Vrms applied.

4. Speed. Electro-optical transient response was measured with the Fig. 22 set-up by gating the 1200 Hz square-wave source for the control box on and off. (The box was set for a particular matrix state in the in the usual way). For a particular output fiber, the detected output

signal and the gated drive voltage were displayed on a dual-trace oscilloscope. The duration of the ac pulse was 20 ms, repeated at 7 Hz. Representative turn-on and turn-off results for 30 Vrms applied are presented in Fig. 25 where the time scale is 2 ms/cm. Very slight modulation exists on the optical signal "plateau", but basically the response is step-like.

Denoting the applied voltage amplitude by V, the observed rise time followed the theoretical V^{-2} dependence. The rise time was 1.3 ms at V = 20 Vrms and τ_r decreased to 0.3 ms at 40 Vrms. The delay time prior to turn-on was 0.3 ms.

In measuring the fall time, we found one or two smaller peaks following the optical down-ramp, after voltage was removed. This optical decay waveform was fitted with an $\exp(-t/\tau_f)$ envelope function. In that way, we determined that the fall time was ~4 ms, independent of V as per theory. Compared with liquid crystal devices in general, this response is quite fast, much faster for example than the decay of 90°-twisted nematic cells.

The liquid crystal layer thickness δ = 6 μm is relatively small, and since theory predicts a δ^{-2} thickness dependence, one would anticipate a fairly speedy decay here, but the actual 4 ms turn-off of the 4 x 4 matrix is surprising at first. However, an earlier research project [26] uncovered reasons why this decay should be fast. It turns out that small rotations of the nematic director produce large changes in the optical TIR effect. Experimentally, in [26], we did find fall times as short as 4 ms in related optical switches. Also, according to the theory worked out in [26], rapid fall times are to be expected in the present matrix in cases where the optical incidence angle of collimated fiber light exceeds the optical critical angle by more than 5°. For the liquid crystal mixture E7, which is quite similar to the present E9 mixture, we calculated in [26] (Fig. 31) that a decay time of 4 ms would be found for $\theta_{inc} - \theta_c = 12^{\circ}$, which compares to $\theta_{inc} - \theta_c = 66.0^{\circ} - 59.6^{\circ} = 6.4^{\circ}$ in the present experiments.

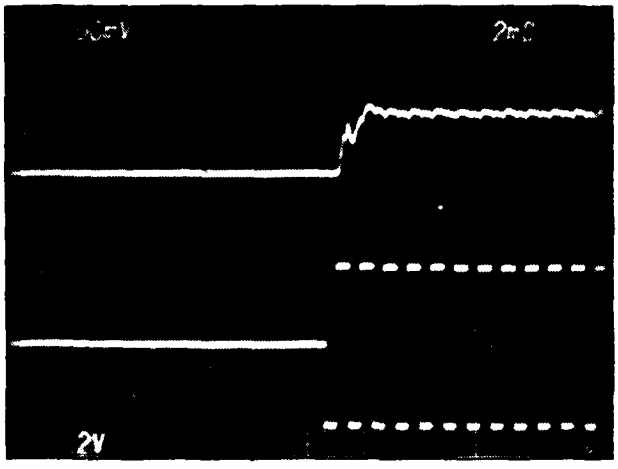

(a) RISE TIME

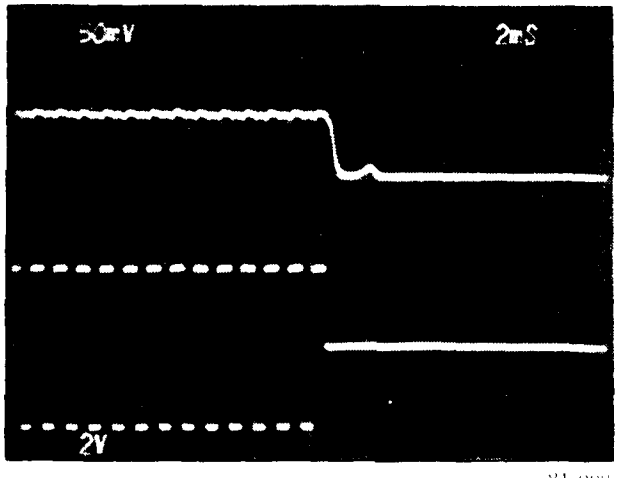

(b) FALL TIME

81-908

FIG. 25 Experimental transient response of final 4 x 4 fiber optic matrix (a) rise time, (b) fall time. Lower trace shows applied voltage waveform; upper trace shows time dependence of switched light.

The overall response time of the present 4 x 4 switch at 40 V is 0.3 ms + 0.3 ms + 4.0 ms, or approximately 5 ms for an on/off cycle.

SECTION XI
DISCUSSION

Tables 1 and 2 summarize the actual construction and performance of our 4 x 4 fiber optical switch. The observed performance of our matrix switch can be judged in three ways: 1) How well does experiment agree with theory? 2) How useful would the performance be in future fiber optic networks? (its "absolute value"), and 3) How does this performance compare with that of competing matrix switches? (the "relative value"). We shall consider these questions in order.

In the first place, we can assert that the overall design was a success. The "multi-bounce" approach to 1 x 4 switching worked well; also, the feasibility and practical value of our dual-switching-array concept were demonstrated. Moreover, the measured performance came close to the theoretical limits in every area except the uniformity of insertion loss from output-to-output and state-to-state. Because fiber light passed through two switching arrays in succession, the optical crosstalk isolation was compounded, and in fact the actual crosstalk levels were extremely low (in most states), as had been expected. So, the usefulness of the 2-stage matrix (and of the liquid crystal TIR effect) have been verified. The only deviations from the expected optical crosstalk performance took place in 5 states because of unexpected electrical cross-coupling between elements.

Secondly, the Table-2 performance does seem useful for fiber optic networks, or capable at least, of meeting future needs. In the repertoire of fiber optic components, switching components are the newest and least-developed, so system designers have not yet created sophisticated, multiple-mode fiber networks that make effective use of the unique capabilities of switches. Thus, we cannot say conclusively that our matrix parameters are those required in an actual 8-terminal optical intercom (or similar fiber system). But, we can project that the matrices will be

TABLE 1

CONSTRUCTIONAL FEATURES OF 4 X 4 FIBER OPTICAL
LIQUID CRYSTAL MATRIX SWITCH

Constructional Feature	Specification
Overall size	2.8 cm x 2.8 cm x 12.0 cm
Liquid crystal layers	Two (mixture E9, EM Industries)
Glass prisms	Four (Scott Optical, type SF14)
Half-wave plate	One 2.3 cm x 2.3 cm x 0.08 cm plastic sheet (Polaroid 280 nm ret.)
Nominal LC layer thickness	6.3 μm (from 1/4-mil teflon tape)
Order of LC layer at V=0	Parallel to walls, parallel to incidence plane
GRINrod lenses	Eight, Selfoc SLS, 2 mm-D, 0.25 pitch at 633 nm
Fiber-optic guides	Eight 1-m strands, Corguide 1515, all-silica, graded index, 5 dB/km
Fiber parameters	50 μm-D core, 125 μm OD, 0.21 NA
No. of electrodes	32, in two sets of 16
No. of addressed electrodes	8 at-a-time
Electrode material	1000Å of indium tin oxide
Optical cement	Devcon 30 minute transparent epoxy
Materials cost (one matrix)	$592 for 4 prisms, 2 LCs, 1 HWP, and 8 lenses

TABLE 2

SUMMARY OF PERFORMANCE OF 4 X 4 FIBER OPTICAL
LIQUID CRYSTAL MATRIX SWITCH

Parameter	Result
Number of "optical conversations"	Four at-a-time
Number of four-fold states	24
Information bandwidth	300 MHz, estimated
Test wavelength	633 nm
Wavelength range of operation	450 to 2500 nm, estimated
Temperature range of operation	+7°C to +84°C, estimated
Switching speed	4.6 ms on/off 0.6 ms rise + delay, 4 ms fall
Circuit parameters	12 megOhm resistance per element 140 pF capacitance per element
Control power	6 μW per element, estimated
Control voltage	40 Vrms at 1 kHz
Optical insertion loss	6 dB min, 15 dB mean, 24 dB max
Optical crosstalk at 40 V	< -53 dB for 19 states, -53 to -44 dB for 5 states
Repeatability	"excellent" (not measured)
Lifetime of operation	several years (not measured)

valuable. To make precise projections, some aspects of multimode networks, such as fiber core sizes, would have to become standardized. In this respect, some system designers distinguish between "telecom" and "datacom" applications; short-haul and long-haul applications, respectively. The 50 μm-core graded fibers are the fibers of choice in telecom situations, while larger core fibers seem better suited for the datacom applications. Our matrix might have difficulty in serving for 100 to 200 μm-core fiber networks because the design was optimized for 50 μm fibers. (See Parts C and D below).

Thirdly, consider the optical matrix switches that are in competition with the present device. Fairly quickly, we can set aside the electro-optic $LiTaO_3$ device [16] because it has not been realized yet in a size larger than 3 x 3, and because the voltages are high (although the $LiTaO_3$ matrix is inherently very fast). It is a different story with the 4 x 4, 8 x 8, and 10 x 10 electro-mechanical matrices that have been made [5,6 and 7]. These do provide a standard for comparison and do compete with our device. In that comparison, we find that the electro-optic liquid crystal matrix is: 1) faster, 2) comparable in the area of optical cross-talk, 3) simpler in construction, 4) potentially more reliable, 5) potentially lower in cost, 6) less demanding in terms of drive power, although requiring higher voltage, 7) comparable in its wavelength-range of operation, and 8) comparable in repeatibility.

On the other hand, the mechanical device presently has: 1) a lower optical insertion loss, 2) possibly a wider temperature range of operation, 3) a more ready adaptation to 100-200 μm-D fiber core sizes, and 4) a greater ability to accomodate larger numbers of fibers, such as 10 x 10 or 20 x 20. It these four areas, note that some refinement and improvement of the present liquid crystal matrix is possible. Therefore, the four "deficiencies" of the liquid crystal matrix can be partly remedied, and the gap between the mechanical and electro-optic matrices can be narrowed on these four issues as discussed below.

A. Insertion Loss

One would typically demand insertion losses < 2 dB for 2 x 2 switches because many 2 x 2s would be "strung together" in most cases. On the other hand, for medium-scale and large-scale matrices, the insertion loss requirements are not as stringent because here there are typically fewer switches in the fiber network, perhaps only one, so the switching loss might be taken only once in the system. Thus, in many fiber systems, it is acceptable to have an insertion loss of, say 10 dB, for the optical matrix.

We realized a loss of 6 dB for a few outputs in Fig. 24, which is an "existence theorem" for low loss. By aligning the fibers better in the 4 x 4 liquid crystal matrix, we estimate that we would obtain an optical insertion loss of 6 dB for all 96 possible outputs. In other words, the potential performance of the matrix switch is 6 dB insertion loss. Furthermore, the potential crosstalk performance is a signal-to-crosstalk ratio of > 50 dB at any output fiber, in any state (see Section IX-B3 above). These performance features would meet most requirements.

B. Temperature Range

This range can be broadened by formulating new liquid crystal mixtures, a process that is on-going in the liquid crystal chemical industry. Operating ranges are presently 80^{o}C to 100^{o}C. Storage ranges are even larger.

C. Fiber Core Sizes

The consequences of enlarging the fiber core diameter in the N x N switch are analyzed in Appendix A. There, we find that we can expand the core size from 50 μm to 100 μm; however, the matrix size will then be cut in half for equivalent matrix performance. For example, if we obtain a 1 dB Selfoc-Selfoc coupling loss in a 6 x 6 switch coupled to

50 μm core fibers, then we will obtain the same loss factors from a 3 x 3 switch coupled to 100 μm core fibers, although the Selfoc lens diameter will be twice that in the 6 x 6, and the overall length of the 3 x 3 switch will be nearly the same as that of the 6 x 6 switch. The 5 x 5 matrix size appears to be the practical limit for 100 μm core fibers.

D. Expandability to Large N

The expansion of the matrix to large sizes such as 10 x 10 is analyzed in Appendix A, where the results are given in terms of the required Selfoc lens diameter (D) and the associated prism height (d), where d is the thickness of the top prism in each half-matrix.

At D = d = 2.8 mm, we find that a 5 x 5 optical matrix switch having 50 μm core fibers is definitely feasible, with performance virtually identical to that of the 4 x 4 switch (1 dB coupling loss, etc.). At ~3 dB higher levels of loss and crosstalk, a 9 x 9 matrix switch is possible, with the 10 x 10 switch representing the practical limit. As before, the 9 x 9 switch has D = d = 2.8 mm and the matrix length is nearly 20 cm.

E. Improved Alignment

In the fiber arrays of Figs. 14 and 15, the output light beams were parallel (in air) with good accuracy, but each beam was not exactly concentric with the cylinder surface of its rod lens, that is, the beams were not exactly orthogonal to the lens faces. This led to alignment errors when index-matching cement was interposed between the lenses and the matrix switch. Alignment is important because, as stated earlier, it is the key to improved insertion-loss performance in the N x N switch. This Section contains some suggestions for improving the alignment.

One idea is to manipulate the fiber behind the lens until the collimated output beam is coaxial with the lens body. Then the fiber is cemented in place. At this point, the coaxial pigtails could be manipulated

one-at-a-time at the matrix input, then attached to the switch; or one could return to the fiber quartet approach, with the four output beams being more nearly perpendicular to the lens faces. The latter would be done by first mounting four lenses with their faces coplanar, flush against the brass fixture. Then fibers would be manipulated for the above coaxial condition. The output array would be prepared in similar fashion.

SECTION XII

SUMMARY

The goal of this contract is to design and fabricate a high-efficiency multimode fiber optic switch capable of switching light from any of N input fibers to any of M output fibers, with a maximum of 50 V and 0.1 A for full switching action. Over the past 12 months, our efforts have been successful and the contract goal has been met with a 4 x 4 electro-optical fiber optic matrix switch, constructed and tested in our laboratory, the first fiber component of its kind. The matrix switch was based on a new design-concept, the dual-switching-array conceived at Sperry Research Center. The dual-array approach means that each optical signal passes through two stages, each stage being a set of 1 x N switches. The tandem-switching effectively filters out leakage light. Additionally, the dual-array technique is general and applies to acousto-optic and magneto-optic matrices as well as electro-optic devices.

An electro-optic effect in nematic liquid crystals, the total or partial reflection of light at oblique incidence, forms the basis of switching in the present matrix, where there are two 6 μm layers of nematic liquid. The voltage-controlled switch is an 8-port device in which four input fibers and four output fibers (graded index, 50 μm core diameter) are coupled to the matrix by means of quarter-pitch graded-index rod lenses (GRINrods). There is a 4-fold pairing of inputs with outputs in each state of the matrix, and the switch has 24 different states. For selecting the optical flow-paths, there are two sets of 16 independent electrodes, and eight electrodes are voltage-addressed at any instant to choose a state. The matrix is reconfigured by choosing a different set of eight.

We have demonstrated, for the first time, a low-voltage, low-power, multimode, electro-optic N x N matrix. Construction is compact

and simple, using only four glass prisms, two liquid layers, and one half-wave plate. All components are permanently cemented together with optical index-matching adhesive, giving a rugged, free-standing package.

The electro-optic approach to multimode switching is generally regarded as being more challenging to implement than the electro-mechanical approach. At other laboratories (mainly in Japan), researchers have made progress with electro-mechanical matrices consisting of arrays of moving prisms, etc; but to our knowledge, no one has heretofore attempted to make a sophisticated electro-optic switch such as the nonblocking 4 x 4 matrix switch. The most that has been done in previous electro-optic experiments is to implement a 2 x 2 switch.

Extensive measurements of the electrical and optical properties of the 4 x 4 matrix have been made. The observed on/off response time of 5 ms was relatively fast for a liquid crystal device, while the control voltages were in the 30 to 40 Vrms range. Optical crosstalk in 19 states was extremely low, more than 53 dB below the input. Due to some unwanted electrical cross-coupling (which can be eliminated in future versions), the crosstalk was -53 to -44 dB in the other 5 states.

The main problem encountered during this work was that the optical insertion loss of the switch varied from state to state, and from output to output within a state. The cause of the nonuniform loss was found to be mechanical misalignments of the fibers with respect to the switch axes. This is not a fundamental problem, and the alignment can be greatly improved in future models via procedural changes during assembly. The measured insertion loss had a minimum value of 6 dB, a mean value of 15 dB, and a maximum value of 24 dB. The 6 dB result is within 1 dB of the theoretical insertion loss. In the 5 dB theoretical loss, 3 dB is due to the fact that only one polarization-component of the unpolarized fiber light is switched.

SECTION XIII

ACKNOWLEDGEMENT

The author is pleased to acknowledge the valuable technical assistance of Larry E. Sheppard, who performed the photolithographic operations, rf sputter deposition, and fiber preparation.

SECTION XIV

REFERENCES

1. C. Dahne and A.L. Harmer, Electronics Letters, 16, 647 (1980).

2. R. Watanabe and K. Asanti, Electronics Letters, 16, 258 (1980).

3. M. Nunoshita and Y. Nomura, Applied Optics, 19, 2574 (1980).

4. E.G. Rawson and M.D. Bailey, Optical Engineering, 19, 628 (1980).

5. Y. Fujii, J. Minowa, T. Aoyama and K. Doi, Electronics Letters, 15, 427 (1979).

6. J. Minowa, et al, Electronics Letters, 16, 422 (1980).

7. H. Yamamoto et al, Journal of Optical Communications, Vol. 1, No. 2, pp. 74-79 (1980).

8. [1-7] are just a small sample of the numerous articles on electro-mechanical switches.

9. W.B. Spillman, Jr., Applied Optics, 18, 2068 (1979).

10. R.B. Kummer et al, paper presented at the 5th European Conference on Optical Communication, Amsterdam, (Sept. 1979).

11. W.J. Tomlinson et al, Electronics Letters, 15, 192 (1979).

12. R.A. Soref, A.R. Nelson, D.H. McMahon, W.B. Spillman, Jr. and L.E. Sheppard, Applied Phys. Lett., 32, 408 (1978).

13. D.H. McMahon and R.A. Soref, Optics Letters, 3, 136 (1978).

14. S. Iguchi et al, paper presented at the 6th European Conference on Optical Communication, York, England (1980).

15. M. Kondo et al, paper Th-P4 presented at the 1981 Conference on Lasers and Electro-optics, Washington, D.C., (June 1981).

16. R.A. Soref, in "Fiber Optics--Advances in Research and Development", Plenum Press, New York, (1979), pages 415-429.

17. M. Shiraki, N. Tagaki, and T. Obokata, Appl. Phys. Lett., 38, 833 (1981). Fiber coupling was not used here.

REFERENCES (cont.)

18. R.A. Soref, W.B. Spillman, Jr. and M. Kestigian, Proceedings of the National Electronics Conference, Vol. 33, p. 188, Chicago, IL, (Oct. 29, 1979).

19. R.A. Soref, Optics Letters, 4, 155 (1979).

20. R.A. Soref, S.P.I.E. Proceedings, Vol. 176, 124 (1979).

21. R.A. Soref and D.H. McMahon, Optics Letters, 5, 147 (1980).

22. R.A. Soref, FOC'80 Proceedings, pp. 21-25 (Sept. 1980).

23. R.A. Soref, in "Physics of Fiber Optics", Bendow and Mitra, Editors, pp. 432-443, American Ceramic Society, Columbus, Ohio (1981).

24. R.E. Wagner and J. Cheng, Applied Optics, 19, 2921 (1980).

25. R.A. Soref, Optics Letters, 6, 275 (1981).

26. R.A. Soref and M. Kestigian, Final Technical Report on RADC Contract No. F19628-79-C-0086, Sperry Research Center CR-80-25, (April 1980).

APPENDIX A

EXPANSION OF THE N x N MATRIX TO N > 4

APPENDIX A

EXPANSION OF THE N x N MATRIX TO N > 4

How might we expand the switch to larger sizes such as 10 x 10 while preserving low loss? In answering this question quantitatively, we note that the optical insertion loss is related to the fiber core diameter (C) and to the available diameter of the GRINrod lenses (D). The fiber core diameter enters into the relation that describes the degree of collimation of the fiber light produced by the microlens. The input fiber is butt-coupled to a Selfoc microlens and the light emerges from that lens with a beam diameter of approximately 0.5 D and with a beam divergence of $\pm\theta$. If that light enters a glass medium (the matrix switch) whose refractive index is n_g, then at a distance X from the lens, the beam diameter will be $0.5\ D + 2X\theta/n_g$. From a computer-aided ray tracing analysis of Selfoc-Selfoc coupling by W.B. Spillman of SRC, we find that the fiber/Selfoc→Selfoc/fiber coupling loss will be about 1 dB when the beam diameter has expanded at the second lens to a size approximately equal to the second-lens diameter. Let S_a denote the lens-lens separation for which the coupling loss is 1.0 dB. Then, we write $0.5\ D + 2S_a H/n_g = \alpha D$. Solving for S_a:

$$S_a = (\alpha-0.5)n_g D/2\theta \qquad (1)$$

with $\alpha \simeq 1.0$ at 1.0 dB coupling loss. Thus,

$$S_a(1\text{-dB}) = n_g D/4\theta. \qquad (2)$$

Now, from Selfoc lens theory, we note that the focal length of the quarter-pitch lens is $1/n_o\sqrt{A}$, and the output beam divergence is:

$$\theta = C/2f = Cn_o\sqrt{A}/2 \tag{3}$$

where C is the fiber core diameter, n_o is the index of the rod lens, and $\sqrt{A}$ is the radial index-profile parameter of the graded lens. Substituting (3) into (2), we find the 1 dB loss spacing is:

$$S_a(1\text{-dB}) = n_g D/2Cn_o\sqrt{A} \ . \tag{4}$$

Small cores allow large spacings.

Assuming that the mechanical alignment of the 2N fibers has been properly attended to, the fiber-to-fiber coupling loss becomes the dominant factor in the insertion loss when we consider expanding the N x N matrix to large N. This happens because the matrix becomes larger physically, and because the coupling loss goes up sharply with increasing lens-lens separation. Hence, there is a trade-off between insertion-loss and N. Recall from QSR-1 that we found the longest optical path (S_b) in the matrix is given by:

$$S_b = 2d(2N-1)/\cos\theta_p \tag{5}$$

where d is the height of the top prisms, θ_p is the prism angle, and N the matrix size. Our calculation here will assume that the coupling loss is held to a small value irrespective of which N is chosen. This implies that the maximum path length will always be smaller than (or equal to) the 1 dB loss separation, namely, $S_b \leq S_a$.

If we take the limiting case of 1 dB loss, then we have $S_b = S_a$,

that is, $0.5n_g D/Cn_o\sqrt{A} = 2d(2N-1)/\cos\theta_p$. Solving for the required lens diameter:

$$D(1-dB) = 4Cn_o\sqrt{A}\, d(2N-1)/n_g \cos\theta_p \qquad (6)$$

Returning to the analysis of QSR-1 (Appendix B, page 22) we find that the overall length of the N x N matrix is:

$$L = 2d\left|(2N-1)\sin^2\theta_p/\cos\theta_p + \cos\theta_p\right| \qquad (7)$$

which neglects the 12 mm overhang of the bottom prism (the overlap can be made in the orthogonal direction instead). Now, we shall compute the required lens diameter and the resulting matrix length using (6) and (7). A constraint of (6) is that the prism height d shall always be greater than the lens diameter, namely $D < d$. If this were not true, the optical beam would be "truncated" at the matrix output and would fill less of the capture-lens than it might.

We now use the actual parameters of the SLS lenses:

$\sqrt{A} = 0.229\ \text{mm}^{-1}$

$n_o = 1.558$ at 633 nm

and the actual switch parameters:

$\theta_p = 66^o$

$n_g = 1.740$ at 633 nm

$C = 0.05$ mm (the actual fiber size)

Hence, we find that:

$$D(1\text{-dB, 50 } \mu\text{m core}) = 0.1008\ (2N-1)d \tag{9}$$

$$L = 4.1037(2N-1)d + 0.8134\ d \tag{10}$$

For N = 5 or less, we find that D < d as desired, and for the 5 x 5 matrix:

$$D(1\text{-dB, 50 } \mu\text{m core, 5 x 5}) = 2.54 \text{ mm at } d \approx 2.80 \text{ mm.}$$

(We actually used d = 2.80 mm in our 4 x 4 matrix).

$$L(5 \times 5) = 105.7 \text{ mm at } d = 2.8 \text{ mm.}$$

Unfortunately, from (9), our D < d assumption is violated when N = 6 or greater (for any d); thus the 5 x 5 matrix is the largest we can build at 1 dB coupling loss. However, if we allow the coupling loss to increase to say 2 dB, then $\alpha \approx 2$ in (1) and now:

$$D(2\text{-dB, 50 } \mu\text{m core}) = 0.07128\ (2N-1)d.$$

This allows a 7 x 7 matrix with:

$$D(2\text{-dB, 50 } \mu\text{m core, 7 x 7}) = 2.59 \text{ mm at } d = 2.80 \text{ mm}$$

$$L(7 \times 7) = 151.7 \text{ mm.}$$

The problem here is that the switched optical beam has broadened out internally in the matrix; so, by the time the beam reaches the output surface, it is wider than the output prism height. This gives rise to spurious internal reflections in the matrix, possibly increasing the optical crosstalk. For this reason, one would probably notice a significant increase in optical crosstalk at the 3-dB coupling loss condition, for which $\alpha \approx 3$ in (1). This is probably a limiting case. Here,

$$D(3\text{-dB, } 50\ \mu\text{m core}) = 0.0582\ (2N-1)d.$$

This leads to the 9 x 9 matrix as being the largest:

$$D(3\text{-dB, } 50\ \mu\text{m core, } 9 \times 9) = 2.77\ \text{mm at } d = 2.80\ \text{mm},$$

$$L(9 \times 9) = 197.6\ \text{mm at } d = 2.80\ \text{mm}.$$

We have just shown how expansion to 9 x 9 increases the insertion loss. One way to save ~3 dB of insertion loss in large matrices is to insert half-pitch transfer lenses (GRINrods) for a unitary transformation at the midplane of the switch [6]. The 0.5-p rods capture and retransmit each beam. Thereby, one could nearly double the size of the matrix while keeping loss constant. In our matrix, these lenses would be situated adjacent to the half-wave plate. However, this procedure would be costly because of the need for N^2 added lenses.

APPENDIX B
QUARTERLY REPORT NO. 1

DESIGN AND FABRICATION OF MULTIMODE OPTICAL SWITCHES

Quarterly Status Report No. 1
For the Period 5 June – 30 September 1980
Contract No. F19628-80-C-0147

R. A. Soref

Sperry Research Center
100 North Road
Sudbury, Massachusetts 01776

SRC-CR-80-58
October 1980

Contract Monitor: Mr. R. A. Bradbury (RADC/ESO)

This report is intended only for the internal management use of the contractor and the Air Force.

Prepared for

ROME AIR DEVELOPMENT CENTER
DEPUTY FOR ELECTRONIC TECHNOLOGY
HANSCOM AIR FORCE BASE
BEDFORD, MASSACHUSETTS 01731

SPERRY RESEARCH CENTER

DESIGN AND FABRICATION OF MULTIMODE OPTICAL SWITCHES

I. INTRODUCTION

The goal of this contract is to make a multimode N x M optical switch with high performance in a fiber-optic communication system. To paraphase the work statement: The contractor will conduct a research program necessary for the design and fabrication of a high-efficiency multimode fiber-optic switch capable of switching light from any of N input fibers to any of M output fibers. Consideration should be given to techniques such as liquid crystals. Measurements will be made of insertion loss, crosstalk, switching speed, V/I characteristics, etc., to see to what extent the design goal was achieved. The work will consist of a study-design phase on techniques that will most adequately fill the requirement. Design goal should be for a maximum of 50V and 0.1A for full switching action. After the necessary techniques have been developed and the prototype switches fabricated, the measurements mentioned above shall be made.

Liquid crystal switching has been selected because this technique offers the highest probability of success in meeting the goals of low loss, low crosstalk, and low voltage control. Additionally, these switches do not have any moving parts, and this non-mechanical approach should offer the high reliability that is desired in military applications.

We propose to build the N x M switch with two layers of nematic liquid crystal in a unique "dual array" construction. Most of the effort during the first Quarter was spent designing the switch, specifically the 4 x 4 fiber-optical switchboard discussed in the Proposal. This Status Report, which covers the period from June 5, 1980 to September 5, 1980, discusses the following topics: proposed approach, choice of optical coupling lenses, choice of liquid and glass materials, size and shape of required prisms, and layout of the transparent electrodes.

II. DUAL ARRAY APPROACH

We conceived of a new way of making an N x M switch that we call the "dual array" approach. This was discussed in detail in our Proposal of February 27, 1980, and will be summarized briefly here.

In some respects, this idea harks back to our work on the compound optical switch (Applied Optics, Vol. 14, 2559, (1975) and Vol. 16, 3223, (1977)). wherein two elemental switches were joined at each intersection of an optical matrix switch in order to reduce optical crosstalk significantly.

Here, the N x M is made up of two sub-switches or "half-switches" and, as before, the crosstalk in the N x M is much lower than crosstalk in each half-switch (approximately twice the isolation in dB). The dual array concept is illustrated symbolically in Fig. 1 where the input/output beams are shown for each of the two switching arrays. The first half-switch is a 1 x M switch that is "repeated" N times side-by-side; namely, an inline group of N inputs that leads to an N x M rectangular array of possible output-beam positions. Similarly, the second half-switch is an M-fold-repeated N x 1 switch in which selected beams from the M x N array of possible inputs can be sent to the inline group of M outputs. To complete the N-input M-output switchboard, the rows of the first MN array are one-to-one mapped (optically connected) to the columns of the second NM array. This can be done simply by rotating the second half-switch 90-degrees with respect to the first half-switch. (In an N x N, the half-switches are identical). This dual array concept is general and applies to mechano-optical and acousto-optical switches as well as the electro-optical switches investigated here.

Figure 2 illustrates the structure of a 4 x 3 opto-switch based on two active layers of liquid crystal (LC). Each ordered uniaxial "film" of LC is about 5 microns thick and is held between plane-parallel glass surfaces. Figure 3 shows how an LC layer is divided into NM independently controlled regions by means of NM separate (transparent) conductors on one

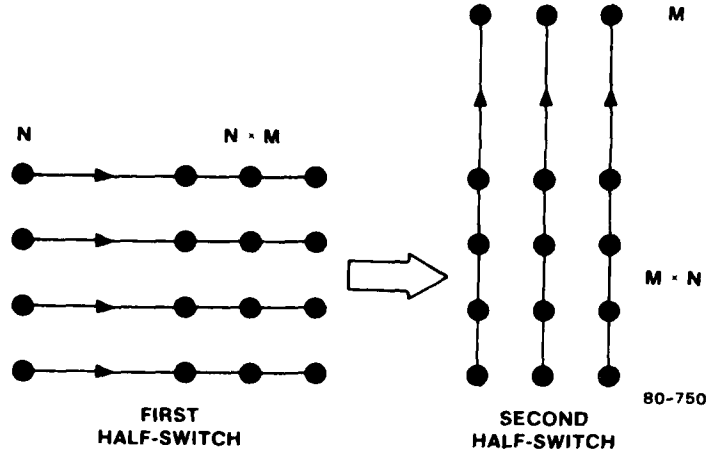

FIG. 1 Dual-array technique for making an N x M optical switch. Half-switches are combined as large arrow indicates.

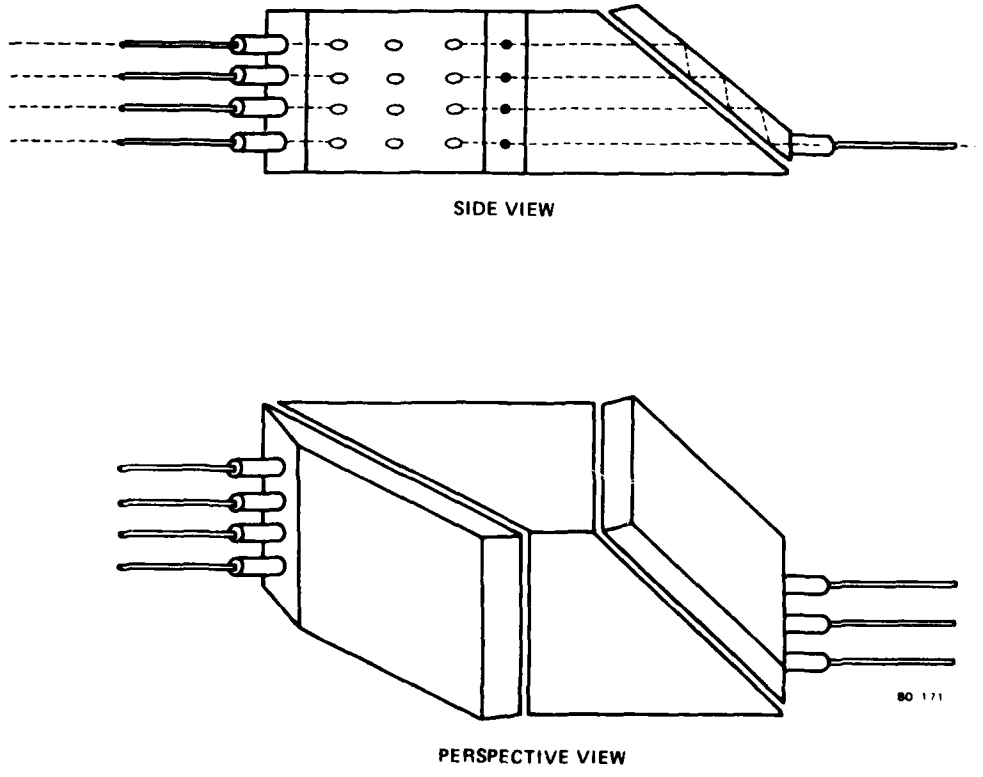

FIG. 2 Configuration of 4 x 3 fiber optical matrix switch (dual array approach).

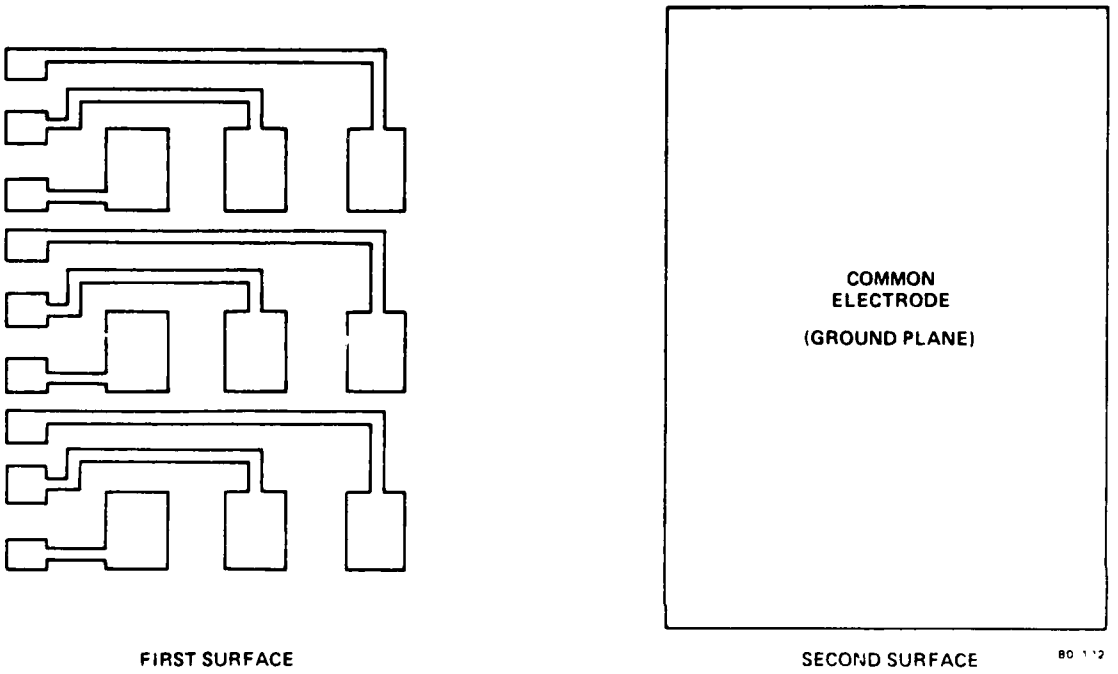

FIG. 3 Plan view of transparent conductors on parallel glass surfaces used to control LC crosspoints in N x M array.

glass surface that face a sheet electrode on the other. The manner in which the electronic control circuit is attached is shown in Fig. 4. A half-wave retardation plate is usually inserted at the mid-plane of the N x M switch as indicated in the beam cross-section diagram of Fig. 5. Further details of the 4 x 3 switch structure are provided in Figs. 6 and 7, a drawing that includes optical ray paths indicated by dashed lines, plus details about LC orientations and optical polarizations. There are four glass prisms in the Fig. 7 switch, two of which (the lens-coupled prisms) have plane-parallel sides as indicated. These prisms are like slab waveguides because of the total internal reflection that occurs both at the glass/air interface and at the LC layer; in other words, light makes regular, multiple bounces within the slab. The multi-bounce arrangement is convenient for obtaining the equi-spaced array of output beam positions that is needed in the half-switch as per Fig. 1. The foregoing description is rather sketchy and we shall provide a complete description of how the N x M structure operates in the Final Report. The 4 x 3 switch discussed above has unsymmetrical half-switches, but a 4 x 4 switch has identical halves and will perform all the functions of the 4 x 3. For this reason, and because of its inherent simplicity, we shall construct a 4 x 4 rather than a 4 x 3.

III. CHOICE OF SELFOC LENSES

One of the first questions to be addressed in designing the 4 x 4 is how to keep the optical insertion loss to a minimum. This, in turn, depends strongly on the microlens coupling. Figure 8 shows schematically the Selfoc Lens coupling in the N x N fiber switch. There are N pairs of input/output Selfoc Lenses, one pair of which is shown. In Fig. 8, the lenses are separated by a distance S that represents the longest optical path in the switch (the worst case). A high-index glass medium ($n = 1.74$) is interposed between the lenses (representing the glass prisms mentioned above).

In designing the switch, we have at our disposal the lens diameter D, the lens profile A (the radial index-distribution factor), and the lens index N_o. What should these parameters be in order to minimize insertion

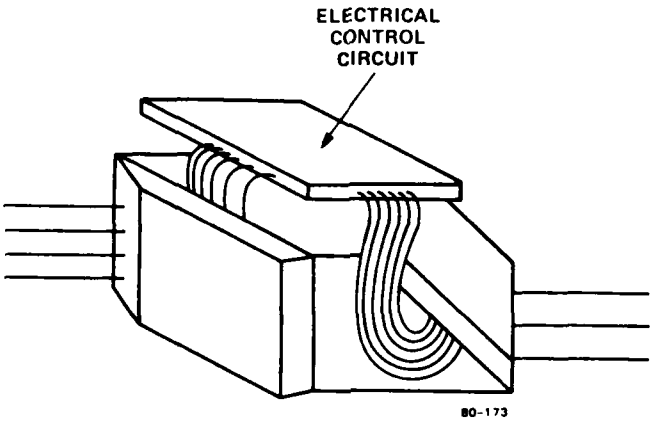

FIG. 4 Configuration of electronic drive for 4 x 3 opto-switch.

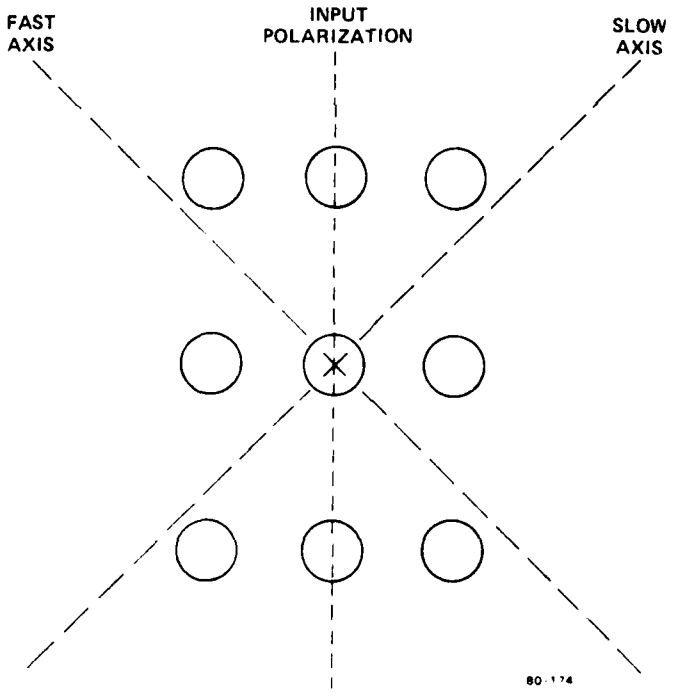

FIG. 5 Position of $\lambda/2$ retardation plate axes relative to optical polarization in N x N opto-beam array for 90° polarization rotation.

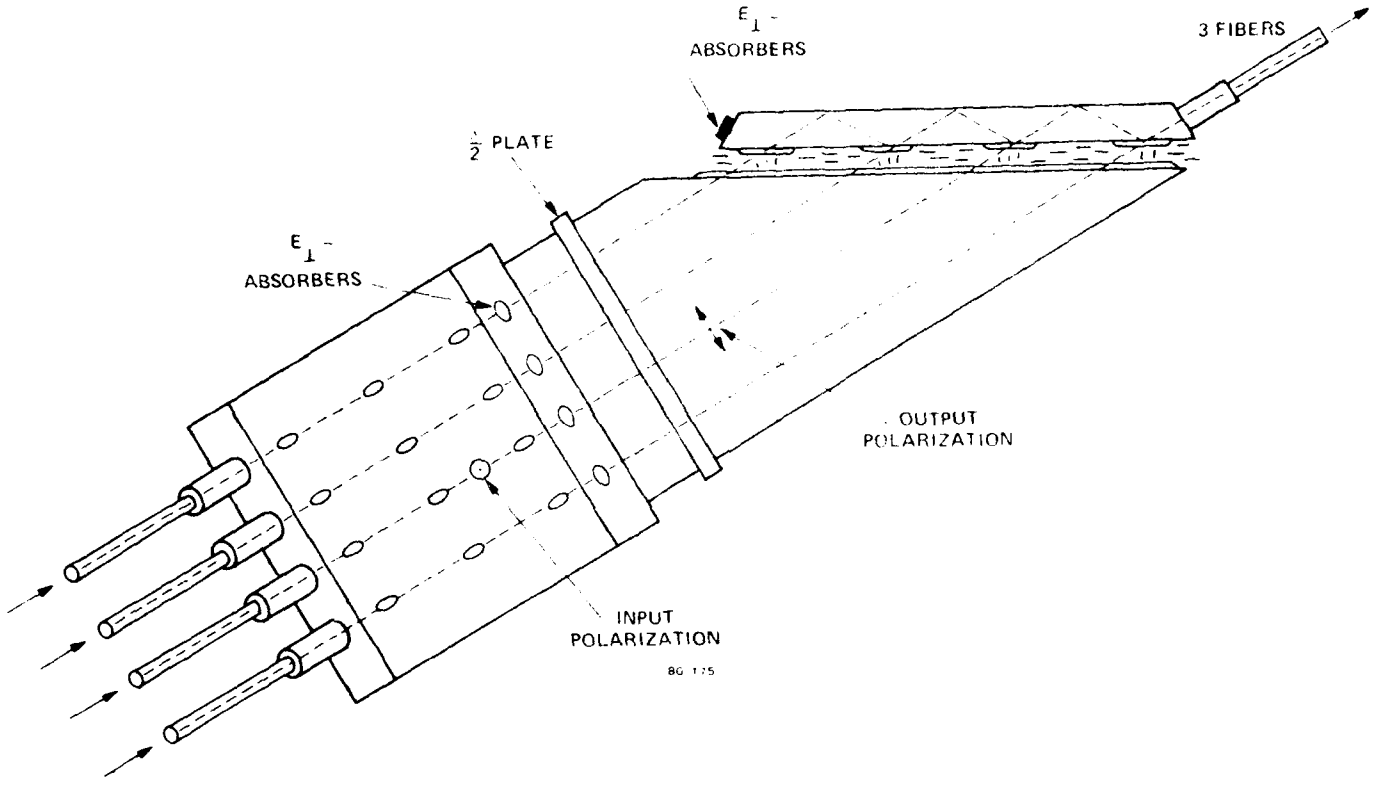

FIG. 6 Configuration of 4 x 3 fiber optical matrix switch with half wave plate.

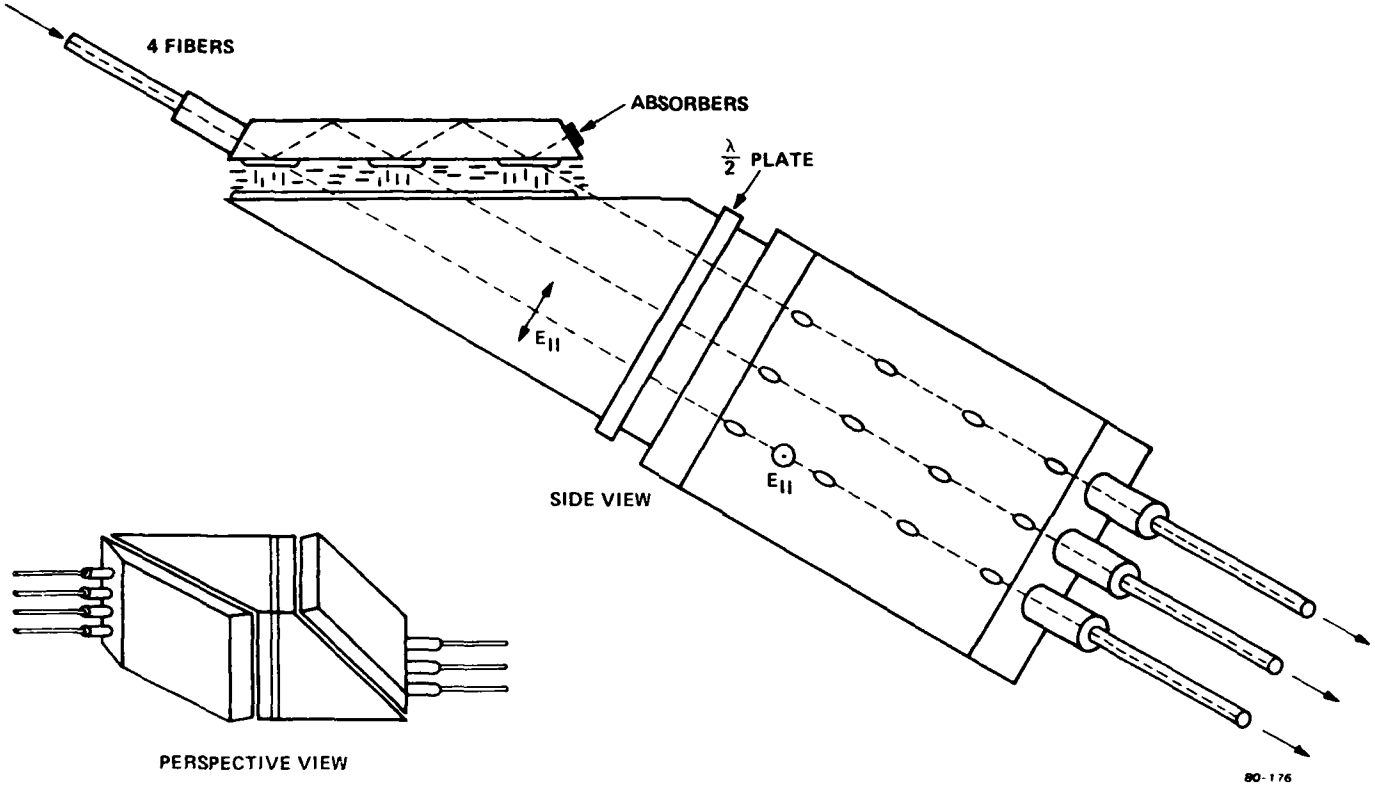

FIG. 7 Additional view of Fig. 6 structure.

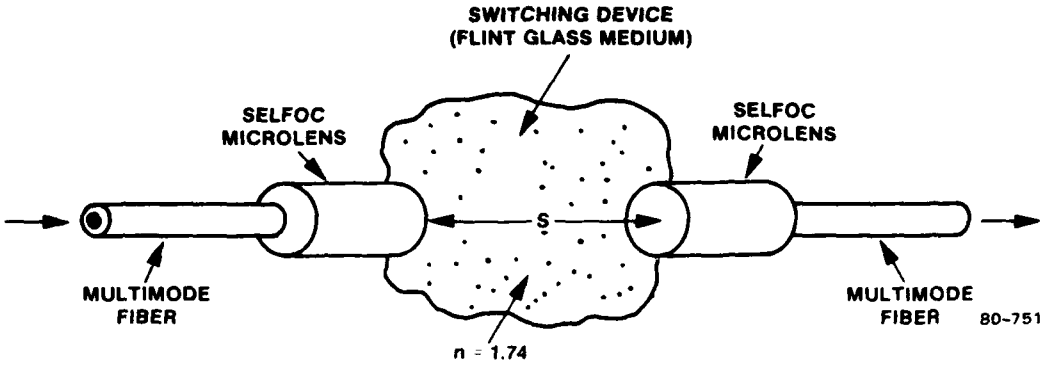

FIG. 8 Microlens coupling of fibers in N x N switch.

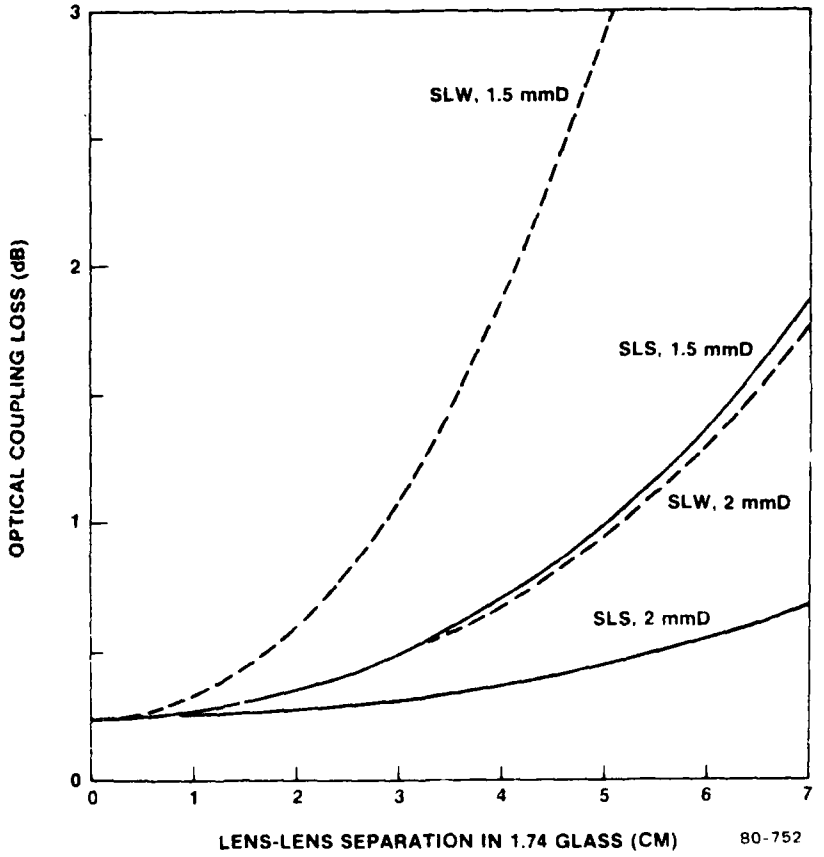

FIG. 9 Calculated coupling loss versus lens-to-lens separation (glass medium) as per Fig. 8.

AD-A113 812 SPERRY RESEARCH CENTER SUDBURY MA F/G 20/6
DESIGN AND FABRICATION OF MULTIMODE OPTICAL SWITCHES.(U)
MAR 82 R A SOREF F19628-80-C-0147
UNCLASSIFIED SRC-CR-81-54 RADC-TR-82-22 NL

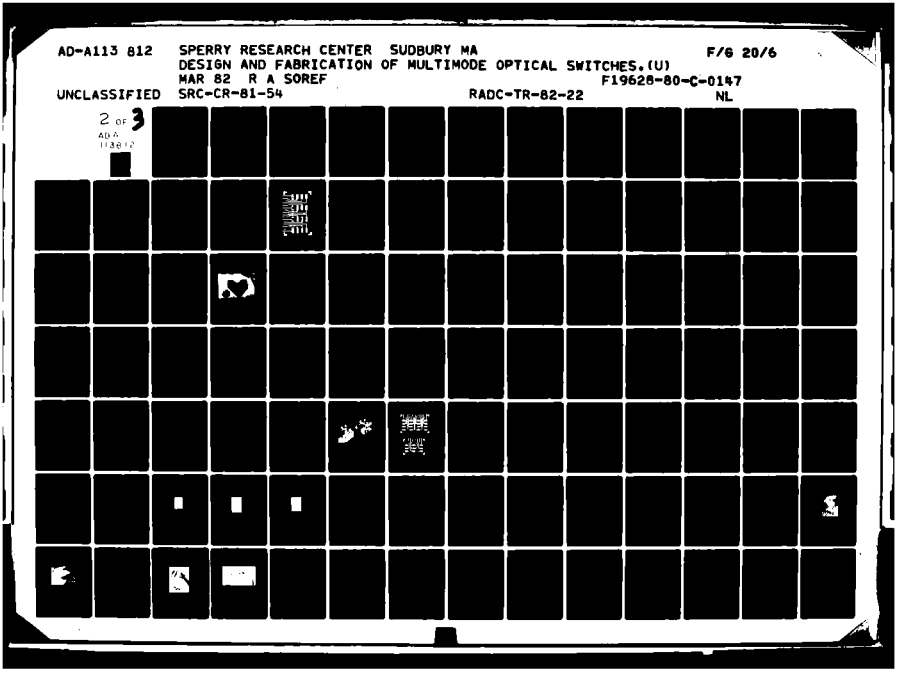

loss in the N x N? We can answer this question by computing the lens-to-lens optical coupling loss (which is the dominant contribution to insertion loss) as a function of S for several choices of lens parameters.

We calculated this loss with the aid of a ray-tracing computer program (441 rays) designed by W. B. Spillman of SRC and described in his recent Research Paper (SRC-RP-80-36, August 1980). In the program, we used values of A and N_o for actual lenses, values obtained from a data sheet supplied by Nippon Sheet Glass Company, the Selfoc manufacturer. Fiber-to-fiber coupling for the following four lenses was investigated:

Selfoc SLW, D=1.5 mm, $\sqrt{A}$ = 0.392 mm^{-1}, N_o=1.610
Selfoc SLW, D=2.0 mm, $\sqrt{A}$ = 0.292 mm^{-1}, N_o=1.610
Selfoc SLS, D=1.5 mm, $\sqrt{A}$ = 0.306 mm^{-1}, N_o=1.558
Selfoc SLS, D=2.0 mm, $\sqrt{A}$ = 0.229 mm^{-1}, N_o=1.558

It was assumed that the fiber was graded-index communications fiber with a 50 μm core diameter and a nominal/launch NA of 0.20. (This would correspond to an all-silica fiber made by Corning, for example). Further, an optical wavelength of 633 nm and a lens length of 0.25 pitch were assumed (both lenses).

Figure 9 shows the results of the loss calculation for lens separations from zero to 7 cm. From Fig. 9, we quickly conclude that the wide-angle Selfoc (SLW) gives lossier coupling than the standard version (SLS); so the SLS profile is immediately chosen.

We now examine Fig. 9 to find the effect of altering the lens diameter. If we assume that a particular loss, say 0.6 dB, is the most that can be tolerated in the switch, and if we note the lens separtion S_1 at which this loss occurs (lens diameter D_1), we find that those critical separations S_1, S_2, etc, do not scale linearly with the diameters, D_1, D_2; in fact, $S_1/S_2 = (D_1/D_2)^2$. Therefore, we conclude that the larger-diameter lens is

Apertures for keeping losses low. Specifically, we have selected the 2-mm diameter SLS lens as the preferred lens for our N x N switches.

IV. CHOICE OF GLASS AND LIQUID CRYSTAL

A number of nematic LC mixtures sold by EM Industries of Elmsford, New York have become popular in the past few years and have proven their usefulness in commercial applications. We have singled out 13 of these as prime candidates for inclusion in the N x N switch. Tables 1A and 1B list the optical, thermal, dielectric, and viscous properties of these liquids. All of them are essentially uneffected by UV, humidity, and other environmental factors.

A variety of high-index glass materials (from several manufacturers) are also suitable for switching. In particular, materials from Schott Optical Glass Company are of high quality, are well documented, and are readily available. For these reasons, we have selected nine Schott materials as candidates for N x N switch construction. These are flint glasses and their optical properties are tabulated in Table 2. Some of the more exotic flint glasses such as barium short flint or lanthanum flint, etc, have been ruled out here because they are relatively "unstable" materials. Even the SF and F glasses will exhibit some staining on their surfaces if not properly handled, although the manufacturer states that they are relatively impervious to acids, etc., and are free from bubbles.

The ordered LC is like a uniaxial mineral with ordinary and extraordinary refractive indices, n_o and n_e, while the isotropic glass has only one index n_g. As discussed below, we often require a specific relationship between the glass and LC indices. If the index ratio is optimized at a particular wavelength, say 589 nm, that optimization will hold at a nearby wavelength, say 832 nm, because the dispersion of glass and LC is similar. All of the indices n_o, n_e, n_g, decrease with increasing wavelength, with about the same functional dependence.

TABLE 1A. Properties of nematic LC mixtures. All are stable and are available from EM Industries. Properties measured at λ = 589 nm and T = 20° C.

Liquid Crystal Type	n_o	n_e	Δn	$\Delta \varepsilon$	Nematic Temp. Range (°C)	Viscosity (cP)
Merck ZLI - 1132	1.493	1.632	+0.139	+10.3	-6 to +70	27
Merck ZLI - 1221	1.494	1.627	+0.133	+ 8.0	-11 to +90	40
Merck ZLI - 1370	1.497	1.637	+0.140	+11.4	-10 to +60	26
Merck ZLI - 1565	1.499	1.630	+0.131	+ 6.0	-20 to +85	19
Merck ZLI - 1557	1.500	1.620	+0.120	+ 4.2	-1 to +61	14
Merck ZLI - 1294	1.503	1.663	+0.160	+10.7	-22 to +66	33
Merck ZLI - 1285	1.508	1.688	+0.180	+13.8	-3 to +68	36
Merck ZLI - 1252	1.516	1.686	+0.170	+14.6	0 to +60	40
Merck ZLI - 1269	1.518	1.707	+0.189	+13.2	-6 to +64	32

TABLE 1B. Properties of nematic LC mixtures. All are stable and are available from EM Industries. Properties measured at λ = 589 nm at T = 20°C. Est = estimated

Liquid Crystal Type	n_o	n_e	Δn	$\Delta\epsilon$	Nematic Temp. Range (°C)	Viscosity (cP)
BDH - E7	1.522	1.747	+0.225	+13.8	-10 to +61	40
BDH - E8	1.52_{est}	1.767	+0.247	$+13_{est}$	-12 to +72	54
BDH - E9	1.52_{est}	1.775	+0.255	$+13_{est}$	+7 to +84	96
BDH - E60	1.52_{est}	1.665	+0.145	$+10_{est}$	-13 to +63	44

TABLE 2. Optical refractive index at λ = 589 nm of glass manufactured by Schott Optical Glass of Duryea, PA. (T = 20°C.)

Glass Type	Refractive Index n_g
F2	1.6200
F1	1.6259
SF2	1.6477
SF12	1.6483
SF9	1.6545
SF5	1.6727
SF13	1.7407
WG345	1.7410
SF14	1.7618

We now examine how the optical crosstalk in the N x N is influenced by the choice of n_o, n_e, and n_g. Recall that our switching device uses oblique incidence on a glass/LC interface with $\Theta > \Theta_c$ at V = 0 for one or both optical polarizations, where Θ is the optical incidence angle and Θ_c is the critical angle for total internal reflection, defined as: $\Theta_c = \arcsin(n_o/n_g)$. As discussed in Ref. 1, in order to achieve the desired switching action, we must choose the glass and LC materials according to the criteria

$$n_g > n_o$$

$$n_g \simeq n_e$$

The incoming light beam is decomposed into s- and p-polarization components and the LC presents effective refractive indices n(s,V) and n(p,V) to those polarizations that depend upon how much voltage (V) is applied to the LC. As the applied voltage is raised well above threshold, say 30 Vrms, one of these indices, say n(p,V) approaches ne. A typical case is:

$$\left.\begin{aligned} n(s) &= n_o \\ n(p) &= n_o \end{aligned}\right\} \text{ at } V = 0 \qquad \left.\begin{aligned} n(s) &= n_o \\ n(p) &\to n_e \end{aligned}\right\} \text{ as } V \to 30 \text{ Vrms}$$

Here, the p-polarization becomes transmitted through the glass/LC interface, rather than being totally reflected. In order to have ideal performance--total transmission without any reflection--it is necessary to satisfy the equality: $n(p,30) = n_g$. If there is a finite index difference $n_p - n_g$, there will be an unwanted reflection (optical crosstalk) which is a few percent of the input level. Since $n_p \to n_e$, we will get fairly low crosstalk if we impose the ON-state requirement

$$n_g = n_e$$

on the glass and liquid. We make an initial selection of glass-LC pairs by identifying those pairs for which the index difference is small, for example,

$|n_e - n_g| < 0.02$. The $|n_e - n_g| < 0.02$ procedure leads to the combinations of materials listed in Tables 3A and 3B.

In actual experiments, the index n_p does not reach n_e and remains slightly smaller than n_e. This happens because the light propagation is not exactly orthogonal to the LC optic axis in the voltage-ON condition. (That would require $\theta = 90°$ grazing incidence because the molecules orient perpendicular to the electrodes). Consequently, a more accurate picture of the ON-state is: $n_p = n_e - 0.01$. This means that a more practical requirement for a low crosstalk switch is that the glass and LC satisfy

$$n_g = n_e - 0.01.$$

For that reason, we shall now refer to Tables 3A and 3B and pick out those glass/LC pairs for which $n_e - n_g$ is most nearly +0.01. The optimum materials combinations chosen in this way are tabulated in Table 4 together with the optical critical angle for each pair. An actual switching device uses one of the pairs in Table 4.

V. CHOICE OF PRISM ANGLE

As Figs. 6 and 7 suggest, the 4 x 4 is comprised of two of the half-switches shown in Fig. 10. Here, the angled faces of the top prism (prism "A") are cut and polished at an angle θ_p with respect to the LC plane, an angle that is the same as the incidence angle. By hypothesis, we use $\theta > \theta_c$ for total internal reflection at V = 0, hence $\theta_p > \theta_c$. But, how much larger than θ_c should the prism angle be? Clearly, as $\theta_p \to 90°$, the prisms become very long and the optical paths within the switch become long. So, as a practical matter, θ_p is only a "few degrees" larger than θ_c. The specific choice of θ_p is arrived at from a tradeoff or compromise between conflicting factors: a small θ_p reduces optical path lengths and minimizes insertion loss, but $\theta_p >> \theta_c$ accomodates larger angular spreads in the quasi-collimated light beams and $\theta_p >> \theta_c$ also leads to faster switching speeds (See Ref. 1). The insertion loss consideration is probably the most important.

TABLE 3A. Glass/LC Combinations selected according to the criterion $|n_e - n_g| < 0.02$. Critical angle = $\sin^{-1}(n_o/n_g)$.

Glass	Liquid Crystal	$n_e - n_g$	Critical Angle (degrees)
SF14	E8	-0.0052	59.6
	E9	+0.0132	59.6
WG345	E7	+0.0060	60.9
	E8	+0.0260	60.9
SF13	E7	+0.0063	61.0
	E8	+0.0263	61.0

TABLE 3B. Glass/LC combinations selected according to the criterion $|n_e - n_g| < 0.02$. Critical angle = $\sin^{-1}(n_o/n_g)$.

Glass	Liquid Crystal	$n_e - n_g$	Critical Angle (degrees)
SF5	ZLI - 1252	+0.0133	65.0
	ZLI - 1285	+0.0153	64.4
	ZLI - 1294	-0.0097	64.0
	BDH - E60	-0.0077	65.3
SF9	BDH - E60	+0.0105	66.7
	ZLI - 1294	+0.0085	65.3
	ZLI - 1370	-0.0175	64.8
SF2	BDH - E60	+0.0173	67.3
	ZLI - 1294	+0.0153	65.8
	ZLI - 1370	-0.0107	65.3
F1	ZLI - 1132	+0.0061	66.7
	ZLI - 1370	+0.0111	67.0
	ZLI - 1221	-0.0011	66.3
F2	ZLI - 1565	+0.0100	67.7
	ZLI - 1132	+0.0120	67.2
	ZLI - 1557	+0.0000	67.8

TABLE 4. Preferred glass/LC combinations selected according to which combination comes closest to satisfying the criterion $n_e - n_g = +0.01$.

Optimum Combination of Glass and Liquid Crystal	Critical Angle (degrees)	Prism Angle (degrees)
SF14-E9	59.6	65
WG345-E7	60.9	66
SF13-E7	61.0	66
SF5-ZLI1252	65.0	70
SF9-E60	66.7	72
SF2-ZLI1294	65.8	71
F1-ZLI1370	67.0	72
F2-ZLI1565	67.7	73

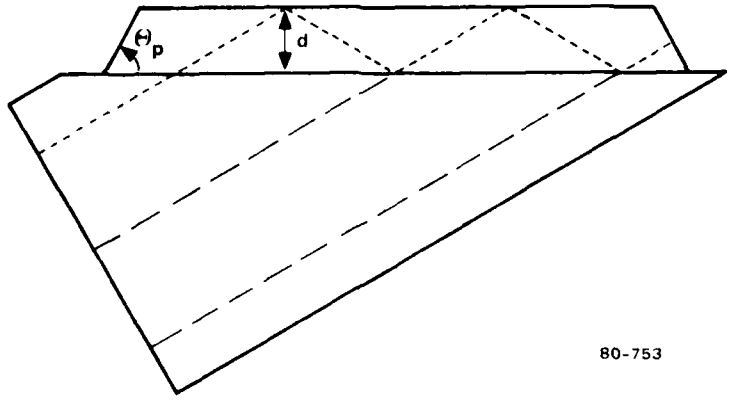

FIG. 10 Dual-prism structure representing one half of N x N opto-switch.

The diagram of Fig. 10 illustrates the longest path in the switch, as shown by the dotted lines. Adding up the segments in this path, we find that the largest path L(max) in an N x N optical matrix is approximately $2d(2N-1)/\cos\theta_p$, where d is the height of prism A as shown. We are concerned about the 4 x 4 and 3 x 3 devices, so we find that

$$L(\text{max, } 4 \times 4) = 14d/\cos\theta_p$$

$$L(\text{max, } 3 \times 3) = 10d/\cos\theta_p$$

This worst-case path length has been plotted as a function of prism angle in Figure 11 for the prism heights d = 2.6, 2.8, and 3.0 mm. According to Fig. 9, long paths are to be strenuously avoided for loss-minimization. Thus, the Fig. 11 graph reveals the importance of choosing a glass-LC combination for which a small prism angle is possible. This means that we strongly favor the first three pairs in Table 4 for which the critical angle is relatively small, and in fact we shall build our first N x N switches from SF14-E9 to obtain low loss.

To complete the story on prism angle, we note that the beam divergence of light from a 125 μm fiber (such as Galite 5020) can be as much as 3° (full cone angle) when collimated by quarter-pitch Selfocs. (This typifys a switching environment that might be encountered in practice). To accommodate such beam-spreads and to allow a 2° "safety margin" for mechanical misalignments, we would choose the prism angle to be 5° larger than the critical angle. Consequently, in a 4 x 4 switch made from the materials SF14-E9 (or SF13-E7), the prism angle would be θ_c + 5° or 60°.

VI. SIZE AND SHAPE OF PRISMS

Figures 12 and 13 show the required prisms (two of A and two of B) and the drawing of Fig. 14 shows how those prisms are put together. Prism B has a uniform sheet electrode on its hypothenuse. Prism A has a

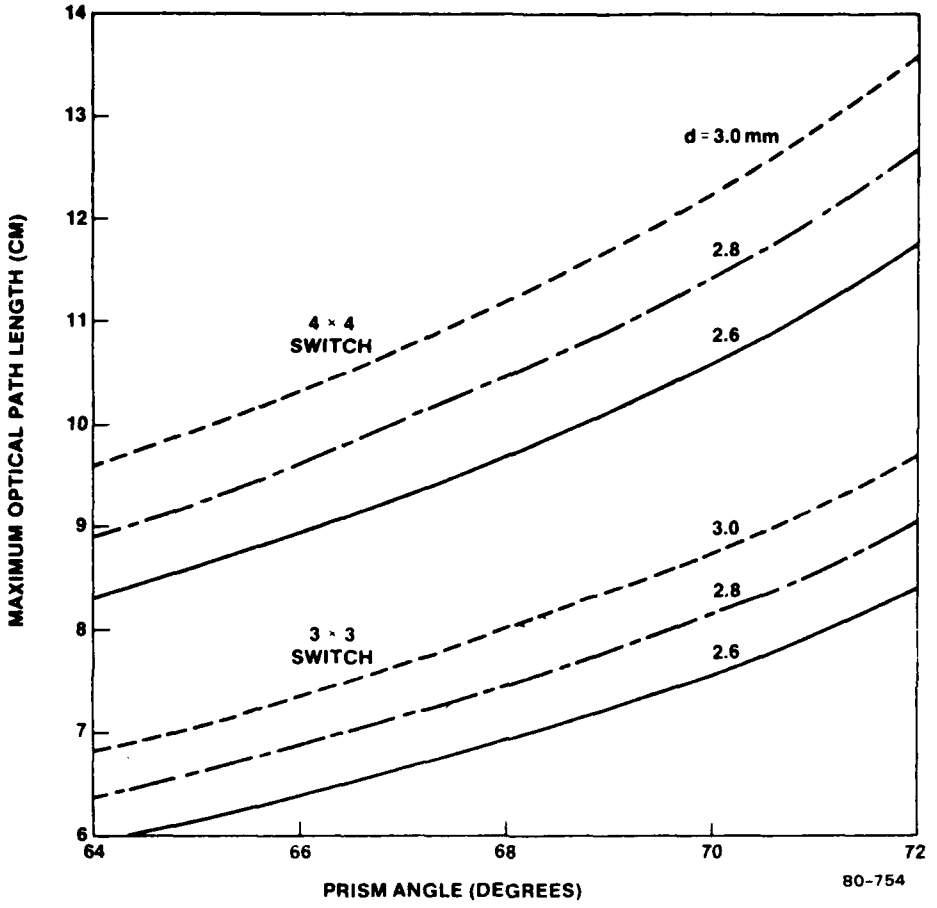

FIG. 11 Optical path length in N x N switch versus prism angle for several prism heights.

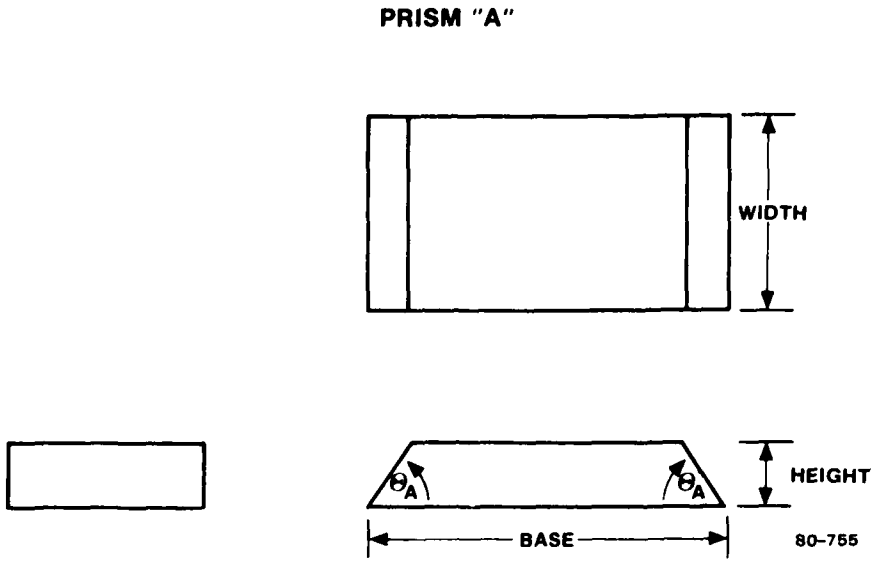

FIG. 12 Outer prism in N x N half-switch to which input (or output) fibers are coupled.

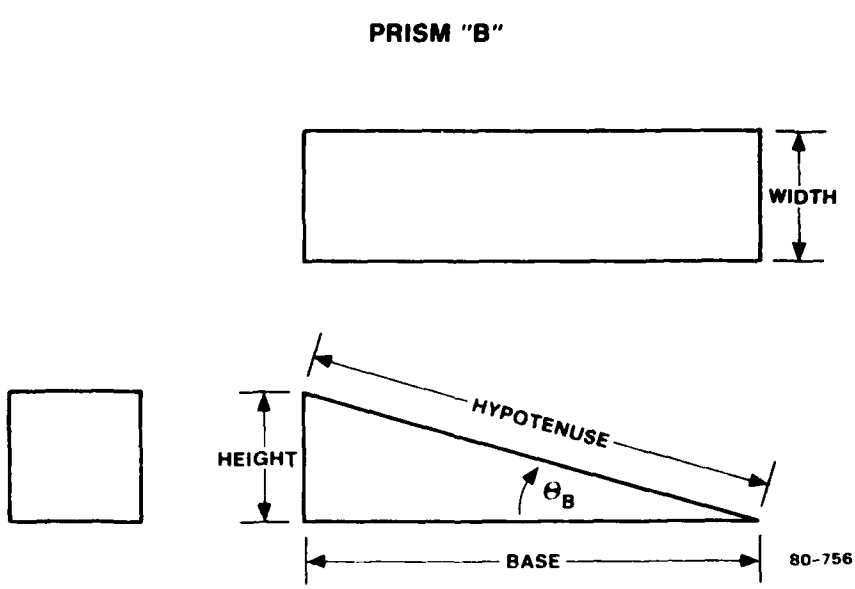

FIG. 13 Inner prism in N x N half-switch.

pattern of N^2 rectangular electrodes on its base surface. Originating from those rectangles, there are N^2 conductive paths that fan out to one side of Prism A where the control circuit is attached. In order to gain access to those N^2 leads, it is necessary to make A wider than B, and to make electrical connections in the overhang region (see Fig. 14). We decided that an overhang of 4.3 mm provided adequate space for lead attachment.

With regard to the prism angles, it is seen by refering to Fig. 10 that θ_A in Fig. 12 is the same as θ_P and that θ_B in Fig. 13 is $90° - \theta_A$. Returning to Fig. 10, we can calculate the physical dimensions of Prisms A and B that are required to contain the various optical beams. Note that the hypotenuse of Prism B is somewhat wider than the base of Prism A. (Fig. 10). Because the width of B equals the height of A, the overlap (hypot of B - base of A) shows up in added width for A. We need room within the width of A for teflon/mylar spacer material (and/or hermetic sealing material) that does not infringe on the conductive rectangles. Therefore, we decided to make the hypotenuse of B 12 mm longer than the base of A to provide a 6 mm border on each side of the electrodes to allow room for teflon/mylar material within A.

The dimensions of A and B are inter-related and in designing the N x N, one goes "back and forth" between A and B. The design sequence is given below. With the aforementioned 4.3 mm and 12.0 mm overlap dimensions, we find the following results in our prism analysis:

1. Height of A = d
2. Base of A = $(2N-1)d \tan \theta_p + d \operatorname{ctn} \theta_p$
3. Hypot of B = Base of A + 12 mm
4. Height of B = Width of B
5. Width of B = (Hypot of B) cos θp
6. Width of A = Width of B + 4.3 mm
7. Base of B = (Hypot of B) sin θp

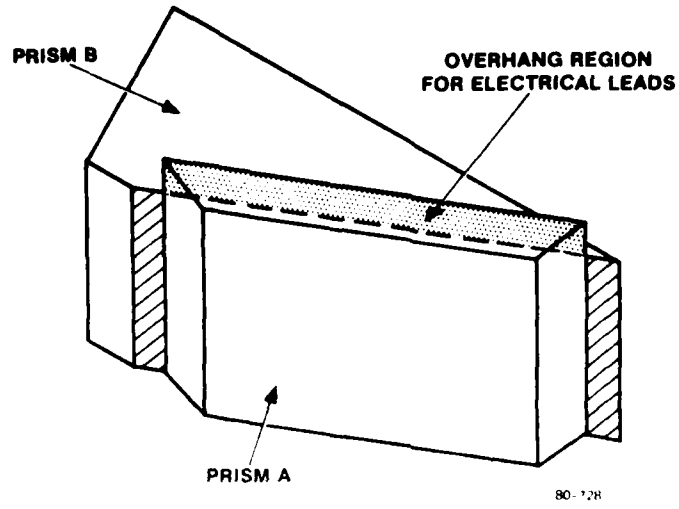

FIG. 14 Assembly of inner and outer prisms in N x N half-switch.

Each 2.0 mm diameter Selfoc lens is cemented to a facet of Prism A whose height is approximately d. We saw in Fig. 11 how sensitive the path length L (max) is to increases in the dimension d. So we want to use small d-values. But, if we make d = 2.6 mm (Fig. 11), there is only 0.3 mm clearance on either side of the lens and we believe that we need more leeway than this in a practical device. Thus, we shall choose the next increment in d shown in Fig. 11, namely, d = 2.8 mm, for our switch.

Now we are able to set forth the specific 4 x 4 switch design by using N = 4, d = 2.8 mm, and $\Theta_p = 66°$ in the above relationships (Θp for SF 14 and SF 13 glass). A 3 x 3 switch design with d = 2.8 and $\Theta_p = 66°$ was also carried out. The results are presented in Table 5. The design has been completed and the prisms have been ordered.

VII. ELECTRODE LAYOUT

The transparent electrodes are made from a thin film of indium tin oxide (ITO) deposited on a prism surface. Via photolithography, the ITO film is etched into the desired shape.

There are N^2 independent electrodes areas, each of which "intersects" a 2-mm-D optical beam. The 66° -incident beam has the form of an ellipse with axes 2.00 mm and 4.12 mm when it falls upon the electrode. To contain this beam, we have made each electrode rectangle 2.6 mm x 5.6 mm in area. Referring to Figs. 6 and 10, we find that the center-to-center spacing of the electrodes is $2d \tan\Theta_p$ in the x-direction and $2d \sin\Theta_p$ in the y-direction. For $\Theta_p = 66°$, these spacings are 12.58 and 5.12 mm. Considerations like these lead to the final design of the 4 x 4 electrode photomask which is shown in Fig. 15. It includes 16 control regions, 16 electrical paths, and 4 reference marks for aligning the substrate (Prism A) in the mask. To keep this drawing simple, we have omitted dimensions here, but some of the sizes have been quoted above. The design has been completed, and the masks have been ordered.

TABLE 5. Size and shape of glass prisms for 4 x 4 and 3 x 3 opto-switches; SF14 glass with $\Theta_A = 66°$ and $\Theta_B = 24°$.

PRISM		DIMENSIONS IN MILLIMETERS 4 x 4 SWITCH	3 x 3 SWITCH
A	BASE	45.3	32.7
A	WIDTH	27.6	22.5
A	HEIGHT	2.80	2.80
B	BASE	52.3	40.8
B	WIDTH	23.3	18.2
B	HEIGHT	23.3	18.2
B	HYPOT.	57.3	44.7

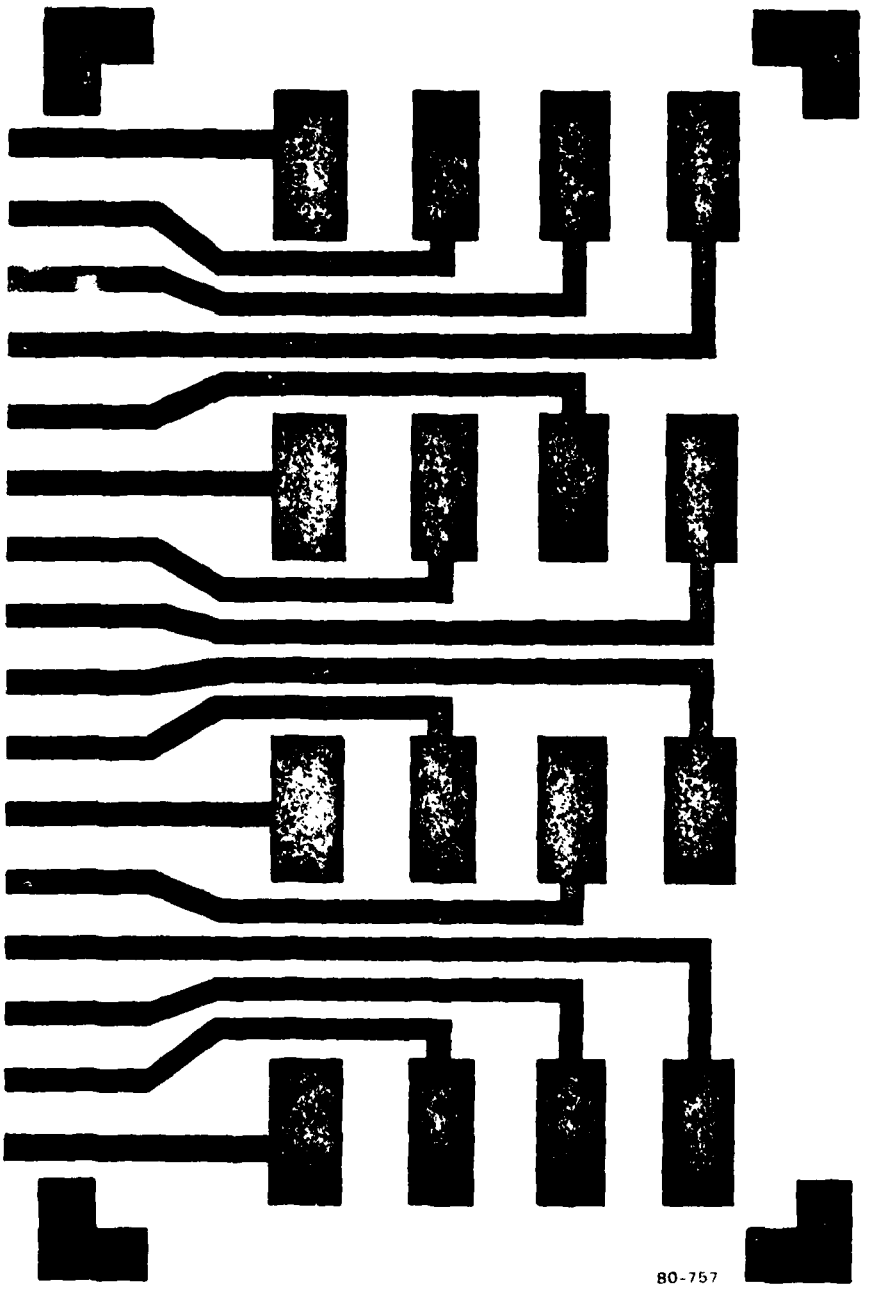

FIG. 15 Electrode pattern used to control 4 x 4 opto-switch.

VIII. SUMMARY

Good progress has been made on the design of 4 x 4 and 3 x 3 electro-optical switches for multimode fibers. Ways of reducing crosstalk and loss in the switch were investigated. The design of initial prototype switches has been completed. Optimum glass and liquid crystal materials were identified. Customized glass prisms have been ordered from Optics for Research, Inc. Electrode photomasks were also ordered from another vendor.

IX. PLANS FOR NEXT QUARTER

The vendor for the prisms has quoted a ten-week delivery time. This will seriously delay (or preclude) switch-building during the second quarter, and other activities--both theoretical and experimental--will take the place of 4 x 4 construction next quarter. We shall examine alternative designs for an N x N liquid crystal switch that uses polarizing beamsplitters (multilayer dielectrics) to split the s- and p-polarizations. (The active regions will be liquid crystal that operate off of 3V.) In the laboratory, we shall work on the technology that will be needed after the prisms arrive, including photoresisting and ITO etching techniques.

X. REFERENCES

1. R. A. Soref and M. Kestigian, Final Report on RADC Contract No. F19628-79-C-0086, Sperry Research Center, Report CR-80-25, April 1980.

APPENDIX C
QUARTERLY REPORT NO. 2

DESIGN AND FABRICATION OF MULTIMODE OPTICAL SWITCHES

Quarterly Status Report No. 2
Contract No. F19628-80-C-0147

Sperry Research Center
100 North Road
Sudbury, Massachusetts 01776

SRC-CR-81-3
January 1981

Contract Monitor: Mr. Richard Payne (RADC/ESO)

This report is intended only for the internal management use of the contractor and the Air Force.

Prepared for

ROME AIR DEVELOPMENT CENTER
DEPUTY FOR ELECTRONIC TECHNOLOGY
HANSCOM AIR FORCE BASE
BEDFORD, MASSACHUSETTS 01731

DESIGN AND FABRICATION OF MULTIMODE OPTICAL SWITCHES

I. INTRODUCTION

The goal of this contract is to make a multimode N x M optical switch with high performance in a fiber-optic communication system. Our approach was spelled out in the first Quarterly Report. During the second Quarter, work was done on 2 x 2, 3 x 3, and 4 x 4 switches, but progress on the 3 x 3 and 4 x 4 devices was quite limited because the custom-made glass prisms for these devices did not arrive from the vendor until ten days before the end of the Quarter. Therefore, most of the effort was spent on the 2 x 2 switch since we were able to assemble this device from standard, *off-the-shelf polarizing* beamsplitters rather than from specially fabricated parts.

We designed, built, and tested a novel 2 x 2 optical switch consisting of four 2 x 1 "sub-switches" coupled together in conformance with our dual-array principle. This compound switch gives significantly lower levels of optical crosstalk than prior-art electro-optical switches, and is actuated by only 4V rms. Optical insertion loss is also low.

II. RESULTS ON 3 x 3 AND 4 x 4 SWITCHES

Experimental work on 3 x 3s and 4 x 4s was limited due to the unavailability of glass prisms for these devices. The vendor, Optics for Research, delivered the prisms to us at the end of the Second Quarter. During this Quarter, plexiglass fixtures for clamping prisms A and B together while assembling the switch (Fig. 14 of QSR-1) were designed and are being built in our machine shop. Electrode masks with 9 and 16 elements per our design (Fig. 15 of QSR-1) were received from Photronics Inc. Work

was done on SiO slope evaporation and on prism spacing techniques needed for the N x N liquid crystal "package". The SiO deposition was also used for the twist cells described in Section III below. With regard to spacers, we tested Ablefilm 539 type II, which is a 1/4-mil mylar film coated on both surfaces with 1/8-mil of thermosetting adhesive, a total film thickness of 1/2-mil or 12.5 microns (the thinnest available). We cut this material into strips and used it as gasket material (spacers) for LC cells. After putting clamping pressure on the glass plates during the 125°C oven curing cycle, we found that the Ablefilm compressed to 9 to 10 microns, with some of the adhesive flowing laterally before hardening. When the temperature was raised to only 90°C rather than 125°C, we found that the cells did not have good mechanical strength (the plates could be pulled apart). Our 3 x 3 and 4 x 4 opto-switches will require LC film thicknesses of only 6 microns. Because the Ablefilm did not compress to this thickness range, we conclude that Ablefilm is not optimum in our application, and other techniques will be sought.

III. RESULTS ON 2 x 2 SWITCHES

The attainment of low crosstalk levels is an important aspect of optical switching. In the crosstalk area, results on electro-mechanical switches have been impressive 1-5, but achieving low crosstalk in electro-optical switching (at Sperry and elsewhere) has proved more difficult. During this Quarter, we found a way to reduce crosstalk significantly in electro-optic 2 x 2 devices, which put these devices on a more equal footing with their electro-mechanical competitors. The theory of crosstalk reduction and the experimental results will be given here.

The principle of crosstalk reduction is the tandem cascading of elemental optical switches, and the cascading procedure comes directly from our N x N matrixing idea. Figure 1 illustrates our concept for making an N x N opto-matrix from two groups of 1 x N switches. The first group of multi-pole optical switches is represented by open circles, while the

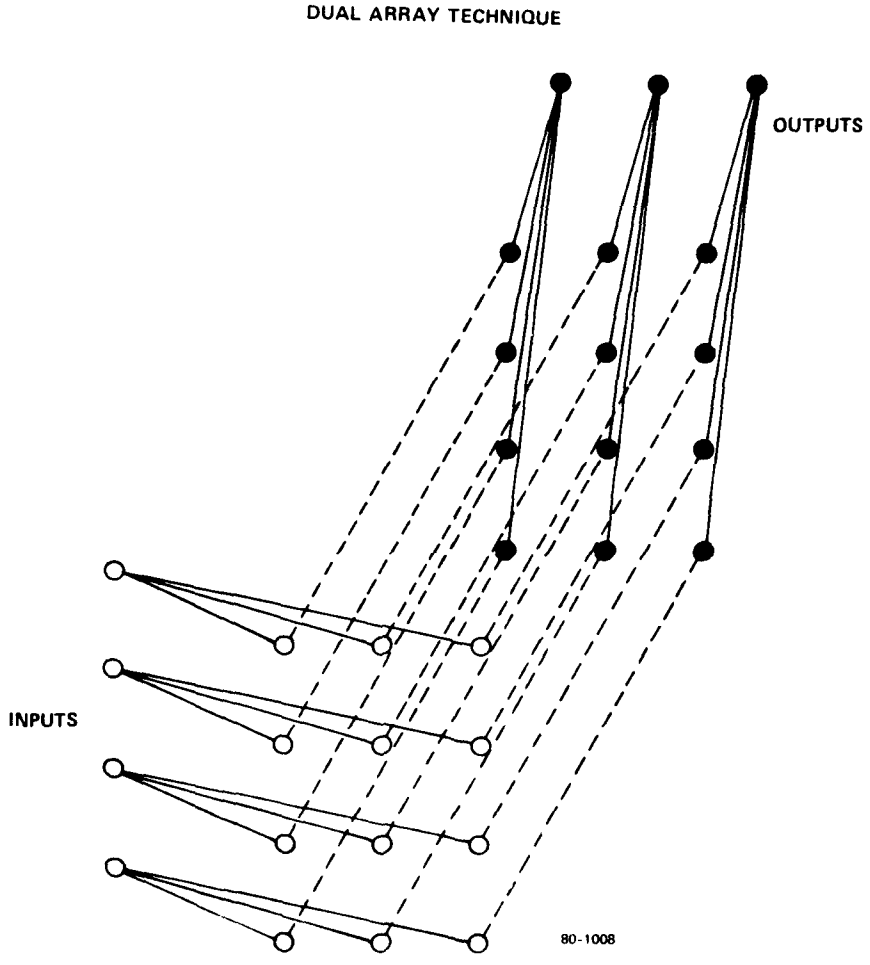

FIG. 1 Method of making N X N switch from two arrays of multi-pole switches.

second array of N x 1s is shown by solid circles. The dotted lines represent optical connections between switches.

The 2 x 2 switch (optical reversing switch) is the simplest example of the N x N matrix. Reducing the Fig. 1 diagram to the N = 2 case, we arrive at the optical circuit diagram of Fig. 2 which is a "compound" switch made from four 1 x 2 switches. Specifically, we see that there is a pair of 1 x 2s (open circles) and a pair of 2 x 1s (solid circles) with four optical paths between the pairs. Two optical paths are parallel ("straight ahead") and two paths cross over each other without interacting. The "cross" and "bar" paths are a consequence of the row-to-column array mapping in Fig. 1. The four switches in Fig. 2 turn ON and OFF in unison (they are ganged).

The compound 2 x 2 has much lower crosstalk than the individual 1 x 2s because each optical signal in Fig. 2 travels through two 1 x 2s and the 1 x 2's fractional optical crosstalk ε is thereby multiplied to ε^2. Thus, the compound switch has twice the optical isolation in dB of an elemental switch, which is an important advance in the art.

We have implemented Fig. 2, with the low-voltage technique described by Wagner and Cheng { Ref. 6 }. They used a 90°-twisted nematic LC cell to turn a 2 x 2 opto-switch ON and OFF with 3V rms. Figure 3 shows the Wagner-Cheng design for a 2 x 2 comprised of two polarizing beamsplitters (PBs) and two 45-90-45 TIR prisms for 90° internal reflection of light beams. The LC twist cell is inserted at the midplane as shown, and provides a 90° optical polarization rotation at V = 0. (In terms of the orthogonal s and p polarizations, the unenergized LC gives a polarization mapping of s → p, and p → s). At 3V, there is no rotation (s → s, and p → p). For fiber-optic applications, four strands of multimode optical fiber and four quarter-pitch Selfoc lenses are coupled at normal incidence to the four ports as shown, and the optical paths within the switch are indicated by the shaded regions in Fig. 3.

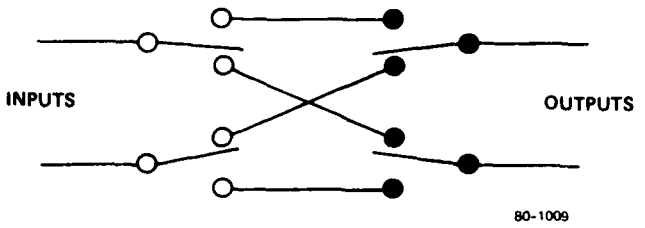

FIG. 2 Low-crosstalk 2 X 2 opto-switch (reversing switch) made from four 1 X 2s.

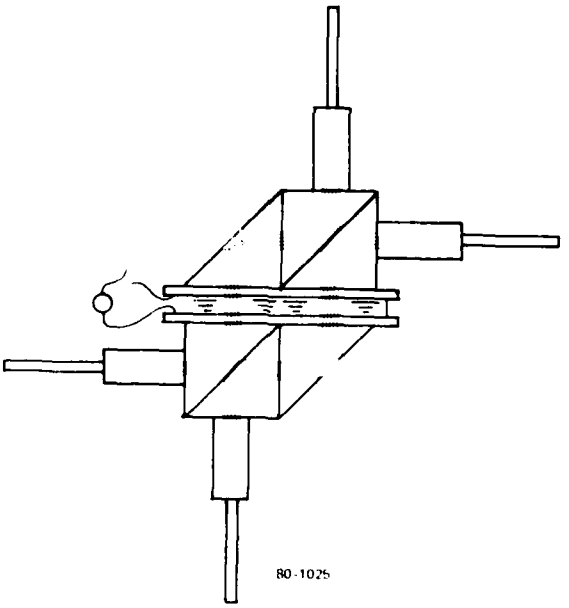

FIG. 3 Low-voltage 2 X 2 fiber-optical LC switch reported by Wagner and Cheng.

In implementing the Fig. 2 structure, we note that each of the elemental 1 x 2s can be a Wagner-Cheng 2 x 2 structure with one of the four ports terminated in an optically absorptive material such as a layer of black paint. We also note that a pair of 1 x 2s can be contained side-by-side in the same glass pieces. The optical paths for independent switches are simply displaced laterally and a pair of ports are terminated. We call this 1 x 2 pair a "subswitch." Next, we take two Wagner-Cheng structures and join them optically with "transfer prisms." The first structure, subswitch #1, has two 2 x 2s with a pair of input ports terminated, giving two 1 x 2s. The second structure, subswitch #2, has a pair of 2 x 2s with two output ports terminated, giving two 2 x 1s. The transfer prisms provide the crossover path of Fig. 2. This procedure leads to Fig. 4, which is the structure of our compound, low-voltage 2 x 2 LC opto-switch. We have shown the optical beam paths in both the voltage-ON and voltage-OFF states. All such paths lie in a plane in Fig. 4. By arranging the subswitches in a symmetric, mirror-image fashion, we are able to use only one liquid crystal twist cell to control both subswitches, which is a convenient and cost-saving arrangement. Let us examine now the first subswitch and look at the four possible output beam positions from the second PB. Two beams exit horizontally and two come out vertically. The horizontal paths go directly to the second subswitch, while the vertical paths are exchanged in going from subswitch #1 to #2. We use three right-angle prisms of unequal size to permute the light beams. (A more sophisticated arrangement for doing this, a multi-faceted prism, is described below). Looking at the lower diagram in Fig. 4, note that the first transfer prism crosses the beams and sends them out horizontally to the next two prisms (one is half the size of the other) which deflect the beams downward into #2 without crossing them.

Wagner and Cheng discuss the idea of placing several 2 x 2 switches side-by-side in the same pieces of glass and they explain the need for segmenting the transparent electrodes in the LC cell in order to control individual switches. It might appear necessary, therefore, in

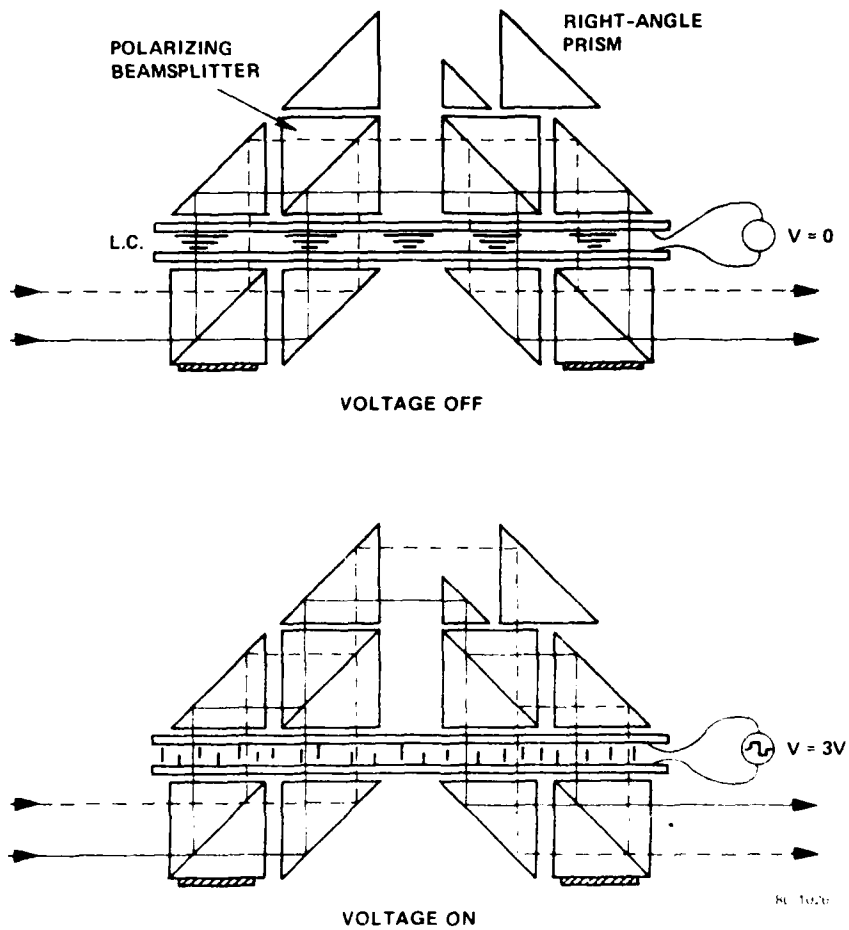

FIG. 4 Two operating states of new, compound 2 X 2 opto-switch based on Figs. 2 and 3. This electro-optical LC switch features low crosstalk and low voltage.

Fig. 4 to divide the LC electrodes into four separate areas to actuate the composite switch properly. However, this is not the case, and we have found a way to operate the compound 2 x 2 with uniform homogeneous electrodes in the LC cell. In other words, the entire LC layer in Fig. 4 is turned ON and OFF in unison, which simplifies the construction and operation of the switch.

Another advantage of the non-segmented LC cell is the fail-safe operation of the switch. By contrast, in many LC switching devices (including the N x N matrix), the electrodes are segmented and it is necessary to apply voltage to some segments at all times; for example, in the N x N matrix, N out of N^2 regions are ON at any instant. However, in the compound 2 x 2, we can operate the switch with four regions ON or with four regions OFF (uniformity) instead of two ON or two OFF. In other words, in our binary-state switch (Fig. 4), V = 0 everywhere is a legitimate switching state. This is useful in practice because optical connections are preserved when the power fails.

The reason fail-safe operation is possible is related to the four possible optical paths in the mid-region between subswitches #1 and #2. If the first input to #1 is excited, light can come out ports A-1 or B-1, with A and B denoting the vertical and horizontal outputs from the second PB. Likewise, the second input leads to outputs A-2 or B-2. We have the option of operating the 2 x 2 with optical conditions (A-1, B-2) or (B-1, A-2) in the midplane, but that would require segmented electrodes, plus four half-wave-retardation plates. Alternatively, we have the choice of using state (A-1, A-2) or (B-1, B-2) as in Fig. 4 where midpaths are both horizontal or both vertical. This choice allows uniform electrodes with the fail-safe feature (a choice not available in the 3 x 3 or 4 x 4).

The shaded regions at the bottom of the first and fourth PBs in Fig. 4 are the optical terminations mentioned earlier. The latter termination absorbs crosstalk light that propagates to the unused ports of the Fig. 4 switch so that this leakage does not appear (via reflections) at the

"real" output ports. The absorber on the first PB is a precautionary measure to reduce stray reflections near the input.

We turn now to the experimental work. The Fig. 4 structure has been realized with standard, off-the-shelf polarizing beamsplitters, 1/2" cubes, whose performance was maximized at the 6328Å He-Ne laser wavelength. The PBs were manufactured by CVI Laser Corporation of Albuquerque. The same company supplied the TIR prisms, diagonally sliced 1/2" cubes with AR coatings on two faces. All 45-90-45 prisms were identical except for the 1/4" x 1/4" x 1/2" prism in the mid-region (a special prism that we cut and polished). The 90° twisted nematic cell was fabricated from two Nesatron ITO plates, 2 1/2" x 5/8" x 1/16", coated at a 60° angle with SiO_x (450Å thickness on a normal incidence monitor) that created the desired LC alignment. The plate spacers were Ablefilm 539 type II, discussed in Section II, that gave a 10 μm LC layer thickness. We used the liquid crystal ZLI-1131, a nematic PCH mixture made by E. Merck (See QSR-1).

Figure 5 is a photograph of the laboratory-prototype 2 x 2 switch made from four PBs, seven prisms, and one LC cell. The wire leads attached to the LC cell with conductive epoxy are visible in the photo. Apart from AR coatings on the prisms (the PBs were not coated), no effort was made to minimize the various Fresnel losses. Numerous reflection losses occur at the interfaces, the air gaps between components. (The components were simply held near each other on a bed of double-sided adhesive tape). We could have filled those air gaps with transparent, index-matching fluid, but did not do so, in order that components could be used later for other tasks. In operation, two parallel, independent beams of light come into the upper left PB in Fig. 5, and two switched beams go out from the upper right PB (light beams not shown).

Crosstalk and insertion loss in the Fig. 5 structure were measured using collimated 6328Å beams. The beams were polarized at 45° to the PB edges, giving 50% s-polarized and 50% p-polarized input light to simulate

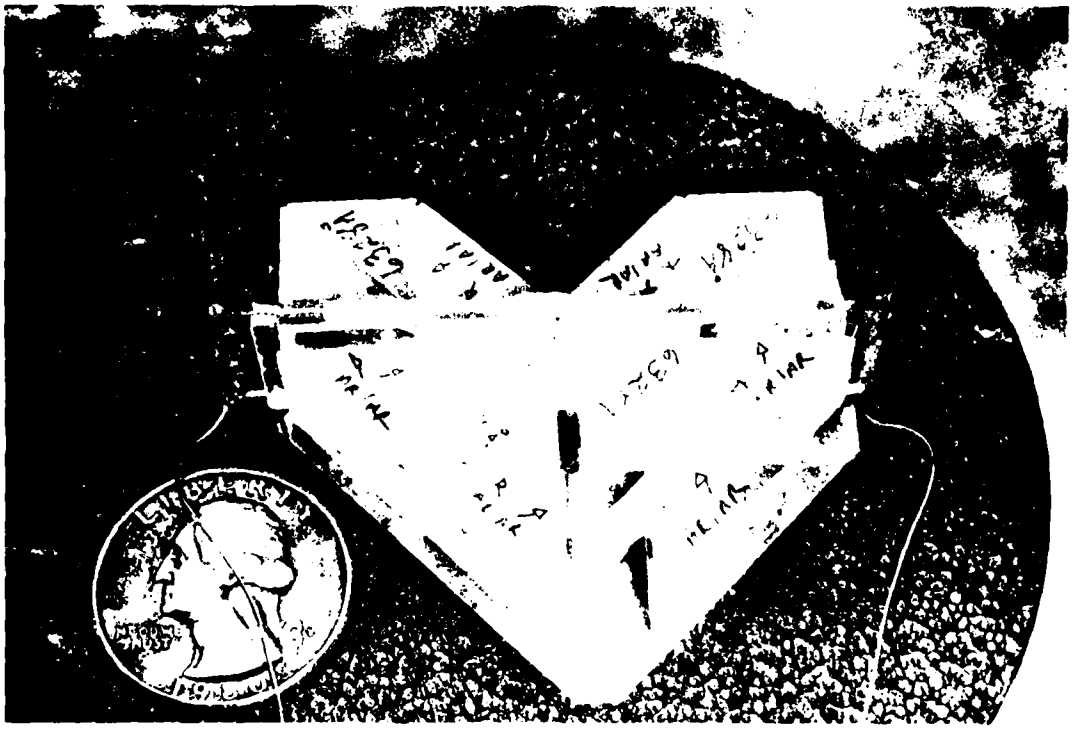

FIG. 5 Laboratory version of the 2 X 2 opto-switch of Fig. 4.

the effect of an unpolarized input. The LC was connected to an audio square wave generator, and control frequencies in the 2 kHz to 50 kHz range produced a steady-state response without noticeable "ripple" on the light.

With one optical input excited, we measured the optical intensity at both outputs of the switch as a function of control voltage amplitude. Then the experiment was repeated for the other input. The results are shown in Fig. 6. This Figure shows the optical turn-on and turn-off vs applied voltage (the rms value of a 4 kHz square wave). Optical output power relative to the optical input level is plotted on a dB scale (unlike the linear plot that is used for many switching devices). Dashed lines indicate the results for the second optical input. The Fig. 6 result exhibits the characteristics of a true reversing switch with "cross" and "bar" states. In terms of crosstalk and loss performance, there is a symmetry between the ON and OFF states, as desired. The two inputs give similar results, as desired. Also, the optical turn-on is rapid; for example, the output levels shift by 12 dB for an increment of 0.6V.

It is seen in Fig. 6 that the switch is OFF from zero volts up to the threshold at 1.3V. The switch is fully ON at 5V, so the required voltage swing is 3.7V, starting at a 1.3V bias. An ON state of 3.5V or 4.0V can be used at somewhat higher loss/crosstalk levels, if desired. We shall consider 5V as the ON state for our discussion.

The optical crosstalk in Fig. 6 is found to be 26 to 27 dB below the input in the ON and OFF states, the best result ever reported for a liquid crystal switch. This 27 dB optical isolation translates into an equivalent electrical isolation of 54 dB.

The insertion loss in Fig. 6 is 2.5 dB in both the ON and OFF states, most of which (~1.7 dB) is due to reflection losses between the 12 constituents. As we mentioned earlier, a large part of this Fresnel loss (~1.3 dB) could be eliminated by interposing a transparent film of index-matching adhesive between each pair of optical parts, which would

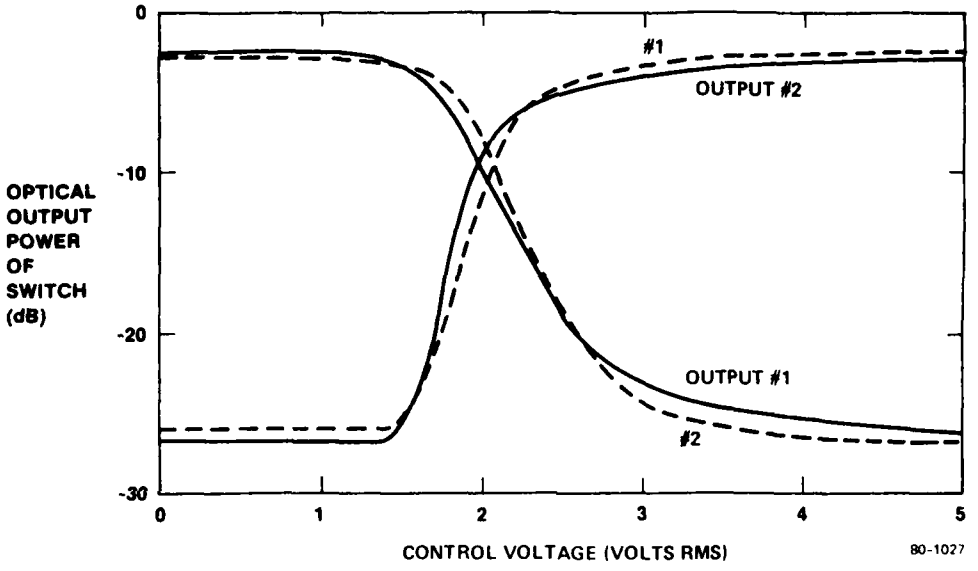

FIG. 6 Experimentally observed switching characteristics of Fig. 5 device. Solid lines show output curves when the first optical input is excited. Dashed curves show output levels resulting from excitation of the second optical input.

have the added virtue of making the structure rugged and "monolithic." Following the discussion of Ref. 6, the total reflection loss should be reducable to less than 0.5 dB. Part of the loss budget in Fig. 5 is a scattering loss of ~0.8 dB for a double transversal of the LC layer (See Ref. 6). In addition, when the 2 x 2 switch is coupled to fibers via Selfoc lenses, a coupling loss of about 0.8 dB will appear (Ref. 6). Putting these factors together, we estimate that the total optical insertion loss (ON or OFF state) of our fiber-coupled compound switch should be reduceable to 2.0 dB.

We wish to point out that our experimentally observed combination of -27 dB crosstalk, 2.5 dB loss, and 5V control (both states) is the best set of performance specifications ever reported for any multimode electro-optical switch.

We did not measure the transient response of this device, but it appears to have a natural decay time of 0.2s and a rise time of < 0.1s as governed by the particular LC twist cell. Several methods have been reported in the literature for speeding up the response of LC twist cells into the 1 to 10 ms range. An interesting speculation concerns "memory" states for the switch. Researchers have obtained stable textures in LC cells that persist after voltage is removed.

The main limiting factor in crosstalk performance is the optical extinction ratio δ of the individual polarizing beamsplitters (See Ref. 6). Extinction ratio is defined as: $\delta = \varepsilon_s + \varepsilon_p$, where ε_s is the fraction of s-polarized light not reflected within the PB, and ε_p is the fraction of polarized light not transmitted by the PB. Wagner and Cheng were able to obtain beamsplitters with $\delta \sim 0.01$ and they observed crosstalk of -19.4 to -18.8 dB in their 2 x 2, which is the best result obtained heretofore with an electro-optic switch.

In the compound 2 x 2 switch, crosstalk light of an intensity δ leaving the first subswitch will suffer an additional attenuation δ

in traversing the second subswitch, so the output crosstalk in theory will have a strength of $(\varepsilon_s + \varepsilon_p)^2$. This leakage does not include a contribution introduced by imperfect ($\neq 90^\circ$) rotation in the LC cell. Figure 2 of Ref. 6 indicates the joint effect of rotation errors and δ. In a typical case, rotation errors of a few degrees will add 2 to 3 dB to the crosstalk level for a double passage through the LC.

If we had possessed PBs with $\delta \sim 0.01$ as did Wagner and Cheng, we could in principle have had a crosstalk of -40 dB in our switch. Unfortunately, our PBs did not have the precisely tailored dielectric layers of Ref. 6 and exhibited more leakage. Specifically, our beamsplitters had $\varepsilon_s = 0.005$ and $\varepsilon_p = 0.030$; in other words, the PB extinction ratio was 0.035 which leads us to predict that our compound 2 x 2 would have crosstalk of $(0.035)^2$ or 0.00123, that is, -29.1 dB, which is close to the level observed, tending to confirm our theory. Extrapolating to the case of improved PBs with $\delta \sim 0.01$, we would anticipate a crosstalk of -35 dB in an experimental version of our switch (-40 dB from δ^2, plus 5 dB from rotation errors and scattering). With regard to the choice of LC material, we feel that the operating voltage of the switch can be reduced by 0.5 to 1.0V through the use of LC materials with lower "untwisting thresholds" such as the mixture E31LV sold by EM Industries. In summary, the optimized fiber switch would have 2 dB loss, -35 dB crosstalk, and 3V control.

Figure 7 is a drawing of what the complete fiber-optic switch would look like in a more commercialized packaging. All glass parts would be cemented together with optical adhesive. The optical crossover (as per the shaded optical paths in the drawing) is accomplished by a 4-facet-roof prism at the top, as shown. The four fibers are grinrod-coupled as indicated, and the optical terminations are shown at the bottom. Note that this switch is completely symmetric and reciprocal (bidirectional). Light can propagate in either direction and the input/output labeling is arbitrary.

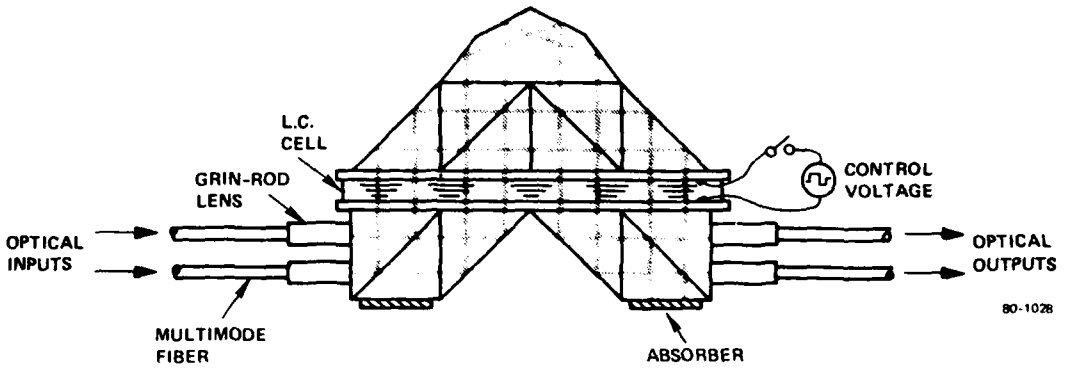

FIG. 7 Proposed structure of low-crosstalk 2 X 2 fiber optical switch based on Fig. 4.

Figure 7 is not the only way to build the compound 2 x 2 switch and we would like to describe the other possibilities here. Note in Fig. 7 that all optical paths lie in one plane, but it is equally possible that light beams from the first pair of 1 x 2s (Fig. 2) can be contained in a first plane, with the second group of paths (2 x 1s in Fig. 2) falling in a second plane. The connecting paths are then "out of plane."

We now present three 2 x 2 structures based on the above ideas. Each structure makes use of elongated beamsplitters and prisms like those of Fig. 4 in Appendix B, components whose size is typically 0.5" x 0.5" x 1.0". Front, side, and perspective views of the first switch are given in Fig. 8. This structure uses two LC twist cells, shown as dotted regions. In Fig. 8, the 1 x 2 switches are placed in parallel planes within the same 2 PBs and 3 prisms. Similarly, the 2 x 1 switches are located in another pair of parallel planes, in 2 PBs and 3 prisms. By analogy with our 4 x 4 matrix (Fig. 1 of QSR-1), the first subswitch is rotated 90° about the mid-beam axes and joined to the second. This gives the row-to-column mapping seen in Fig. 1. The optical parts-count in the Fig. 8 switch is: 4 PBs, 6 prisms, and 2 LCs. Some cost savings are realized in the elongated components, but the requirement of two LC cells is a disadvantage.

Figure 9 presents the front, top, side, and perspective views of another compound 2 x 2 structure. Here, the 1 x 2 and 2 x 1 switches have optical paths in the same two parallel planes, but there is a special multi-faceted prism at the top of the switch to provide an out-of-plane optical beam crossover between those planes. The remaining two optical beams in the mid-region travel straight ahead due to the direct contact between the second and third PBs. Apart from the ten-sided crossover prism, this structure is relatively simple because its parts-count is: 4 PBs, 5 prisms, and only one LC cell.

Finally, in Fig. 10 we present front, side, and top views of a simple "folded" structure in which the light propagation is folded back into

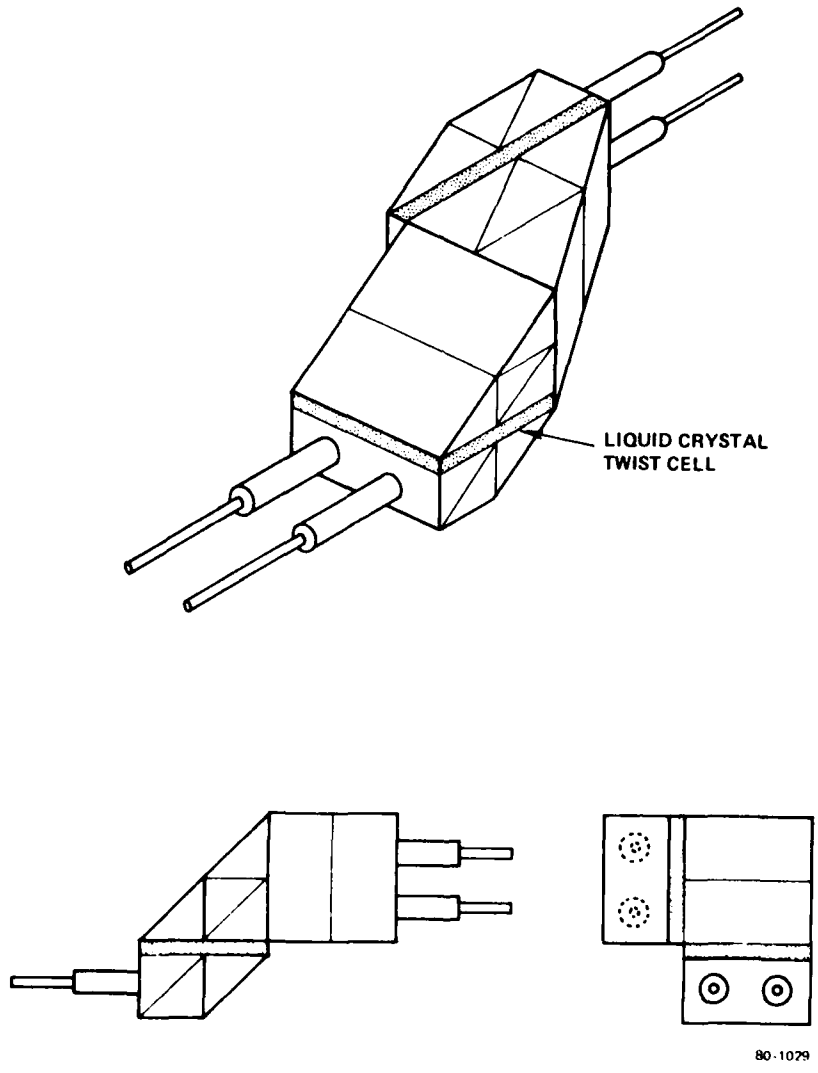

FIG. 8 Low-crosstalk, compound 2 × 2 optical switch (alternative to Fig. 7) in which sub-assemblies are oriented at 90° to one another.

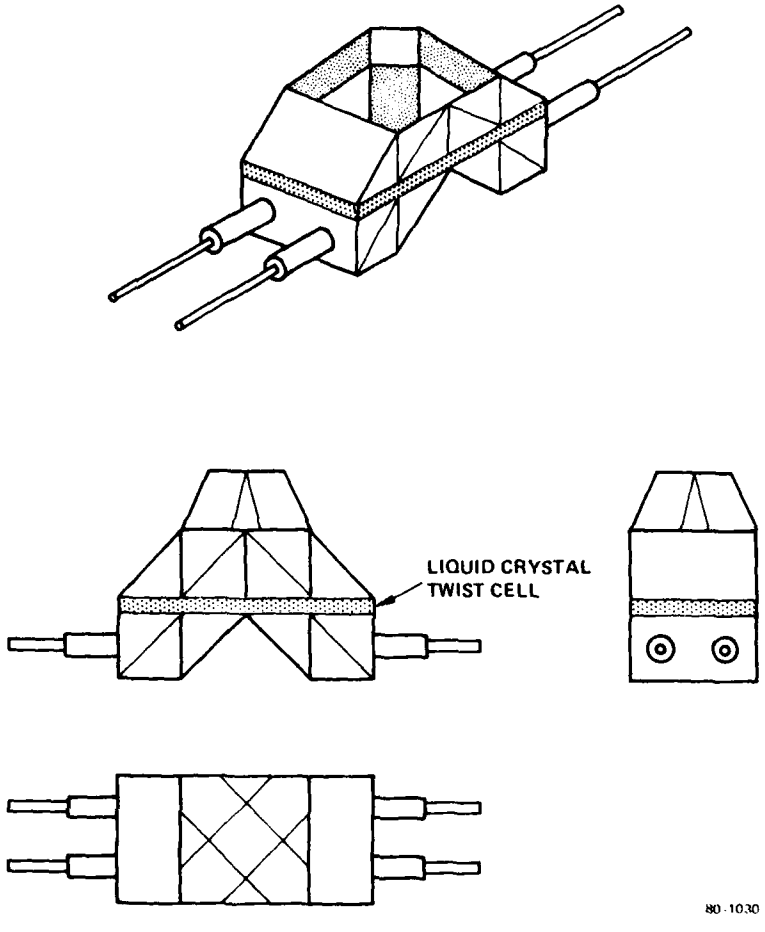

FIG. 9 Low-crosstalk, compound 2 X 2 optical switch (alternative to Fig. 7) with collinear input/output arrangement and out-of-plane crossover prism.

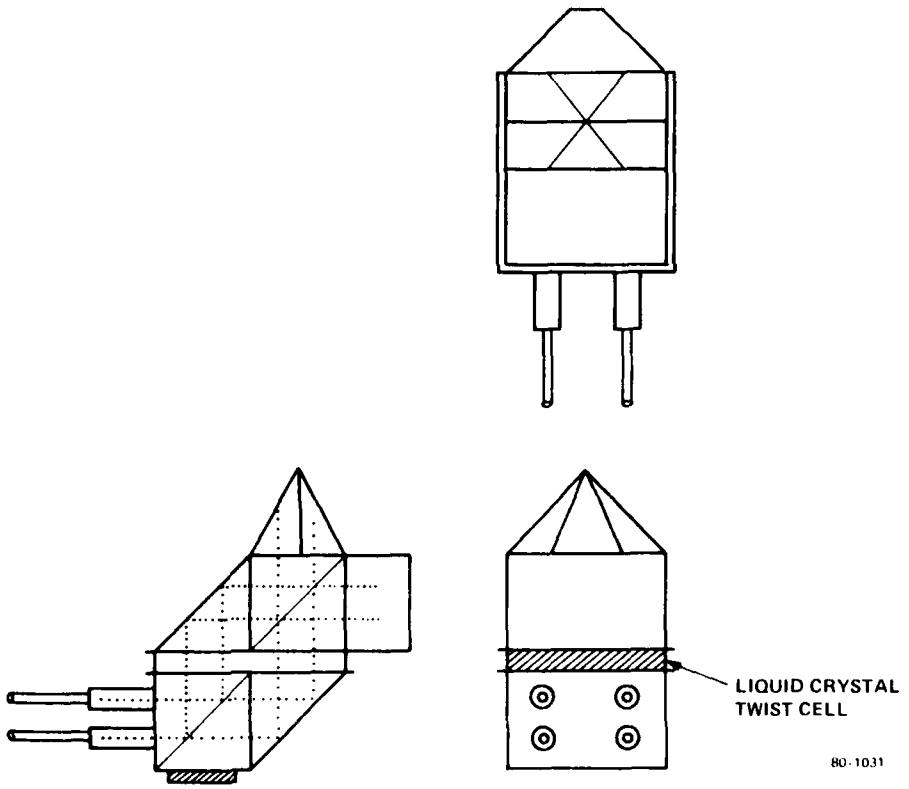

FIG. 10 Low-crosstalk, compound 2 X 2 optical switch (alternative to Fig. 7) with folded optical paths produced by roof prisms. Resulting structure is compact.

the reverse direction (by two reflections) after leaving the first subswitch. The backward traveling beams enter the second subswitch, which is located in a plane parallel to the first, and which shares the same optical components. This means that the fiber optic inputs, as well as the outputs, are located on the same surface on the switch as per Fig. 10. Only one LC cell controls the switch. Retrograde propagation of light is provided by two multi-faceted prisms. Both prisms are fairly simple; the first is a "double pyramid" for beam crossover plus folding; the second is a "single pyramid" for folding only. This structure is the simplest of them all because its parts-count is only: 2 PBs, 4 prisms, and one LC. The switching performance of Figs. 8, 9, and 10 is expected to be identical to that of Fig. 7.

We conclude this Section with a brief discussion of the advantages and disadvantages of the compound 2 x 2 switch. The main advantage is the combination of low loss, low crosstalk, and low voltage. The chief disadvantage is the relatively high complexity (and cost associated with that complexity). By way of comparison, we can examine a 2 x 2 switch made in the same manner as our 4 x 4 matrix. This device is illustrated in Fig. 11. Here, we have gained a considerable simplification over Fig. 7 because there are only 4 simple prisms, and we get the same excellent crosstalk performance of -40 dB (estimated). The Fig. 11 approach is appealing in an N x N because we obtain sophisticated switching (N nonblocking conversations and N! states) with only 4 prisms, but in a 2 x 2, the insertion loss trade-off becomes less appealing due to the simpler network function. Specifically, in Fig. 11, we must trade-off the 4 to 5 dB loss, and the 30V operation (plus the need for two LC layers). So, when we are dealing with 2 x 2 applications, it may be worth dealing with the high parts-count of Fig. 7 to gain the added performance.

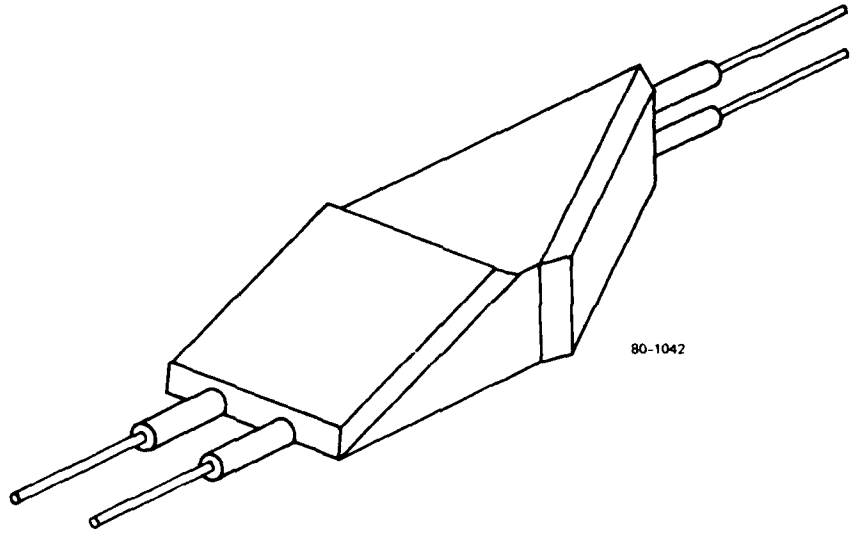

FIG. 11 Structure of 2 X 2 optical switch with a layout identical to the N X N matrix (a special case of Fig. 2 in QSR-1).

IV. REFERENCES

1. C. Dahne and A. L. Harmer, Electronic Letters, vol. 16, 647 (1980).

2. C. M. Miller, R. B. Kummer, S. C. Mettler, and D. N. Ridgway, Electronics Letters, vol. 16, 783 (1980).

3. E. G. Rawson and M. D. Bailey, Optical Engineering, vol. 19, 628 (1980).

4. M. Nunoshita and Y. Nomura, Applied Optics, vol. 19, 2547 (1980).

5. J. Minowa et al, Electronics Letters, vol. 16, 422 (1980).

6. R. E. Wagner and J. Cheng, Applied Optics, vol. 19, 2921 (1980).

APPENDIX A

ELECTRO-MECHANICAL N x N SWITCH

Our February 1980 Proposal to RADC stated that our dual-array approach applied to electro-mechanical and acousto-optic switches as well as electro-optical switches. This Appendix shows specifically how an electro-mechanical N x N fiber optical switch is made with dual arrays. The N x N design is presented here because it is simple, compact, and is expected to offer low crosstalk levels, together with low insertion loss.

Figure A-1 shows front, top, and side views of the N x N opto-switch for the N = 4 example. The light-deflection elements, shown as shaded circles and shaded bars, are cylindrical plungers with a flat mirror at one end, the mirror surface oriented at 45° to the cylinder axis. If desired, an angle-preserving prism can be substituted for the mirror as in Minowa et al, Electronics Letters, volume 16, page 422 (1980). The movable plungers are arranged in a square N^2 matrix, and there are two identical arrays, one above the other, the mirrors in the first N^2 array being oriented at 90° to those in the second N^2 array. A restoring force from springs or magnets (not shown) holds each plunger in a rest position, and the step-wise up/down motion of each plunger is actuated by individual solenoids, etc, (not shown). The ON position is up in the first array and down in the second array. Plungers in the two arrays are addressed in collinear pairs.

Light enters the mechanical matrix from a plane-parallel array of 4 multimode fibers, each having its own quarter-pitch grinrod lens for beam collimation. Orthogonal to this array, a second planar array of fibers and lenses is provided. Note that the two fiber arrays lie in different planes which provides excellent isolation between fiber inputs and outputs.

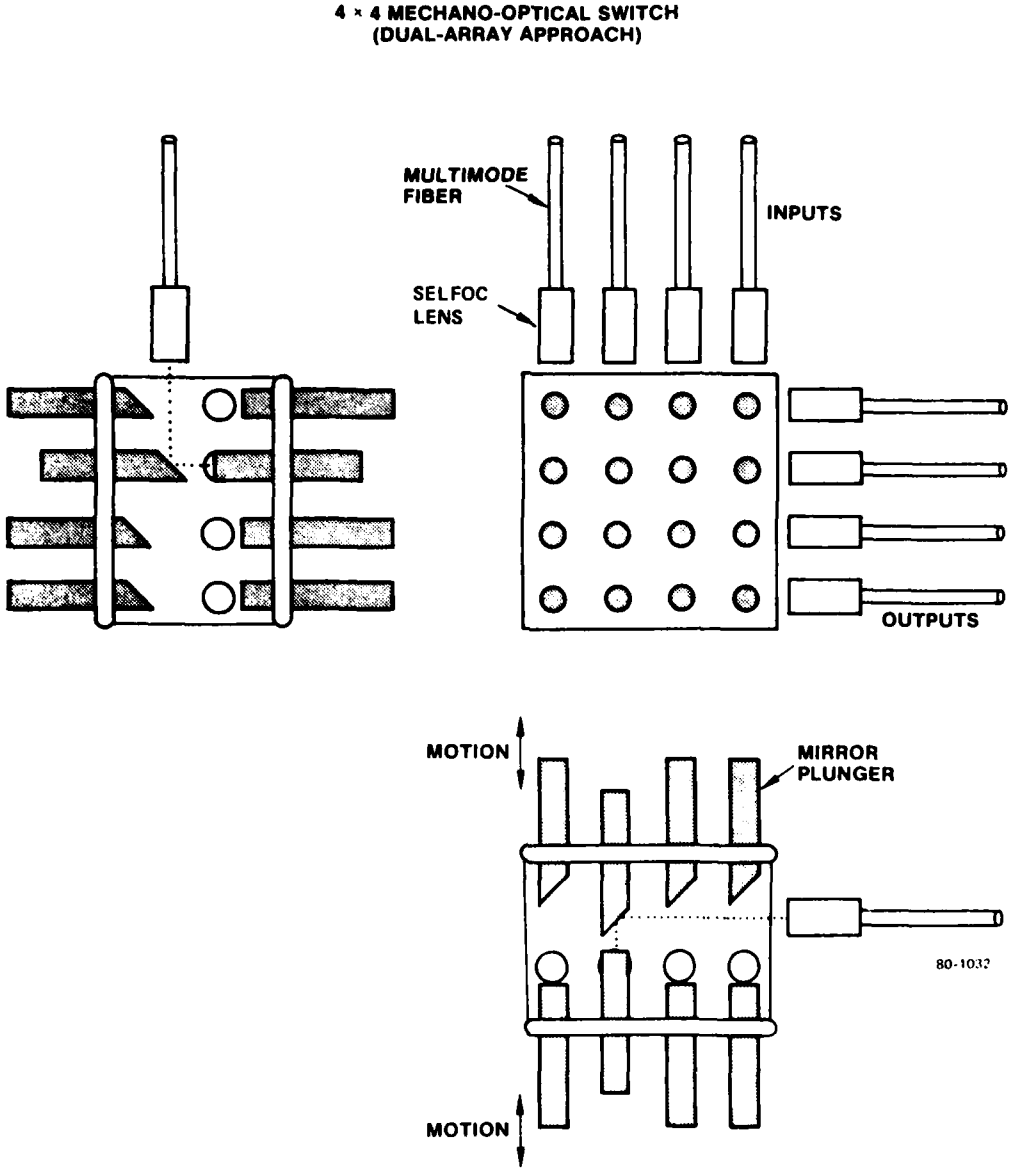

FIG. A-1 Electro-mechanical N X N optical matrix switch based on dual-array concept.

Returning to the electro-mechanical arrays, both are addressed identically: one mirror in each row of the matrix, and one in each column, are turned ON at any instant; that is, 4 out of 16 deflectors are actuated in each array at a given time. Light is deflected twice by 90° in each light path (dotted line) of the addressed matrix. Unpolarized light is switched in Fig. A-1 and the matrix switch can be re-configured into any one of 24 possible states. The light paths are relatively short, leading to low loss.

APPENDIX B

ELECTRO-OPTICAL 1 x N AND N x N LIQUID CRYSTAL SWITCHES

The preferred structures on this contract use four glass prisms, two LC layers, (and oblique optical incidence) to make 1 x N and N x N switches. One drawback of this approach is that ~30V rms is needed to address the switch. Since Wagner and Cheng have made a 2 x 2 switch operable by 3V rms, it is natural to wonder whether there is a low-voltage technique for more complex, multi-way switches. We have found several ways to make 1 x N and N x N optical switches that operate from 3V rms, and we shall present these designs here. None of the designs has been tested in the laboratory, but the straightforward nature of the designs leads us to think that they will work as planned.

We have modified and extended the Wagner-Cheng approach to make 1 x N structures, and we use the same basic constituents; polarizing beamsplitters, liquid crystal twist cells, and right-angle TIR prisms. The switches, however, use relatively large numbers of beamsplitters and numerous LC cells, which is the reason that these structures were not chosen as the primary designs for this contract. Nevertheless, we feel these designs may be useful in some situations, so we offer them here despite their complexity.

Our first design, a polarization-independent 1 x N fiber optical switch is shown in Fig. A-2 (side view of device) for the N = 3 example. It requires 2N beamsplitters and N liquid crystal layers plus the usual quarter-pitch grinrod lenses for collimation/decollimation of light from the 1 + N multimode fibers. The unpolarized input beam is split into s- and p-polarized beams that are recombined at a particular output, or are sent in parallel to the next output, depending upon the state (zero-rotation or 90° optical rotation) of the local LC twist cell. There are N

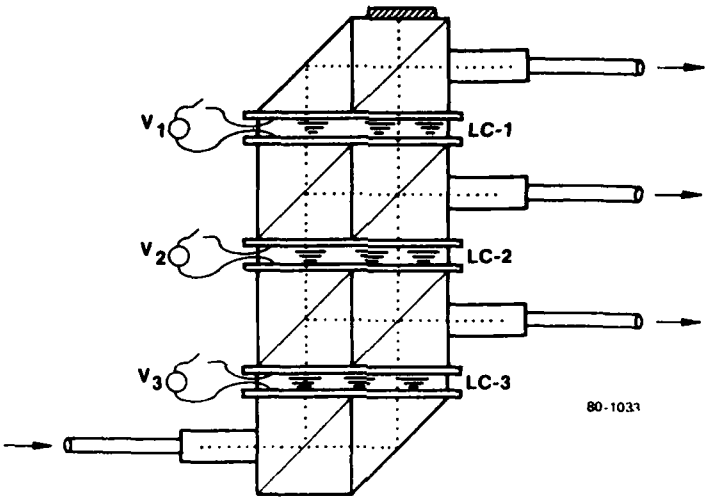

FIG. A-2 Multi-pole 1 X N fiber optical switch (an electro-optic LC device). This design is an extension of Wagner-Cheng. It features low-voltage and two-polarization switching.

such electro-optical decision points. Assuming a 20 dB extinction ratio for each PB, the expected performance of this 1 x 3 switch is -20 dB crosstalk in any of the three states, 1.5 dB maximum insertion loss in any state, and 3V operation. It is quite possible to extend this switch to 1 x 8 or 1 x 10 operation. Then, however, there would be optical beam spreading loss in the switch due to the increased optical path lengths (the maximum path length is Nd, where d is the PB length), which increases the Selfoc-Selfoc coupling loss as per Fig. 9 of QSR-1. Generally, one trades an increased loss for a larger number of fibers. Specifically, in a 1 x 8, we expect 1.6 dB beamspreading loss at the 8th output, and a total insertion loss that ranges from 1.5 to 2.5 dB in going from the first to the eighth output.

If one is willing to accept a 3 dB loss penalty, one can use only half the number of PBs in Fig. A-2 and cut the cost of the switch in half. This is done, as shown in Fig. A-3, by switching only one optical polarizaiton. The 1 x 3 switch of Fig. A-3 absorbs the polarization in the first PB (shaded layer) and sends the s-beam on to the three subsequent PB locations where it is deflected out, or transmitted to the next PB, depending on the local LC twist state. There are N beamsplitters and N liquid crystal cells, with an estimated performance of -20 dB crosstalk (previous assumption), 4 dB insertion loss, and 3V switching. The previous comment about loss vs. large N applies here.

Until now, we have assumed that the PBs are cubes, typically 0.5" x 0.5" x 0.5" in size. It is possible to extend the length of the PBs and TIR prisms in the third dimension to say, 0.5" x 0.5" . 1.5" as shown in Fig. A-4. This can be done at low cost by molding BK-7 glass into these shapes as is often done for the cubic shapes.

Having obtained the elongated components of Fig. A-4, we can readily make extended versions of the Fig. A-1 and A-3 switches wherein the switching function is repeated or "replicated" several times within the same pieces of glass. For example, we can make four independent 1 x 3

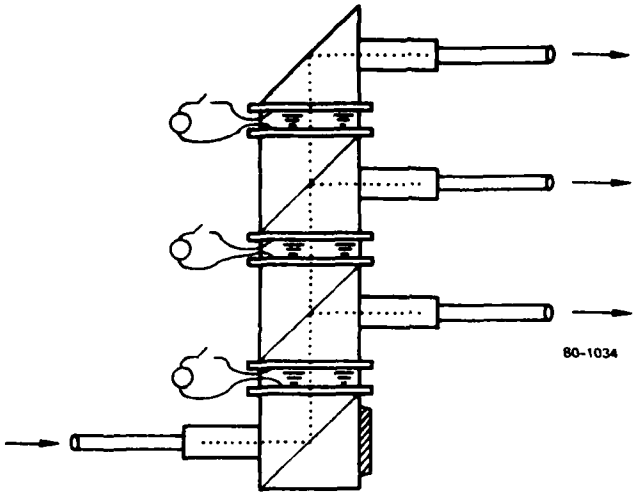

FIG. A-3 Multi-pole 1 X N fiber optical switch, similar to Fig. A-2 except that only one polarization is switched.

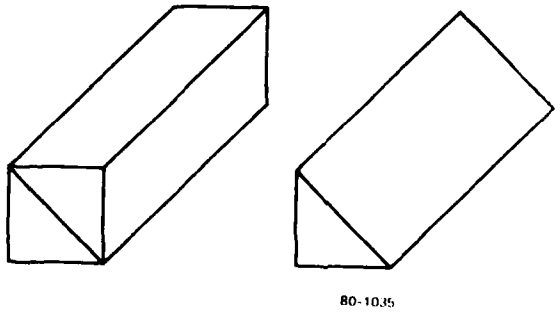

FIG. A-4 Polarizing beamsplitters and prisms with a high width-to-height ratio. These are useful in accomodating several optical switching paths.

switches (polarization independent) as shown in Fig. A-5, an elongated version of Fig. A-2 in which each set of 1 x 3 optical paths lies in a plane, and four such planes are located side-by-side, parallel to one another. In each of the three LC cells, the electrodes are segmented into four parts; four rectangles that are independently controlled (segmenting not shown).

Further, as per Fig. 1 of this Report, we can apply the dual-array principle to Fig. A-5 and employ the A-5 device as one half of a polarization-independent N x M matrix. Two Fig. A-5 switches, a 4-fold 1 x 3 and a 3-fold 4 x 1, are attached at their input/output planes as shown in Fig. A-6 after the second switch has been rotated 90° with respect to the first about the output beam axis. This creates a 4 x 3 opto-matrix, which is a fairly complicated structure because it requires 7 LC cells and 14 PBs, although it performs a sophisticated switching function. Estimated performance is -40 dB crosstalk in any state, 2 dB insertion loss and 3V control.

Returning to the 1 x N switch, we now inquire as to whether a single LC cell with segmented electrodes can be used to control N optical outputs. The answer is yes, provided that the number of PBs is increased over Fig. A-2 and A-3, and that the optical path is folded back upon itself in a zig-zag pattern. The alternative design for a 1 x N switch, N = 4 example, is presented in Fig. A-7. This is a single-polarization switch that has a slightly higher loss than Fig. A-3. This structure uses only one elongated LC twist cell whose conductive surfaces are divided into three independent parts (segmented electrodes). The control voltage sources are not shown. There are also a series of TIR and double-TIR (roof) prisms that cause the light beam to "meander" back and forth through the LC cell by multiple 90° reflections. The operation of the switch is as follows: Light comes into the first PB where the transmitted polarization is absorbed (shaded region) and the reflected polarization travels through the LC to the next PB (the first

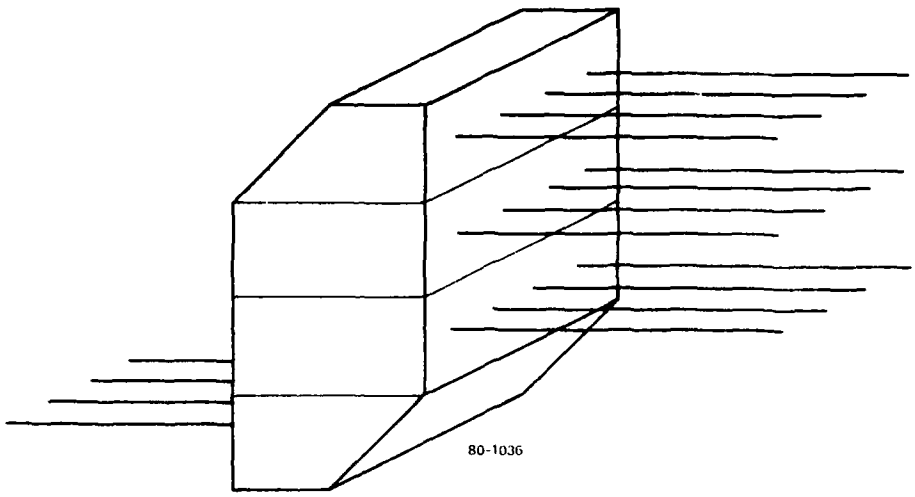

FIG. A-5 Monolithic structure containing four independent 1 X 3 fiber optical switches based on Figs. A-2 and A-4.

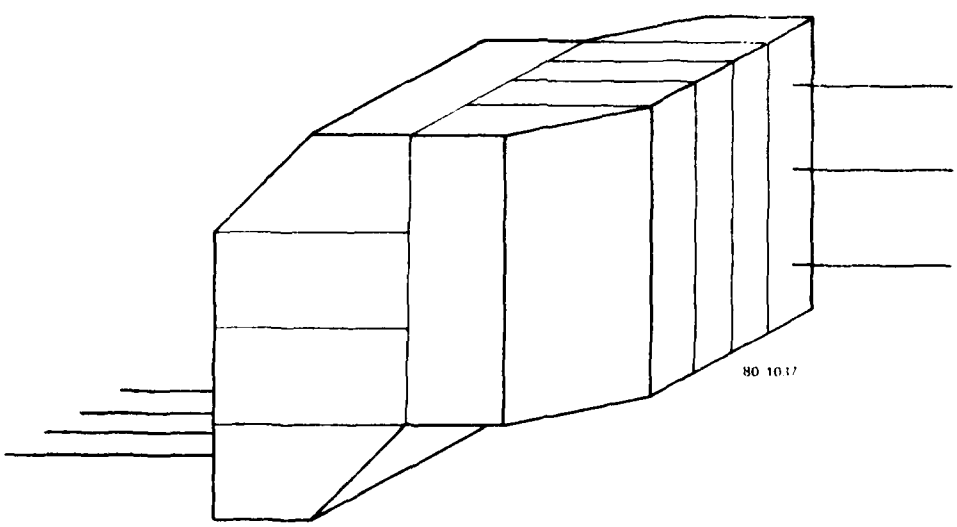

FIG. A-6 4 X 3 fiber optical matrix switch made from two subassemblies like Fig. A-5 (sub-switches at right angles to each other).

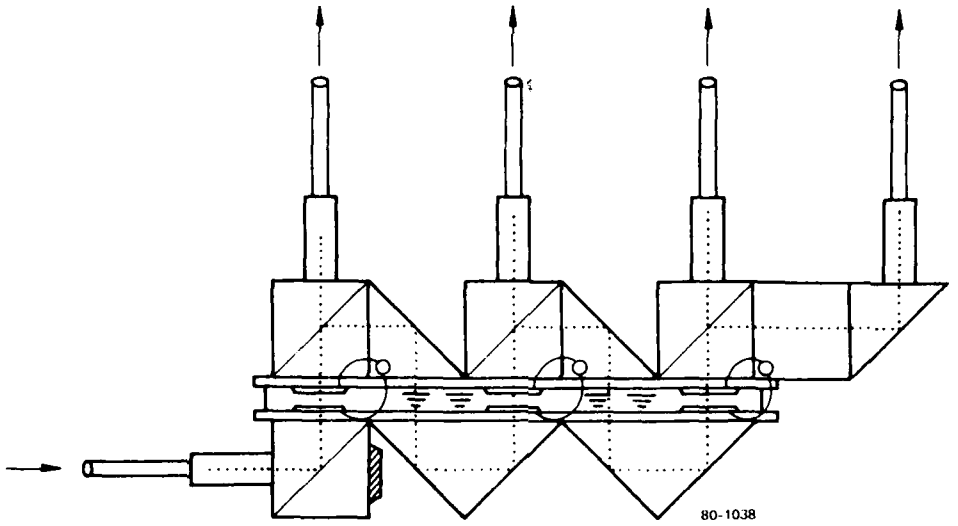

FIG. A-7 1 X 4 fiber optical switch using one LC cell.

output location). The LC operates on the polarization-state of the light. As before, the N local LC regions can have 90° rotary power, or no rotary power, depending upon the voltage applied locally. The local rotation state provides an electro-optic selection mechanism because, in one case the light will exit the j-th PB, while in the other case, light will be reflected in zig-zag fashion to the (j+1)-th LC/PB combination.

The four outputs in Fig. A-7 are all taken above the LC cell, which actually is an inefficient use of space because light can easily be switched out of the zig-zag path above and below the LC as shown in Fig. A-8. Here, there are six outputs and six electrically controlled areas of the LC twist cell as indicated (voltage sources not shown). Both Figs. A-7 and A-8 switches have 4 to 5 dB insertion loss for unpolarized light, with -20 dB crosstalk and 3V control. Returning to Fig. A-7, two devices of this kind can be joined to make an N x N matrix as illustrated in Fig. A-9, the N = 4 example. The matrix assembly procedure is the same as discussed for Fig. A-6. Although there are only two LC layers in Fig. A-9, the complexity of this 4 x 4 structure is high and the loss is 3 dB higher than in Fig. A-6.

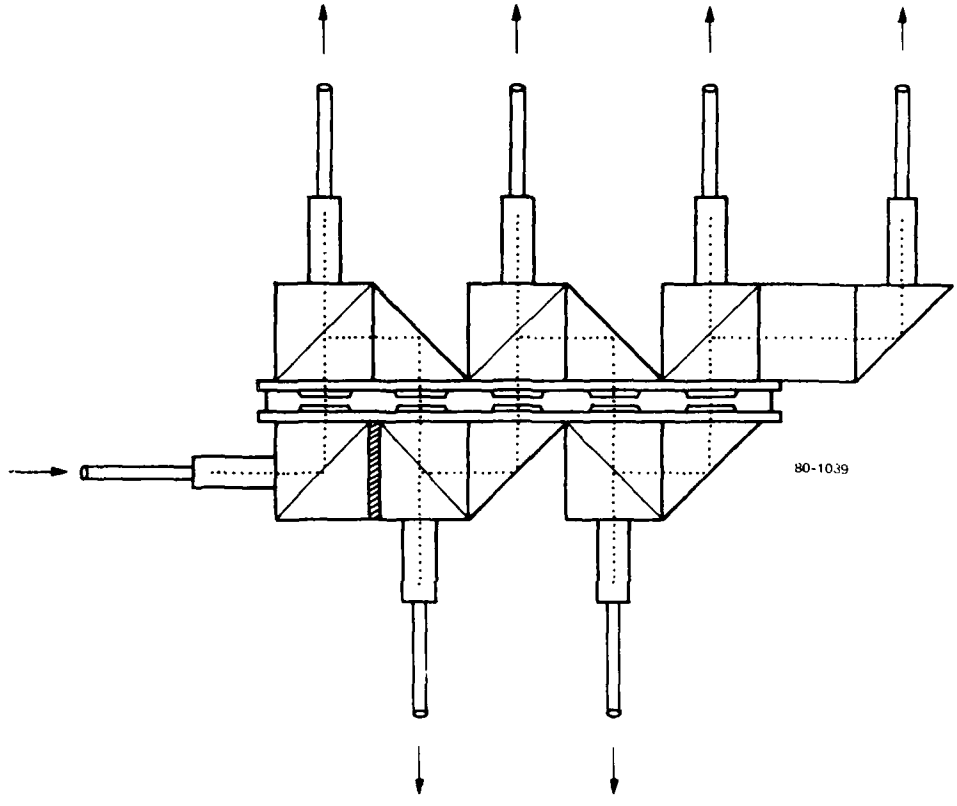

FIG. A-8 1 X 6 fiber optical switch similar to Fig. A-7 except that outputs are taken from both sides of LC cell.

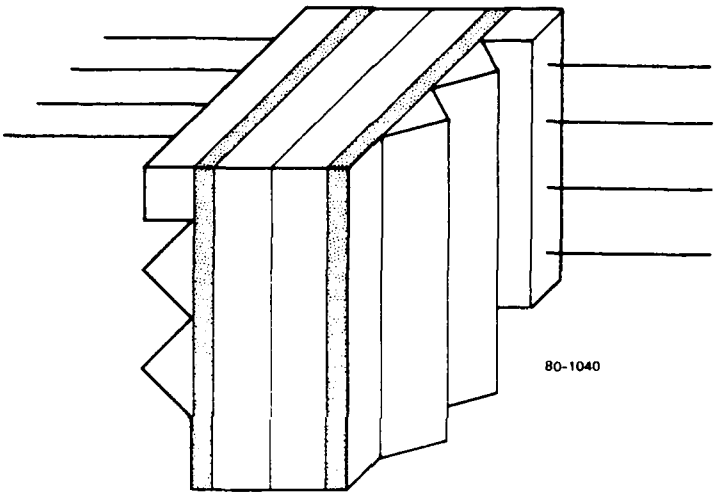

FIG. A-9 4 X 4 fiber optical matrix switch made by joining two sub-switches per Fig. A-7 at 90°.

APPENDIX D
QUARTERLY REPORT NO. 3

DESIGN AND FABRICATION OF MULTIMODE OPTICAL SWITCHES

Quarterly Status Report No. 3
For the Period 1 January - 31 March 1981
Contract No. F19628-80-C-0147

R. A. Soref

Sperry Research Center
Sudbury, Massachusetts 01776

SRC-CR-81-25
March 1981

Contract Monitor: Mr. R.A. Bradbury (RADC/ESO)

This report is intended only for the internal management use of the contractor and the Air Force.

Prepared for

ROME AIR DEVELOPMENT CENTER
DEPUTY FOR ELECTRONIC TECHNOLOGY
HANSCOM AIR FORCE BASE
BEDFORD, MASSACHUSETTS 01731

DESIGN AND FABRICATION OF MULTIMODE OPTICAL SWITCHES

I. INTRODUCTION

The goal of this contract is to make a multimode N x M optical switch with high performance in a fiber-optic communication system as spelled out in the First Quarterly Report, Part I.

Good progress has been made this Quarter. All of the parts (prisms, masks, etc.) were received, an rf sputter machine was utilized for electroding, photolithographic etching of ITO was done successfully, the half-matrix switches, both 3 x 3 and 4 x 4, were successfully assembled, and electro-optic measurements have been made on those switches. A surface-treatment problem was uncovered and was solved during this Quarter.

Generally speaking, the experimental work is on schedule, although we did encounter difficulty in obtaining a uniform 6-μm LC layer, a difficulty that we hope to overcome next Quarter. During the Fourth Quarter we shall address the problem of mechanically aligning the Selfoc lenses and fibers along optical paths in the matrix.

As the Appendices to this Report indicate, we have also made progress during this Quarter in designing low-voltage fiber-optic LC switches, both 1 x N and N x N, using the twisted-nematic polarizing-beamsplitter approach.

II. SWITCH MATERIALS AND CONSTRUCTION

Prisms made from Schott SF14 glass, cut and polished to our specifications by Optics for Research, Caldwell, NJ, were delivered to us in January 1981. The dimensions of these flint-glass prisms are given in

Table 5 of QSR-1. The prisms had a refractive index of 1.762 at λ = 589 nm, and they cost about $85 each.

The nematic liquid crystal (LC) in each switch was the cyanobiphenyl mixture, type E9, from EM Industries (BDH Chemicals Ltd.) whose 598-nm refractive indices are n_o = 1.52 and n_e = 1.775, and whose mesophase temperature range is +7 to +84°C (see Table 1B of QSR-1). In conjunction with SF14 prisms, this LC had an optical critical angle of 59.6°, while the prisms gave a 66° optical incidence angle on the LC layer.

Prisms A and B were separated by two pieces of 1/4-mil-thick teflon tape, thereby producing a nominal 6.3-μm LC layer. A custom-designed plexiglass fixture with four clamping screws was built in our machine shop to hold prisms A and B together under pressure during assembly. Figure 1 shows these fixtures.

For electroding the prisms, we used an International Vacuum rf diode sputtering system that had a 6"-diameter mixed oxide target of 88% In_2O_3 and 12% SnO_2. Photomasks, 3"-square iron oxide masks per our design (Fig. 2), were received in January 1981 from Photronics Laboratories of Brookfield, CT.

III. INITIAL DEVICES

We ordered sufficient parts for four 3 x 3 half-switches and eight 4 x 4 half-switches. This Quarter, we built three of the former and two of the latter, so we have several opportunities left in the Fourth Quarter to make one 3 x 3 half, and six 4 x 4 halves. Unfortunately, one 4 x 4 A-prism is chipped, so we have only five "good chances" for additional 4 x 4 halves, and the remaining 3 x 3 A-prism is chipped, so a good 3 x 3 result may not be obtained.

This Quarter, all five devices were fabricated using positive photo-resist. Late in this Quarter, we discovered that this led to an unwanted border of conductive material around the electrode pattern in some devices due to an edge-buildup of photoresist. The thick rim of

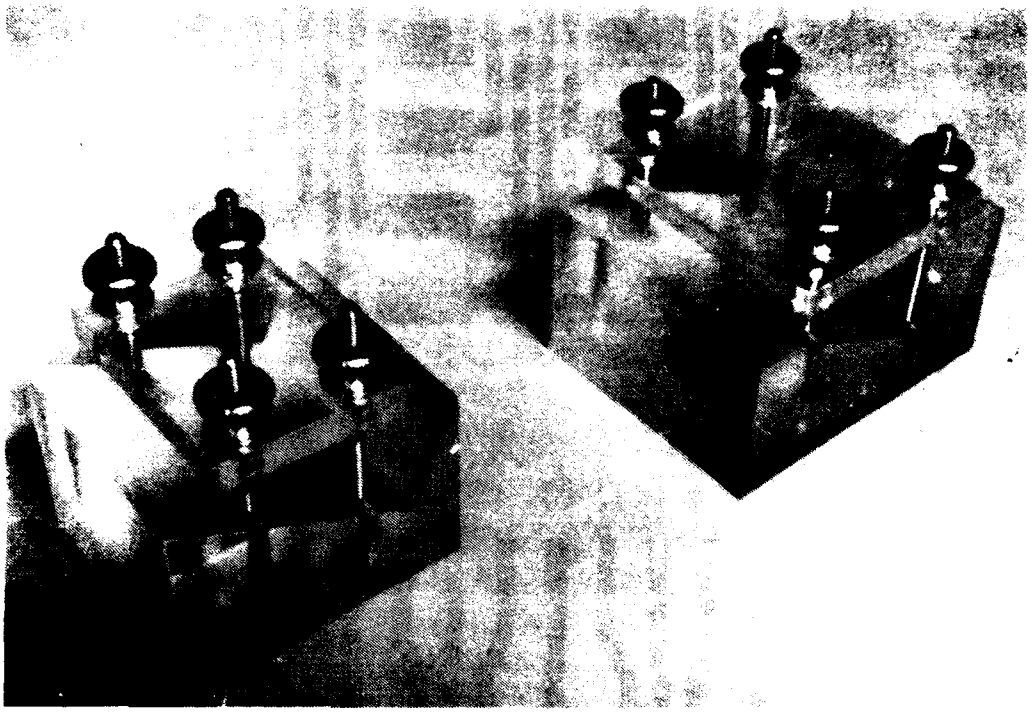

81-340

FIG. 1 Clamping fixtures for assembling 3 x 3 and 4 x 4 switches.

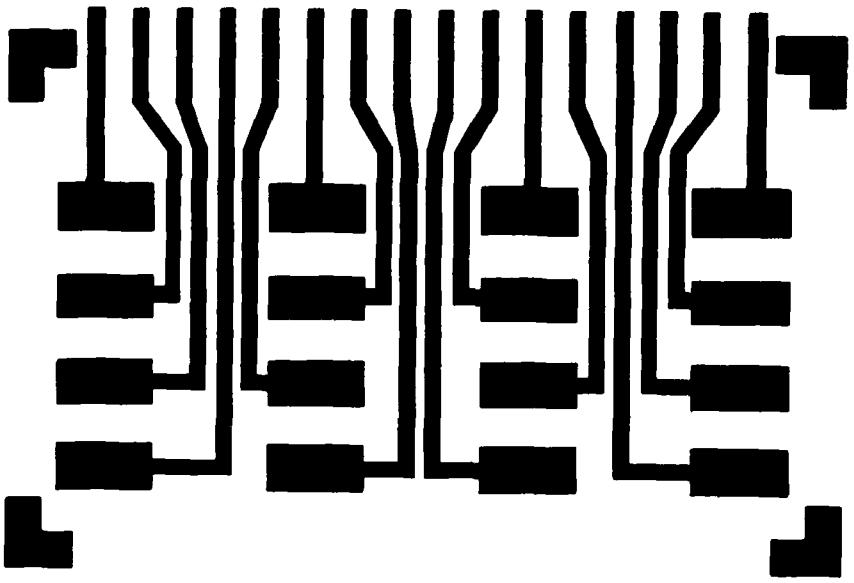

80-757

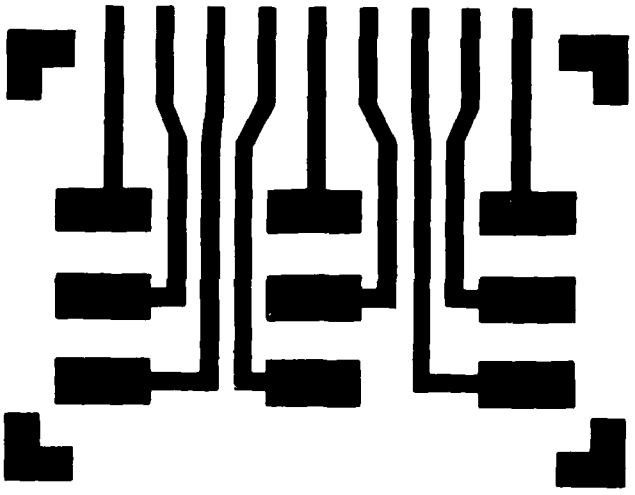

81-337

FIG. 2 Pattern of transparent electrodes for 3 x 3 and 4 x 4 switches.

resist at the edges of prism A was underexposed to UV and that resist did not wash away completely during development. Consequently, the conductive film was not etched away completely along the periphery of prism A. However, this problem does not arise with negative resist, and we shall make the remaining 4 x 4 switches with negative resist during the Fourth Quarter.

IV. TECHNICAL PROCEDURE

We present in this Section a detailed description of the process (arrived at after several trials) that give the best results in the construction of electro-optical switches.

A. Cleaning

Clean prisms with successive baths of acetone, detergent solution, filtered water, and methanol. Blow dry with filtered air after each step.

B. Sputter Deposition of Indium Tin Oxide

Fill cold trap with liquid nitrogen. Pump system down to 2×10^{-5} Torr. Backfill with flowing argon and adjust throttle valve to give 0.020 Torr partial pressure of argon. Presputter target onto metal shutter for 5 minutes at 50 W. Then, sputter-deposit ITO film on prisms for 62 minutes in 0.020 Torr pure argon at 85 W rf power (45 Å/m). Prism B is sputtered obliquely because the base of the prism is in thermal contact with the J, while its exposed surface is at 26° to the target surface. Prism A is sputtered at normal incidence. The resulting ITO film is approximately 1000Å thick, is highly transparent (with a faint interference color), and has an initial resistance of 800 ohms across a 2 cm gap. After 24-hr. exposure to room atmosphere, the ITO resistance increases two-fold and stabilizes, with the transparency unchanged. The ITO film is not uniform across the Prism-B area, as seen in bands of interference colors, but because the film resistance is sufficiently low everywhere, the nonuniformity does not affect the switching performance.

C. Photoresisting and Etching

Positive masks and positive photoresist, Shipley AZ1350, were employed for the first five switches. Later, this was changed to negative masks and negative resist. The AZ resist was spun at 5000 rpm for 30 seconds on the clean ITO surface of prism A. In a contact-printing operation, the resist was exposed to UV through the N x N electrode mask for 40 seconds. Following development, the resist pattern was baked at 60°C for 30 minutes. Then, the prism was immersed in a bath of undiluted hydrochloric acid for 20 seconds to etch away unwanted areas of the ITO film. An acetone bath removed the resist. As Section V indicates, an edge buildup problem in the resist was sometimes present.

D. Surface Treatment

Oblique SiO was used in the first switch. Subsequent devices had rubbed surfaces. This is discussed in Section V below.

E. Assembly and Spacers

The surface-treated prism B was placed in the lower half of the plexiglass jig. Then two pieces of 1/4-mil teflon tape, 3 cm x 1.5 mm, cut from a 1/4" ribbon with a razor blade, were placed on opposite sides of the prism B surface, while making sure that the tape was not wrinkled. The treated prism A was then carefully placed on top of B on the teflon spacers, A having the proper alignment and overlap with respect to B. Guided by four threaded stainless steel rods, the lid of the jig was then placed on top of prism A and tightened down with equal pressure at the corners. At the gap of the A/B sandwich, six small dots of Torr-seal epoxy (Varian Associates) were put on, three on each side, to cement A to B. This assembly was placed in a 45°C oven for 80 minutes to cure the epoxy.

F. Liquid Crystal Filling Step

After the epoxy cured, the empty (but cemented) switch was removed from its jig and was placed on a hotplate with prism A up. Thirty minutes

of heating allowed the switch to reach thermal equilibrium at a temperature of 95°C, a temperature sufficient to melt the LC. A bottle of E9 was heated simultaneously on the hotplate. We transferred molten LC from the 5 gm bottle to the switch with clean 25 ml glass pipettes. Two pipettes containing LC were held at the top of the prism A ramp at the open slit between A and B. The isotropic liquid then flowed in along the order-direction to fill the 6 μm cavity in about 2 minutes. Then the hotplate was turned off and the switch cooled slowly to room temperature.

G. Wire Attachment

In the region where A overlaps B, there are 9 or 16 parallel bars of ITO, the electrical fan-out leads. These ITO strips were covered with narrow bars of Tracon type 2902 silver conductive epoxy adhesive, and a 4 cm piece of tinned #26-gauge copper wire was inserted in each silver bar to provide an electrical connection to the outside world. In addition, for access to the uniform conductive surface of B, there is a 2 mm x 2 cm overhang of B with respect ot A. Here, a #26 wire was attached with silver epoxy to give a "ground" or common electrode for the switch.

V. TEXTURE-CHANGE PROBLEM

Surface treatment in the first 3 x 3 switch consisted of depositing a thin film of silicon monoxide in the usual fashion. SiO powder from a baffle boat was evaporated at 10Å/second onto prism A and B surfaces at 60° to those substrates, the boat being 30 cm from the surfaces to give the desired homogeneous in-plane orientation of the LC director at each surface (with zero tilt angle). The SiO film thickness was 480Å as measured by a normal incidence quartz monitor. The SiO was put on top of the photoetched ITO pattern and therefore covered a combination of bare-glass and conductive areas. The device was assembled and filled with E9 liquid crystal that flowed in (in the isotropic phase at 95°C) along the order direction. The LC texture was uniform, free from threads and air bubbles, and was "clear" although a closer inspection revealed a light "haze" throughout the LC

film. With red light incident at 66°, this LC film reflected both s- and p-polarized light as desired. However, a serious problem was revealed by electro-optic measurements.

After applying a 60 Hz sine-wave voltage of sufficient magnitude, the texture of the LC could be changed permanently in any of the 9 elements (the ac voltage had a frequency of 400 to 8000 Hz). Although the elements turned on and off properly at low voltage with no aftereffects, we found that the LC molecules became "detached" from the prism walls when a voltage of 40 Vrms or more was applied across the 0.25 mil LC for two seconds or longer ($E > 6$ V/μm). After voltage was removed, the LC was transformed into an optically scattering texture; a fine-grained, chaotic, random texture that covered the electrode rectangle. In other words, due to high-field application, the initial anchoring forces at the walls were overcome and the planar texture was destroyed. This texture change is unwanted and renders the switch useless because some s- and p-light now leaks through the LC film at V = 0 and because the film has high loss in the quiescent state. It is interesting to note that the original planar ordering could be restored by heating the entire LC film into its isotropic phase (done by placing the switch in a 100°C oven for 10 minutes) and by cooling it to room temperature. If this is not done, the texture change is permanent in the nematic phase. Even after restoration via heating, we could again destroy the LC order with voltage.

It is not clear why destruction of wall anchoring occured in the SiO cell. We did not see this in prior devices, but those had uniform electrodes, unlike the present devices in which "accentuated" E-fields are present at the boundaries between bare and conductive areas. (The bunching of field lines at electrode edges and corners may trigger the texture change).

It might be possible to operate an SiO-treated switch by imposing a 40 V "ceiling" on its operation. But that ceiling is close to the actual operating voltage (Section VIII below) and there would be little margin for

error. Thus, from the above experiment, we conclude that the SiO surface treatment is not acceptable for our switching matrices and that an alternative method is needed.

For many years, almost from the beginning of LC technology, the simple (but not well understood) technique of rubbing the electroded surfaces has done a good job of orienting LC molecules in planar arrays. Because of the secure anchoring forces that are offered, we felt this method would be a good one to use here, and our tests confirmed this.

Some workers deposit polyvinyl alchohol on a surface and stroke it with a clean cloth or piece of paper to produce the LC anchoring. Similar results are produced with the simpler expedient of rubbing an ITO surface with a cotton swab. This is "unscientific" because it involves manual manipulation, but the consequences of rubbing are quite reproducible and are therefore useful. LC order is believed to be caused by the linear mechanical disturbance (microgrooving) of an organic impurity-film deposited on the surface by the swab.

We tried unidirectional rubbing on the N x N switches with good results. After photoetching of the A/B ITO layers, we stroked the surface in one direction in a parallel raster of strokes. We used three different Q-tips and rubbed for 45 seconds on each prism. An added benefit of rubbing is to smooth out microscopic point defects on the ITO film that act as E-field singularities. High-field application did not change the LC texture in any of our rubbed devices, and the LC always reverted to planar order after field removal.

VI. DEVICE SUMMARY

Table 1 summarizes our results on the first five switching devices with respect to three technical problems that we encountered: 1) a permanent change in LC texture due to application of 7 V/μm rms fields, 2) nonuniformities in the thickness of the LC layer, and 3) the presence of an unwanted conductive ITO border around the 3 x 3 or 4 x 4 electrode pattern

Table 1. Results on 3 x 3 and 4 x 4 half-matrix switches with SF14 glass, E9 liquid, and ¼-mil teflon spacers.

Switch	Surface Treatment	LC Texture Change?	Uniformity of LC Layer	Unwanted Conductive Areas?	Estimated LC Layer Thickness
3 x 3 x ½ - A	SiO at 60°	Yes	Good	No	6 to 8 μm
3 x 3 - ½ - B	Rubbed	No	Fair	No	6 to 9 μm
3 x 3 - ½ - C	Rubbed	No	Fair	No	6 to 10 μm
4 x 4 - ½ - A	Rubbed	No	Good	Yes	6 to 8 μm
4 x 4 - ½ - B	Rubbed	No	Poor	A Few	6 to 15 μm

that acts as a "high-resistance short-circuit" giving undesired electrical coupling between electrode elements. Unfortunately, none of these five devices combined a uniform LC layer with uncoupled electrodes - a deficiency that we hope to overcome in the Fourth Quarter. On the other hand, all 16 switching elements turned on in each device. Sample 2 x 3-1 had a special 90°-twisted order discussed in Section VIII.

VII. UNIFORM-LAYER PROBLEM

The LC layer thickness depends on prism spacing, and there are several reasons why the separation between the prism-A and prism-B surfaces can turn out to be non-uniform. The most obvious cause is inadequate flatness of the "plates." We specified that both surfaces be flat to within one wave over the ~3 cm x ~5 cm area, but do not know at present whether the vendor lived up to this requirement. Another cause is unequal tightening of clamping-screws in the assembly jig which prevents the top prism from sitting with equal pressure on the supporting spacers of teflon tape. Wrinkled tape is a third cause.

To determine whether clamping has been done properly, it may be necessary to examine the switch with monochromatic light before the LC is added, specifically to look at the optical interference pattern of the air-gap cavity between prisms A and B. This will be attempted during the Fourth Quarter. At present, our technique is mechanical rather than optical. In the assembly jig, we try to tighten the four nuts with equal force ("finger tight").

A. Interference-Color Results

When polarized white light is passed through a thin uniaxial liquid crystal layer, optical interference colors are observed due to the birefringence. This phenomenon is a useful diagnostic tool to determine whether the LC layer is indeed uniform in thickness. This was recognized nine years ago by ourselves (J. Appl. Phys., 43, 2029, (1972)) and by others. For example, in 1972, we correlated a yellow interference color

with a 6.3 μm layer thickness in a field-ordered planar film of MBBA ($\Delta n = 0.18$).

In our N x N switch, we can immediately detect non-uniformities in a dramatic visual fashion by placing the device between crossed polarizers in a beam of white light and by photographing the result. The device is illuminated through the large polished faces. Figure 3 illustrates our experimental set-up which takes into account refraction of the beam by the prism-shaped switch. A large-aperture f/2 lens images the LC layer onto an opal-glass screen for photography. The input light is polarized at 45° to the LC optic axis, and the analyzer is set at -45° (crossed). Figures 4,5, and 6 are color photographs (rendered here in black and white halftones) of the optical interference patterns from switches 3 x 3 - ½ - B, 4 x 4 - ½ - A and 4 x 4 - ½ -B. The LC in switch 4 x 4 - ½ - A exhibits good uniformity, whereas 4 x 4 - ½ - B shows very strong non-uniformities in the LC, particularly in the bottom area of the switch. We see in the 3 x 3 that the LC layer has a different thickness in the two end regions than the rest of the layer. This is discussed in Section VIII.

VIII. ELECTRO-OPTICAL PERFORMANCE

A. Electrical Control Technique

Because dc drive reduces the life of the LC, we used ac drive throughout. In theory, the LC turns on by an amount proportional to the rms value of the applied voltage waveform, so it should not matter whether a sine-wave or square-wave source is used. We found some violations of this principle in practice. For some devices, at a given audio frequency such as 2000 Hz, the square wave drive was 40% more effective than sine-wave drive on an equal-rms basis. We do not presently understand this, and plan to make further tests of the effect next Quarter. The tests described below were all done with square-wave control.

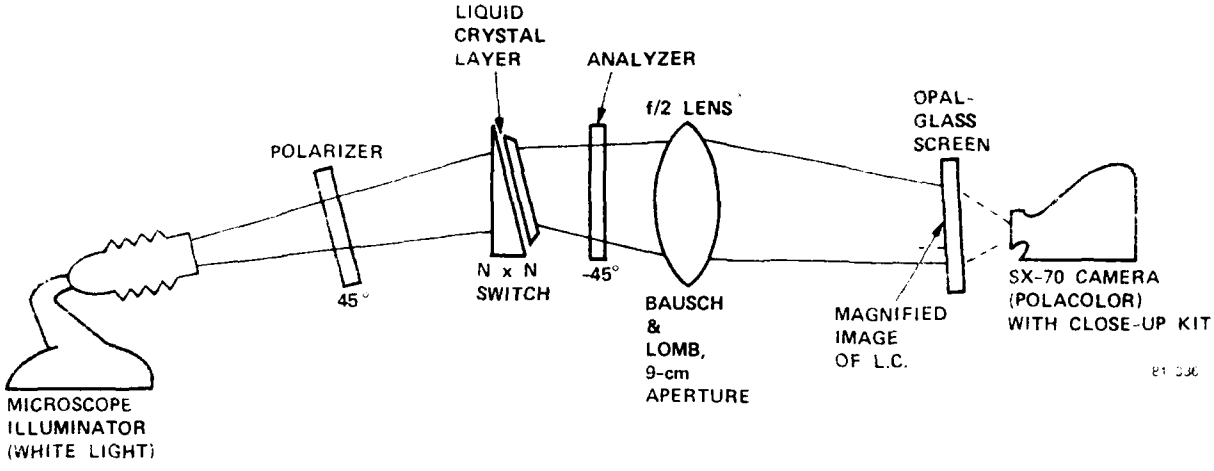

FIG. 3 Optical set-up for determining interference colors of LC film.

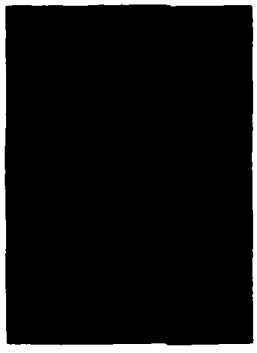

81-354

FIG. 4 Interference-color photograph of planar nematic liquid crystal layer in optoswitch 3 x 3 - ½ - B.

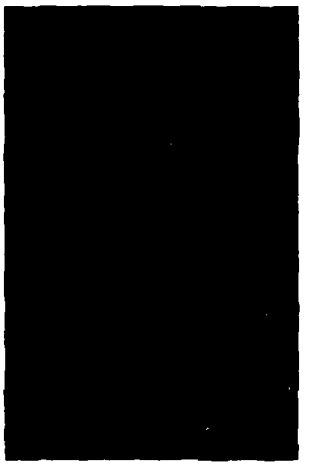

81-355

FIG. 5 Interference-color photograph of planar nematic liquid crystal layer in optoswitch 4 x 4 - ½ - A.

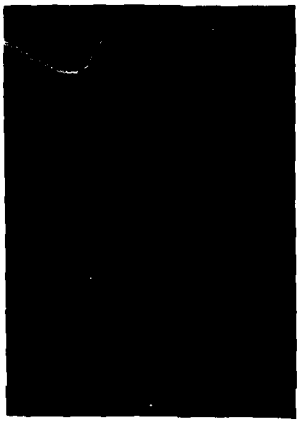

81-356

FIG. 6 Interference-color photograph of planar nematic liquid crystal layer in optoswitch 4 x 4 - ½ - B.

B. Tests on 3 x 3 - ½ - B

We determined the performance of this switch with a 1.2 mm-diam He-Ne laser beam (λ = 633 nm) polarized in the plane of incidence to provide 100% p-polarized light (this is the switched component). In a separate test, with s-polarized beams, we found the s-light was totally reflected by the LC irrespective of voltage, as expected. Unpolarized light is also totally reflected at V = 0.

This switch has three "rows" of addressable elements, so there are three locations where the light-beam can come into the switch, locations that are accessed one at a time in our initial experiments by moving the switch 5 mm laterally with respect to the fixed laser beam. Before two devices are assembled into a matrix, an individual device functions as a 3-fold 1 x 3 switch.

It is possible for light to enter the small facet of prism A. We call this the "forward propagation direction." Equally possible is the entry of light into the square face of prism B, whereby the beam can encounter any of three separate electrodes on the LC layer, depending on entry height. This arrangement is termed "reverse propagation." Figure 7 presents a side view of the experimental set-up for both forward and reverse propagation. In the first case, the beam undergoes five TIR bounces (with voltage off) before exiting the rear of prism A. With voltage applied, light is switched out from locations 1, 2, or 3 in parallel paths. For reverse propagation, there are three equi-spaced input locations instead of one. Here, with V = 0, the input beam bounces off the LC and penetrates the base of B. With voltage on, the beam passes through the LC, entering A where it travels to the A-output over a multi-bounce path.

Figure 8 presents the observed electro-optic turn-on characteristic of switch 3 x 3 - ½ - B. The switched optical output (the beam-power transmitted in a direction parallel to the input) is plotted as a function of rms control voltage. Curves are shown for light entering each

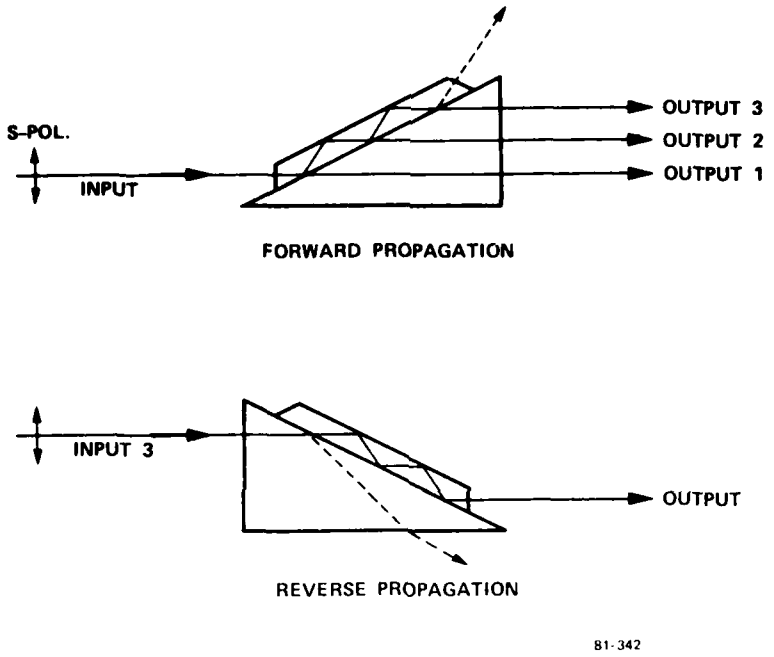

FIG. 7 Method of using one device for either 1 x N or N x 1 optical switching.

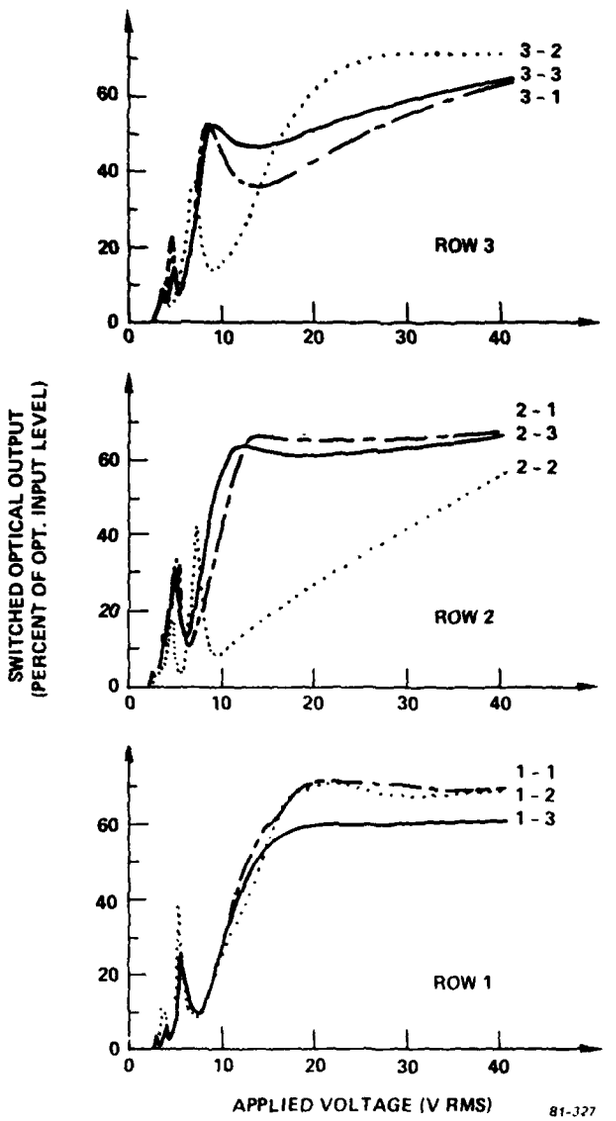

FIG. 8 Electro-optical response of switch 3 x 3 - ½ - B to 100% p-polarized light, $\lambda = 633$ nm. Switch has 66°-incidence on E9 liquid crystal, with Schott SF14 glass. Nominal thickness of LC is 6.3 μm. Voltage source is cw 400-Hz square wave.

of three rows of the switch. The rectangular electro-optic elements in a row were turned on one at a time with the results indicated. When one element in a row was addressed, all other elements were electrically connected to ground (the common electrode on prism B).

As is characteristic of tilted birefringent LC elements, the turn-on has several local maxima and minima at low voltage, near the threshold. This was seen in our earliest switches (Optics Letters, 4, 155, (1979)) that had the same LC orientation. One would expect the oscillatory initial response to be smoothed out when Selfoc lenses are added to the device. Then the turn-on should follow an averaged "envelope" response. By the time that 30 to 40 V has been applied, the response has closely approached its asymptotic value and has "saturated"; in particular, in Fig. 8, the response at 40 V for all nine elements is fairly uniform as would be expected from the interference-color result of Fig. 4. (Element 2-2 is in some sense "defective"). We see in Fig. 8 that the great majority of p-polarized light is switched, as expected. Since the SF14 prisms have a high index, the reflection loss at the air/glass interface is significant, specifically, this reflectance is $(1.76 - 1.00)^2/(1.76 + 1.00)^2$, or 7.6%, this Fresnel loss being taken twice in our laser-beam experiment at the input and output surfaces of the switch. Therefore, the ideal transmission of a laser-coupled switch is $(0.942)^2$, or 85.4%, which is the largest possible ordinate in Fig. 8. Normalized to the 85.4% level, the actual switched power ranged from 73% to 85% of the ideal transmission for the nine elements in Fig. 8 at 40 V applied.

C. New LC Orientation

As a brief digression, we examined the effect on 1 x N switching of a different LC orientation, the 90°-twisted nematic order. In a 1980 RADC Contract Report, we stated a hypothesis concerning the oblique incidence of light on a twisted LC layer. If light impinges on the LC at an angle beyond the critical angle of the glass/LC sandwich (for example, 70°), we asserted that the electro-optic turn-on characteristics of such a device would be quite similar to those of switches with the planar

(0^{o}-twist) LC order. (Note that this oblique-incidence device differs markedly from the familiar wristwatch display). We anticipated that both s- and p-light would be totally reflected at V = 0, that only p-light would be switched, and that it would take a large multiple of the threshold voltage (rather than 3 V) to turn the switch on completely. During this Quarter, we performed a brief experiment that confirmed these predictions.

A 3 x 3 half-matrix switch, SF14/E9, was prepared with a 1/4 mil thick 90^{o}-twisted LC layer (V = 0) achieved by rubbing prism A at 90^{o} to the rubbing direction on prism B. The orientation of the LC at low and high voltages are shown in the side view diagrams of Fig. 9. With a cw 400-Hz square wave applied, the electro-optic transmission of this switch had the behavior shown in Fig. 9. Rather than showing results for all nine elements, we present in Fig. 9 the transmission measured for a "typical" element (first element, third row) and show what happens in both the forward and reverse propagation directions. The general behavior followed our theory (100% s/p reflection at zero voltage, p-switching, and a close similarity between forward and reverse switching) but we found that the turn-on was smooth and that this turn-on was more gradual than in the planar LC case. The Fig. 9 switch might be useful when one wishes to avoid an oscillatory turn-on, but because the 0^{o}-twist switch reaches its final throughput at lower voltages than the 90^{o}-twist switch, the former is probably preferable in a matrix switch.

D. Results on 4 x 4 - ½ - B

Returning now to our planar-LC half-matrix switches, we shall present experimental results for our early 4 x 4 - ½ devices. As indicated in Table 1, device 4 x 4 - ½ - A had an unwanted border of conductive material that coupled various elements, making it impossible to turn on all 16 elements on an individual basis (some were excited in pairs and trios). This is unfortunate because the LC film in 4 x 4 - ½ - A is considerably more uniform in thickness than that in 4 x 4 - ½ - B. However, switch 4 x 4 - ½ - B offered individual control of the 16 elements and its performance was therefore measured.

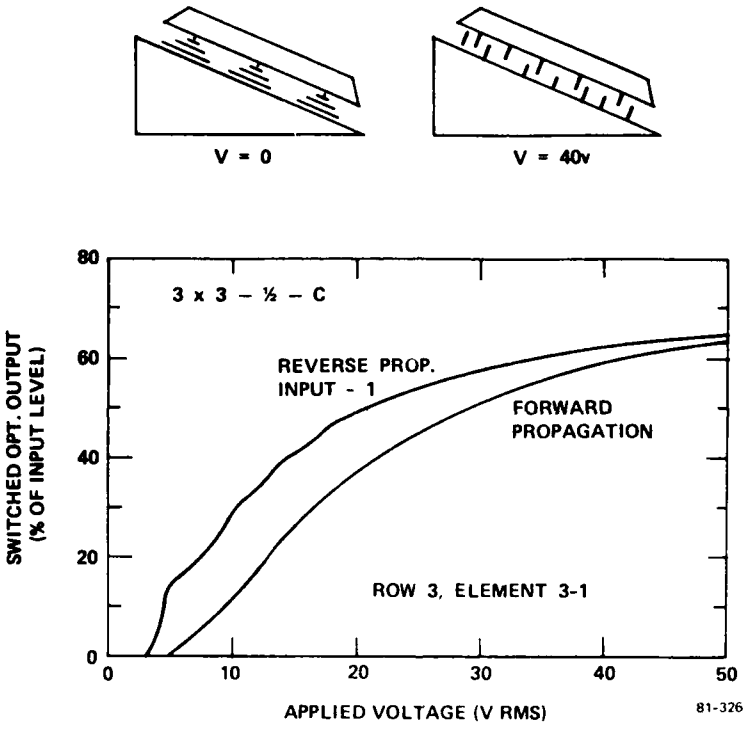

FIG. 9 Electro-optical response of switch 3 x 3 - ½ - C with 90°-twisted LC. Same conditions and specifications as Fig. 8.

Figure 10 shows the voltage-controlled optical output of switch 4 x 4 - ½ - B with 633 nm laser light entering each of four rows in succession. Results are given for the four elements in each row. As discussed above, the maximum possible throughput is 85.4%. The switching performance of each element is directly affected by the LC film thickness (d) at each location. Judging from Fig. 6, the LC film thickness increases significantly at the bottom of each row, especially in row 1 where element 1-1 has an LC thickness of perhaps 15 μm. The situation is similar for elements 2-1 and 3-1 for which we estimate d = 12 μm and d = 10 μm, repectively. Row 4 has the best uniformity of the rows, with 4-1, 4-2, and 4-3 all having d ~ 6 μm. The thickness variations discussed here show up rather dramatically in Fig. 10 where we find that the turn-on of element 1-1 is quite slow, with element 2-1 going somewhat faster, and 3-1 faster still. The weak turn-on of element 2-3 was due to the partial turn-on of 2-1 with 2-3, and the slow rise of 3-2 occurred because of unwanted coupling between 3-2 and 3-1. Apart from these problems, we see a fairly consistent, repeatable turn-on from row-to-row and element-to-element. It is gratifying that the turn-on curves have the same quasi-stepfunction shape of Fig. 8. The row 4 curves are closely bunched as desired, and the curve shapes are similar for 1-2, 1-4, 2-2, 2-4, 3-3, 3-4, 4-2, 4-3, and 4-4, with the switched optical power ranging from 67 to 76% of ideal throughput at 40 V applied. If the LC had been as in Fig. 5, it seems fair to conclude that the response of the Fig. 10 switch would have been step-like and uniform for all 16 elements.

The threshold is 2.5 V in Fig. 8 and 4.5 V in Fig. 10. Below threshold, the intensity of transmitted light (crosstalk) is extremely low. Crosstalk will be measured during the Fourth Quarter.

To conclude this Section, we present a set of four photographs showing the 4 x 4 - ½ switch in operation. Figure 11 is a close-up of the switch with its 17 electrical control leads attached. Figure 12 is a similar view taken with low room-illumination showing a red laser beam entering from the left. The beam undergoes five internal reflections in

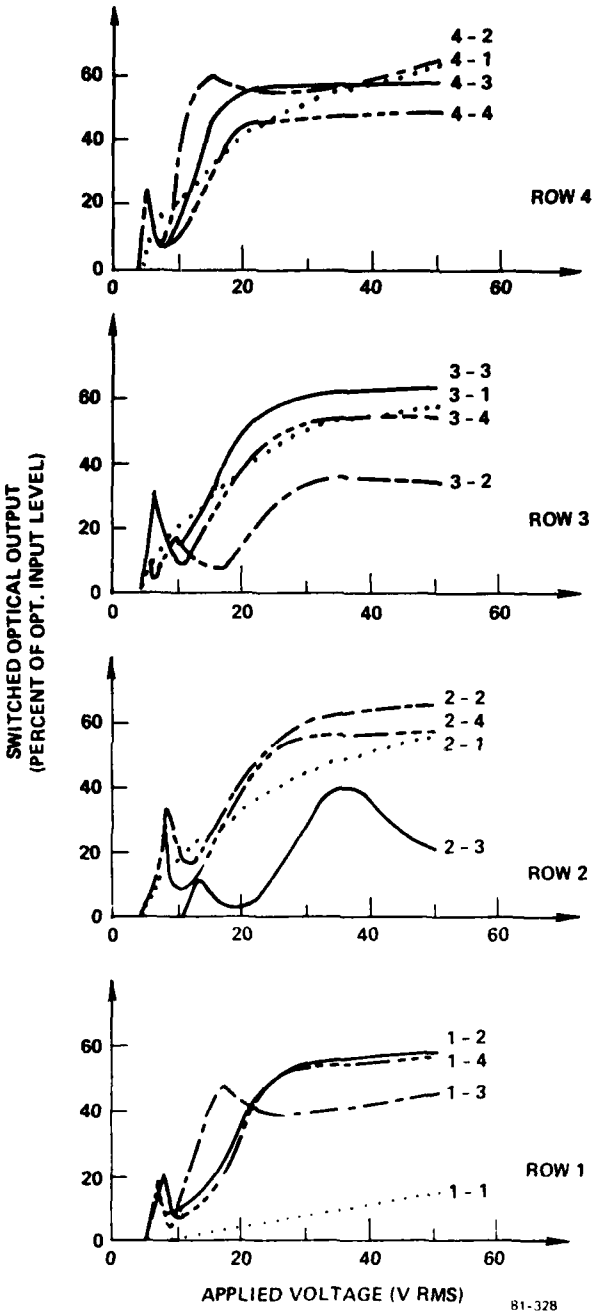

FIG. 10 Electro-optical response of switch 4 x 4 - ½ - B. Same conditions and specifications as Fig. 8, except that voltage is 1300-Hz square wave.

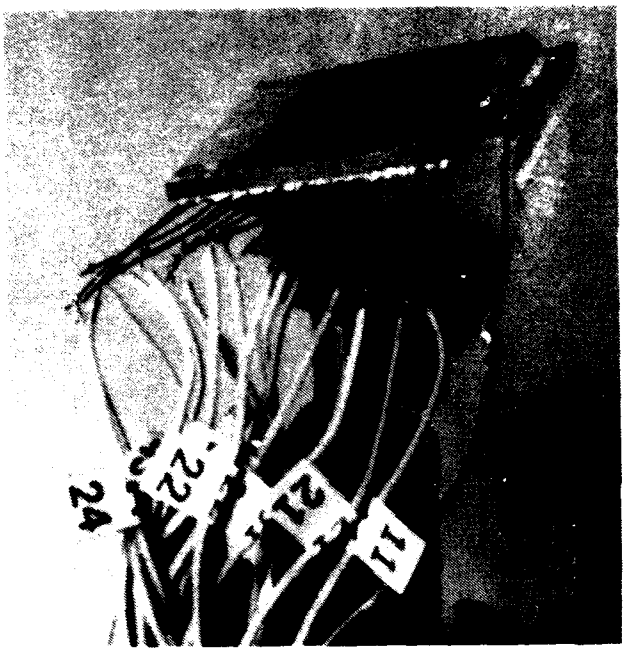

81-350

FIG. 11 Experimental model of 4 x 4 - ½ switch.

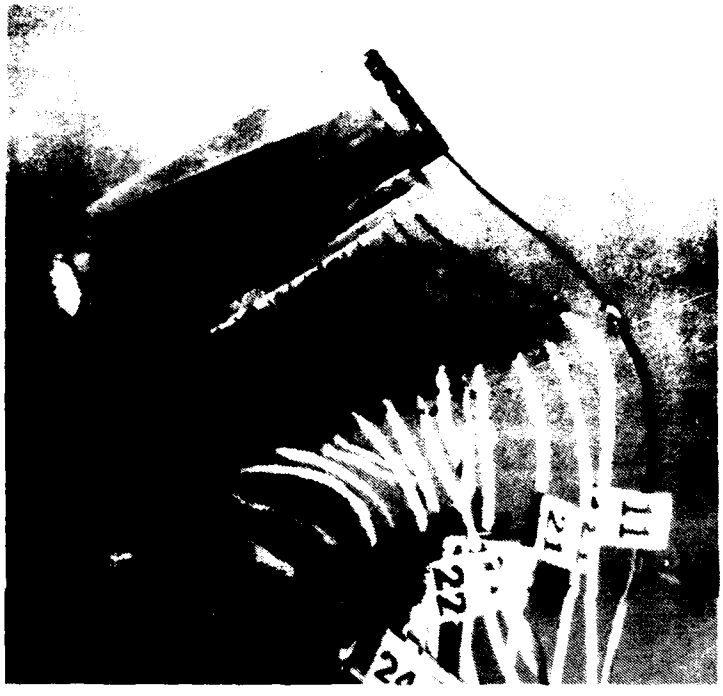

81-351

FIG. 12 Same as Fig. 11, except that the optical path in prism A has been highlighted.

succession as it travels within the switch. Figure 13 shows an end-on perspective of the device in which a portion of the optical beam has been switched out of each of four elements in row 2. The four output beams are seen in Fig. 13 on a screen placed at the rear of the switch. Figure 14 again illustrates 4-way switching, but here the camera is aimed at the output surface, the square face of prism B. Also visible in the photo are the laser source (at the left) and the viewing screen (at the right).

IX. Plans for Next Quarter

During the final Quarter of this contract, we plan to assemble four 4 x 4 - ½ switches and one 3 x 3 - ½, hopefully with better control over the LC thickness. The best of these will be coupled to fiber/lens pairs. We shall ascertain ways of mutually aligning several fiber/lens assemblies along optical paths in the switch. After determining suitable alignment techniques, the complete matrix, the "optical PBX", will be assembled and tested.

FIG. 13 Experiment showing 4 position electro-optical switch using Eq. 11 device

81-353

FIG. 14 Electro-optic switching viewed from output-end of 1 x 4 switch.

APPENDIX A

LIQUID CRYSTAL SWITCHING TECHNIQUES

The purpose of this Appendix is to survey the possible LC switching techniques, and to contrast the two principal techniques that have been used.

Switching techniques are based on the known electro-optical effects in LC materials. After surveying the LC literature, we have selected six candidates: 1) frustrated TIR from oblique incidence on a uniaxial field-effect LC, 2) polarization-rotation by a twisted-LC, plus external beamsplitters, 3) optical scattering from dynamic scattering or from a cholesteric-nematic phase change, 4) selective absorption from dichroic dye molecules dissolved in a LC, 5) refraction by a wedge-shaped layer of birefringent field-oriented LC, and 6) refraction by a bistable-texture LC.

The first two effects are our "favorites", as we have discussed in QSR-1 and QSR-2. At present, we feel that the last four are not suitable for low-loss N x N switching. Taking these in turn, we judge the scattering effects to be overly lossy because it is not obvious how to capture a large portion of the off-axis scattered beam for transmittal to an output port. With regard to absorptive effects, one could imagine a loss-modulation approach in which an LC shutter would block a portion of an optical beam that had been spread out spatially with a cylindrical lens. But in a 1 x N switch, the optical throughput would be only 1/N, which is too low. Refractors have two drawbacks: the refraction angles are very small in practice, and transmission losses through a portion of the refractor would be high since one LC region is typically 25 μm thick. With regard to bistable-anchoring reported recently, the switch could remain indefinitely in either state without electrical sustaining power, an appealing feature. On the other hand, from data presented thus far it is not obvious how one would obtain low-loss wide-angle deflection of light beams from the bistable texture change.

Over the past two years, we have tested numerous switching structures that rely on the first two electro-optic effects: frustrated TIR, and polarization rotation. The TIR effect has the advantage of using fewer optical components, and the TIR structures are generally simpler and less costly. But there are trade-offs. The rotation-type switches operate at noticeably lower voltages, and all of the parts are designed for normal incidence, which simplifies some aspects of manufacturing. The choice between these two approaches depends upon economic constraints as well as the detailed technical requirements of the optical network under consideration.

We have found that 30 to 40 V is usually needed for complete turn-on of the oblique-incidence switches. Here, the LC layer is typically 10 λ thick. In principle, it is possible to reduce the control voltage into the 5 to 10 V range by reducing the LC layer-thickness to some value in the 2 λ to 4 λ range, but this is technologically difficult.

Switching devices may be classified according to whether they switch one or both polarization-components of the fiber light, and as to whether the switching structure is simple or compound. The term "compound" means that each light beam passes through two switching operations (sub-switches) before reaching an output port of the switch. This classification scheme applies to either electro-optic effect. Based on the above categories, we have summarized in Table A1 the work that has been done from 1974 to the present. The Table lists proposed switching structures (designs) as well as actual switches that have been demonstrated. References are also given in Table A1 that explain more about each of the specific devices. Table A1 also distinguishes between two types of planar texture. Recall that the LC director is parallel to the prism A/B surfaces in the planar state. We have defined two categories, planar-longitudinal and planar-transverse, both of which have been tested. For planar-L, the director lies in the optical plane of incidence, while for planar-T, the director is perpendicular to the incidence plane. The texture in Table A1 is planar-L unless marked otherwise.

Table A1 Switch designs and actual switching devices implemented during 1979-1981 at SRC

Switching Technique	Simple Structures		Compound Structures	
	1-polarization switching	2-polarization switching	1-polarization switching	2-polarization switching
90°-twisted-nematic LC order, normal incidence, polarizing beamsplitters, ~3 V operation.	1 x 4 multi-way 1 x 6 multi-way 1 x 8 multi-way (ref. e) 4 x 4 matrix (ref. e)	2 x 2 reversing * (Bell Labs) (ref. a)	4 x 4 matrix (dual array) (ref. e)	2 x 2 bypass * (ref. b) 2 x 2 reversing (ref. d) 3 x 4 matrix (ref. d)
planar LC order, oblique incidence, ~30 V operation	2 x 2 tap/feed * (ref. f) 1 x 3 multi-way * 1 x 4 multi-way * (refs. c, d, e)	2 x 2 reversing *# (ref. g)	4 x 4 matrix (dual array) (refs. c,d,e)	2 x 2 bypass # (ref. b) 2 x 2 reversing (ref. d)

* an experimental model was tested

\# planar-T texture

a. R. Wagner & J. Cheng, Appl Opt., 19, 2921 (1980)
b. unpublished report, R. A. Soref
c. QSR-1
d. QSR-2
e. this report
f. Opt. Lett., 4, 155 (1979)
g. Opt. Lett., 5, 147 (1980)

APPENDIX B

LOW-VOLTAGE 1 x 4, 1 x 6 AND 1 x 8 OPTICAL SWITCHES

The purpose of this Appendix is to present new designs for low-voltage multi-way switches that are fully compatible with TTL control circuits and other semiconductor IC logic circuits. We have not tested these multi-way structures but are confident that they will perform as planned because related 2 x 2 structures have been tested successfully.

The 4 x 4 opto-matrix of this contract is a combination of 1 x 4 switches that require 30 or 40 V for operation. The same 1 x 4 function can be performed with a lower voltage technique (albeit with more pieces of glass), namely the 3 V twisted-nematic polarizing-beamsplitter approach, and we shall show how this is done.

There is fairly close analogy between the designs of the 3 V and 30 V switches. The 30 V 1 x 4 switch of this contract is a succession of optical 1 x 2 branching operations performed on a beam of light. The technique proposed in this Appendix is also a branching process, except here we use a symmetrical switching "tree" well-known from the electrical switching art. In this tree, each stage doubles the number of optical outputs, and it is a simple matter to extend the number of optical outputs from four to eight, for example.

Like the 1 x 4s on this contract, the 3 V devices switch only one polarization component of the unpolarized fiber light entering the switch. This means that the 1 x N multiway switch will have 3 dB insertion loss in principle, and a 4 or 5 dB loss in practice due to additional losses from Selfoc-Selfoc coupling and from other factors. If we demand a fairly complex switching function, such as 1 x 8, the one-polarization switching will not be such a drawback. Then, the value of an 8-way network switch may outweigh the 4 to 5 dB loss, or at least make one willing to trade loss for complexity. Therefore, we think it is worthwhile to present a design

for a 3 V 1 x 8 switch that can be realized with a very simple structure.

Our concept for a 1 x N switch is illustrated in Figs. B-1 and B-2. Here, the optical components are polarizing beamsplitters for separating s- and p-polarized beams by 90°, right-angle prisms for deflecting internally either beam by 90°, and a 3 V, 90°-twisted-nematic LC cell for rotating the optical polarization plane by 90° at V = 0 (s → p and p → s) or for transmitting the light without rotation at 3 V applied (s → s and p → p). The transparent electrodes that bracket the liquid crystal layer are segmented into several areas for independent voltage control. Looking at the 1 x N trees of Figs. B-1 & B-2, we note that $N = 2^{M}$, and that there are M layers LC, plus (M+1) stages of beamsplitters (PBs). The unpolarized input light in Fig. B-1 is first converted into a totally polarized p-beam by PB-1 that "throws away" the s-light. Then the first LC converts the retained beam to s or p, the first optical branching. The second PB/prism sends s or p light into parallel paths to the next LC. Then, LC-2 provides optical branching on either of its two inputs (s → s or s → p, and p → s or p → p), a symmetric process that yields a total of four possible outputs spatially separated in parallel fashion by a third stage of PBs/prisms.

Extending this concept to the 1 x 8 in Fig. B-2, we see there are three LC layers and four PB stages, with two-fold additional splitting arising from the last LC/PB. The third PB stage has two isotropic glass cubes that serve to separate output beams by an amount appropriate for the next stage. All components are of the same size, and all optical paths lie in one plane (so the switch is also planar). The number of independent voltage-controlled areas are: one in LC-1, two in LC-2, and four in LC-3.

The structures of Figs. B-1 and B-2 are somewhat "clumsy" in their use of multiple LC layers. From a practical standpoint, it would be much better to require only one layer of LC, thereby simplifying construction and lowering costs. We have found a way to do this. Our technique uses three ideas: 1) the optical path is "folded" in zig-zag fashion, 2) LC-2 and LC-1 are placed side-by-side in the same plane to capture the meandering light beam, and 3) the first PB serves a double purpose; an input splitter and a

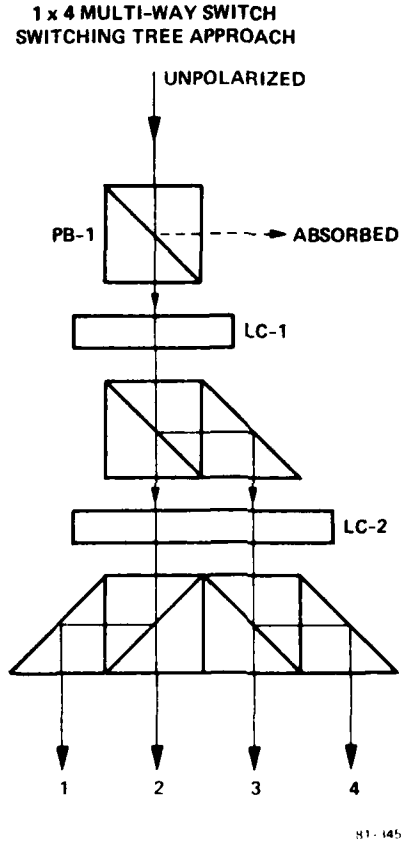

FIG. B-1 Multi-way 1 x 4 electro-optical liquid crystal switch based on switching-tree approach.

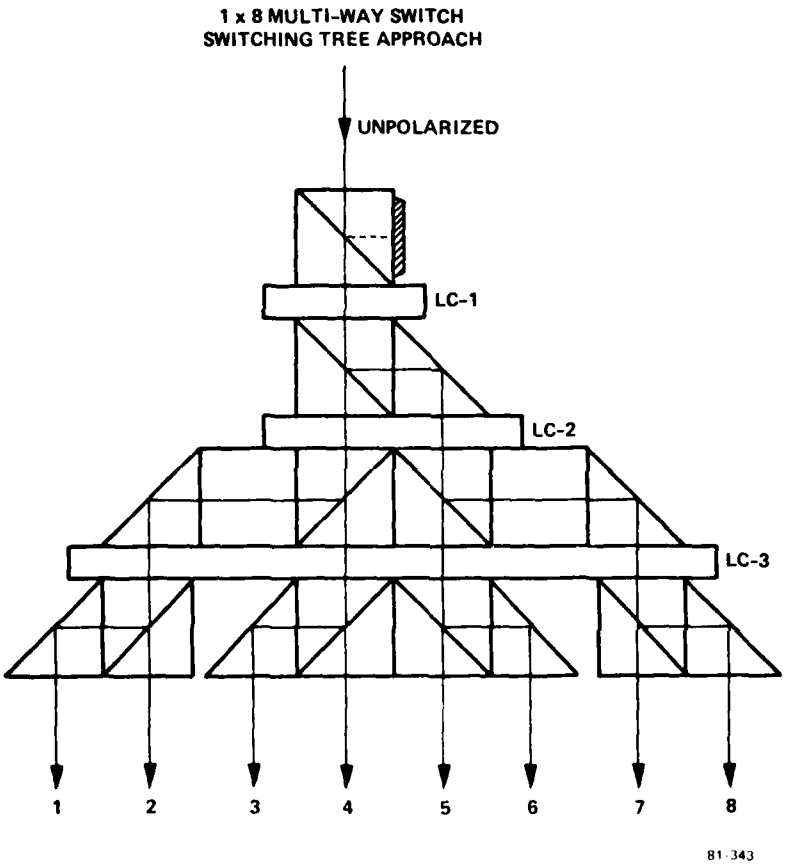

FIG. B-2 Multi-way 1 x 8 electro-optical liquid crystal switch based on switching-three approach.

third-stage splitter. These ideas are applied below.

Figure B-3 illustrates our new way to make a 3-V 1 x 4 switch with only one LC layer (a side view of the planar structure). Multimode light enters the side of the first PB as shown in a direction 90° with respect to the output direction. Half of this light is reflected upward through the first region of the electrically active LC cell (that has three separate regions) and the other 50% travels horizontally through the next PB into an absorptive region between the second and third PBs where that light is "lost."

The first LC region operates on the deflected half-beam with two possible results shown optically by the solid and dashed rays in the upper portion of the switch. These two polarized beams have their polarization state acted on by the second pass through the same LC, either region 2 or 3.

Examining this 1 x 4 structure in detail to see how light is switched to each of four output positions, we illustrate in Fig. B-4 four possible addressing conditions for the LC cell, (0° or 90° in region 1, 2, and 3) with the resulting optical beam paths indicated. The top drawing in Fig. B-4 shows the 0°, 0°, 0° rotation state of the LC layer, corresponding to the applied voltage state (3v, 3v, 3v). Here, the light remains in the s-state through four successive PB reflections and emerges from port 1 as shown. The second drawing shows what happens for 0°, 90°, 90° rotation, or (3v, 0v, 0v) applied. Here, the beam changes from s to p in the second LC region and is transmitted through the next PB, exiting from port 2. The third drawing illustrates 90°, 90°,0°, the (0v, 0v, 3v) state in which we get an s → p change, sending the beam to the upper right TIR prism, followed by a beam exit througn port 3 (the state of LC region 2 is irrelevant here). A similar thing occurs in the fourth drawing where the region-2 state does not influence the result. Here, the LC has 90°, 90°, 90° rotation, or (0v, 0v, 0v), and the beam shifts from s to p, with a second p → s change that conveys the beam to the fourth output. Note that the state of region 3 was not relevant in the first two drawings.

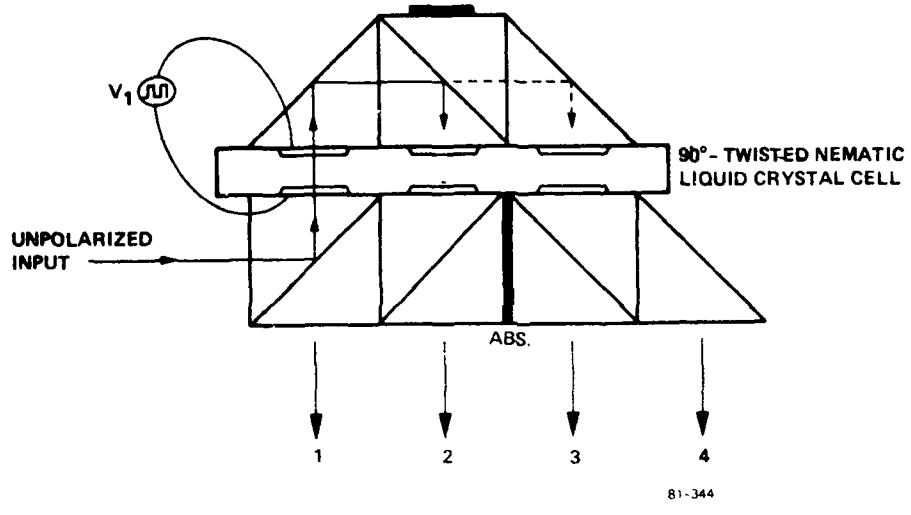

FIG. B-3 Compact 1 x 4 optical switch using only one LC layer.

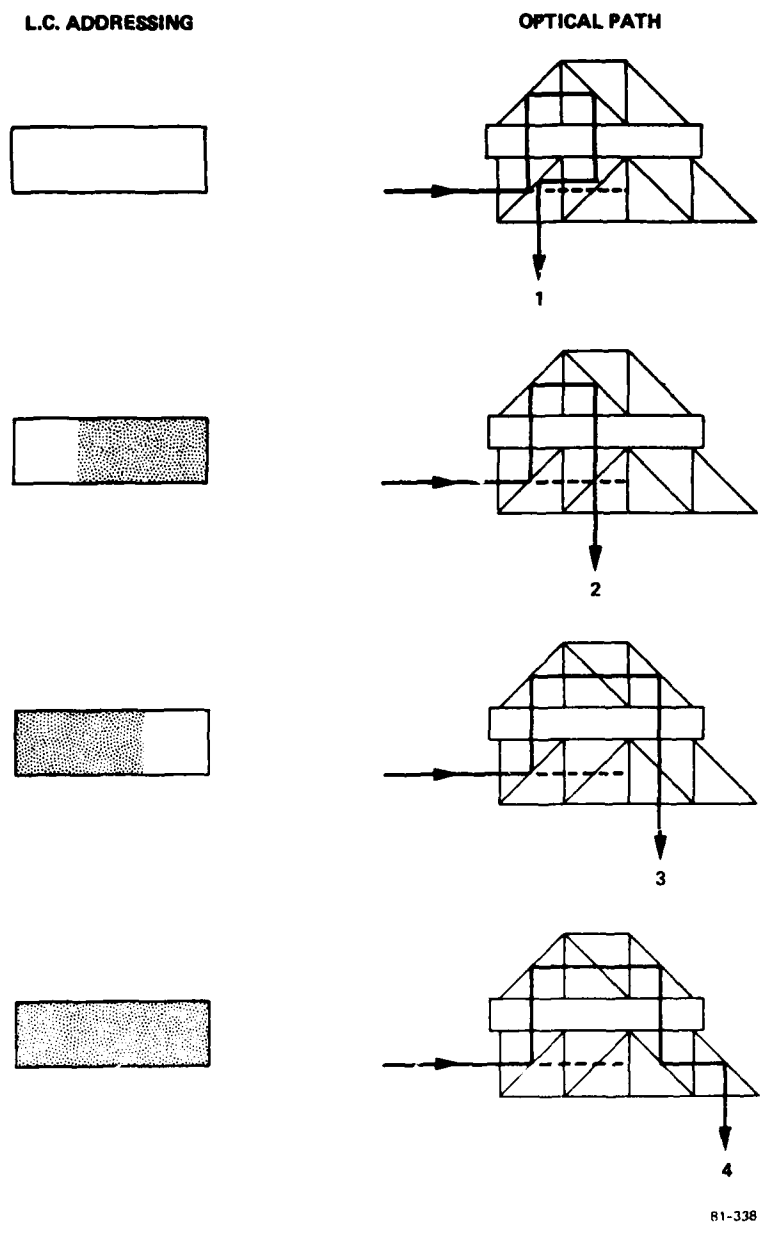

FIG. B-4 Four-position optical switching resulting from voltage-addressing states #1 through #4.

AD-A113 812 SPERRY RESEARCH CENTER SUDBURY MA F/G 20/6
DESIGN AND FABRICATION OF MULTIMODE OPTICAL SWITCHES.(U)
MAR 82 R A SOREF F19628-80-C-0147
UNCLASSIFIED SRC-CR-81-54 RADC-TR-82-22 NL

With regard to optical crosstalk levels at the switch's outputs, we would expect the 1 x 4 to have a crosstalk performance of approximately -20 dB at each port, which is the average s + p extinction ratio of a high quality PB.

Since each LC region has two states, there are actually 2 x 2 x 2 = 8 addressing possibilities, four of which have already been discussed. The remaining four conditions are shown in Fig. B-5. By noting the polarization state of the beam as it passes back and forth through the voltage-controlled LC in Fig. B-5, we can trace the set of beam deflections and will find that light can emerge from any one of the four ports as shown.

An 8-way version of this switch would be more valuable than the 4-way because the 8-way insertion loss would be nearly the same as that of the 4-way (see our earlier remarks about one-polarization switching). The question now arises: Can we make a 1 x 8 switch with only one LC layer? After some trial and error, we thought of a way to construct a one-layer 1 x 8 as follows: first the input beam is split into s and p beams; second, one of those two beams is "blocked" after traversing the LC; third, either beam is sent to a separate 1 x 4 switch; fourth, both independent 1 x 4s are located side-by-side within the same set of optical components; and fifth, the two input optical paths are folded so that they will pass through the same LC plane as the 2-fold 1 x 4 LC plane.

In the aforementioned paired 1 x 4 switches, the parallel input beams are separated by a distance that is approximately equal to 50% of the PB cube dimension. Thus, it is necessary to make the first PB in the 1 x 8 approximately half the size of the other PBs in order to insert the s and p beams properly.

Taking the above ideas into account, we arrived at the compact design for the 1 x 8 multimode optical switch shown in Fig. B-6. Only one LC twist cell is needed and its transparent control-electrode film is divided into eight independent areas as shown, corresponding to the 1 + 2 + 4 decision points in Fig. B-2. The structure is planar and the optical

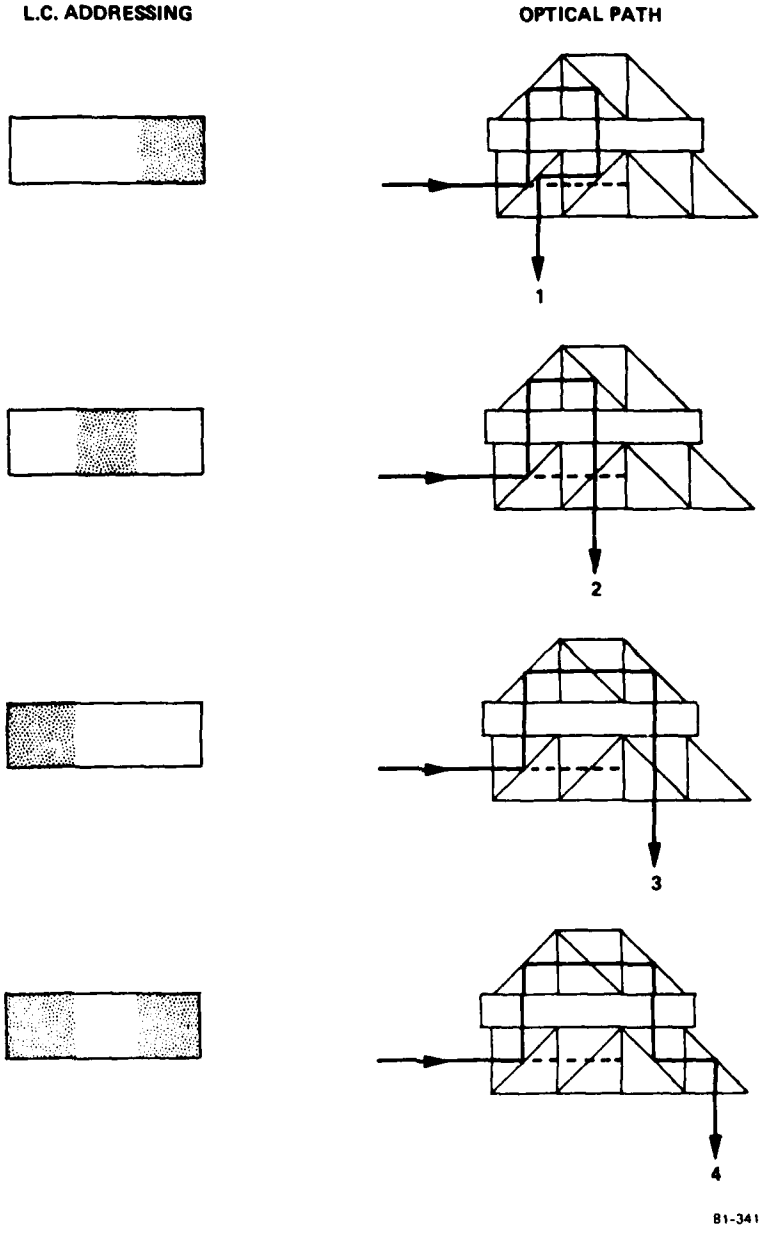

FIG. B-5 Four-position optical switching resulting from voltage-addressing states #5 through #8.

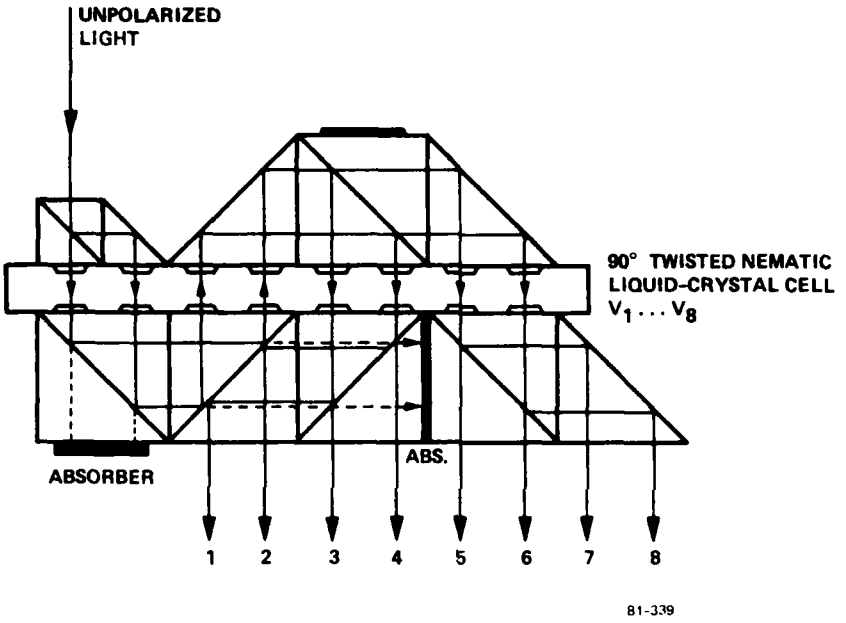

FIG. B-6 Compact 1 x 8 optical switch using only one LC layer.

outputs are conveniently arranged in a parallel array. As in Figs. B-4 & B-5, operation of switch B-6 may be understood by ray-tracing with a similar 3-V or 0-V addressing. The optical components-count here is 5 PBs, plus 6 prisms.

We have also devised a 1 x 6 opto-switch related to the 1 x 8. Figure B-7 presents the structure of a compact, planar 1 x 6 switch that has a smaller parts-count than the Fig. B-6 1 x 8 switch. The 1 x 6 contains a twisted-nematic LC cell divided into 6 independent regions. As in Fig. B-6, the operation of Fig. B-7 begins with a division of the fiber-optical beam into s- and p-polarized components, labeled a and b in Fig. B-7 (each of which traverses the LC and the second PB). As in Fig. B-6, one of these beams is kept and the other is absorbed in the shaded region, depending upon the states of the first two LC compartments. Next, the retained beam passes twice in meandering fashion through the LC and thereby undergoes two optical branching operations. Because one branch is kept inside the switch, there are three outputs for beam-a or beam-b (rather than four outputs). Here, the optical components-count is: 4 PBs and 3 prisms. A disadvantage of Fig. B-7 is that the outputs are arrayed on three sides of the switch, rather than one.

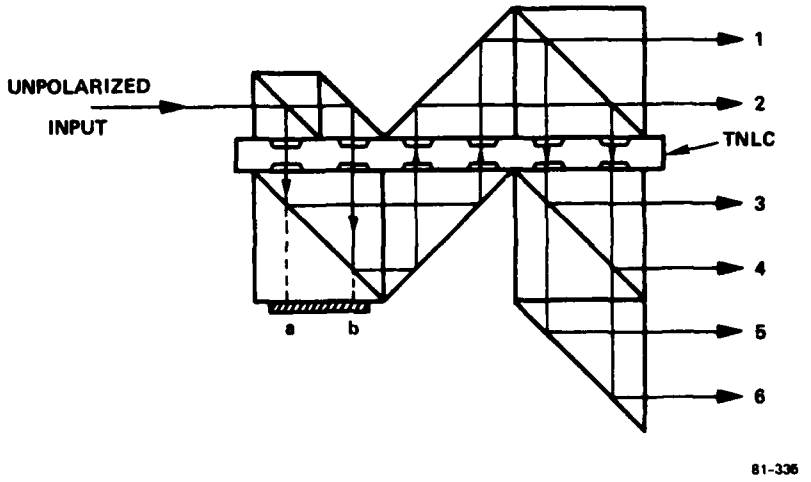

FIG. B-7 Compact 1 x 6 optical switch using only one LC layer.

APPENDIX C

LOW-VOLTAGE 4 x 4 MATRIX SWITCH (DUAL ARRAY)

This Appendix presents a new design for a 4 x 4 optical PBX that operates from a 3 V supply. There is a direct analogy between the 30 V oblique-incidence structures and the 3 V normal-incidence structures. Just as we applied dual-array principle to make a 30 V 4 x 4 matrix from a pair of 4-fold 1 x 4 switches, we can do the same thing in the 3 V case.

We saw in Appendix B how to make a low-voltage 1 x 4 switch (Fig. B-3). This same device serves as a 4 x 1 switch if the propagation is reversed as in Fig. 7 of this report. Since the Fig.-B-3 switch is an in-plane device, we can easily stack four 1 x 4s in parallel planes as indicated in Fig. C-1, where one twisted-LC layer handles all four multi-pole switches (there are 12 independent voltage-addressed areas in the LC). The Fig.-C-1 switch requires four times the number of optical components (PBs/prisms) or the same number of 4x-wide components as in Fig. B-3

Referring to the dual-array combination of Fig. 1 in QRS-2, we see immediately that we can combine two Fig.-C-1 switches to make a complete 4 x 4 optical PBX (matrix switch). This is shown in Fig. C-2. Here we have taken two identical Fig. C-1 switches and have joined them "back-to-back" after having rotated one switch 90° with respect to the other, so that the column-outputs of the first device are mapped onto the row-inputs of the second device.

This is a convenient structure because it requires only two LC layers, each of which is actuated by 3 V pulses. As in Fig. B-3, only one polarization in the multimode light is switched, but this loss tradeoff is tolerable because of the sophistication of the matrix. The 16 outputs of the Fig. C-1 submatrix have definite s/p polarization states. In order for the second submatrix to accept those 16 beam-polarizations properly, it is necessary to interpose a half-wave retardation plate, shown in Fig. C-2.

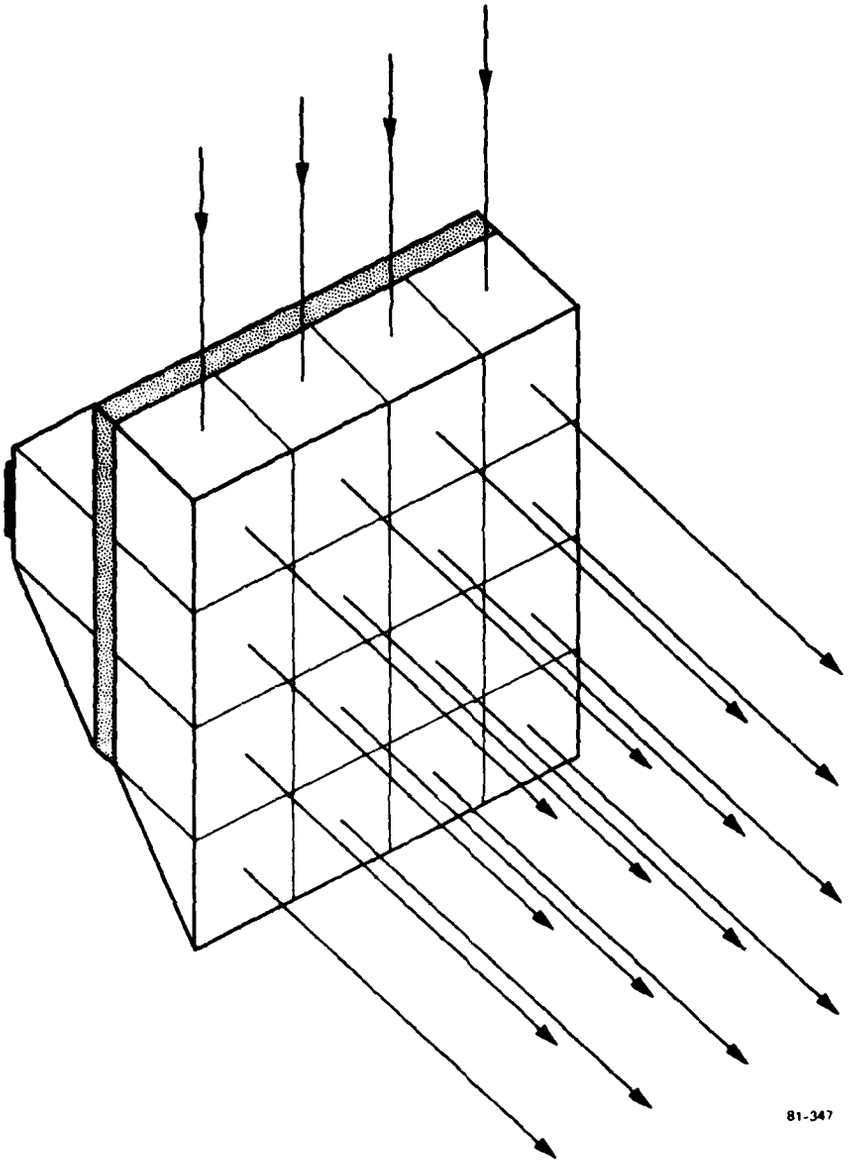

FIG. C-1 Four independent 1 x 4 optical switches stacked in parallel planes and controlled by one TNLC layer.

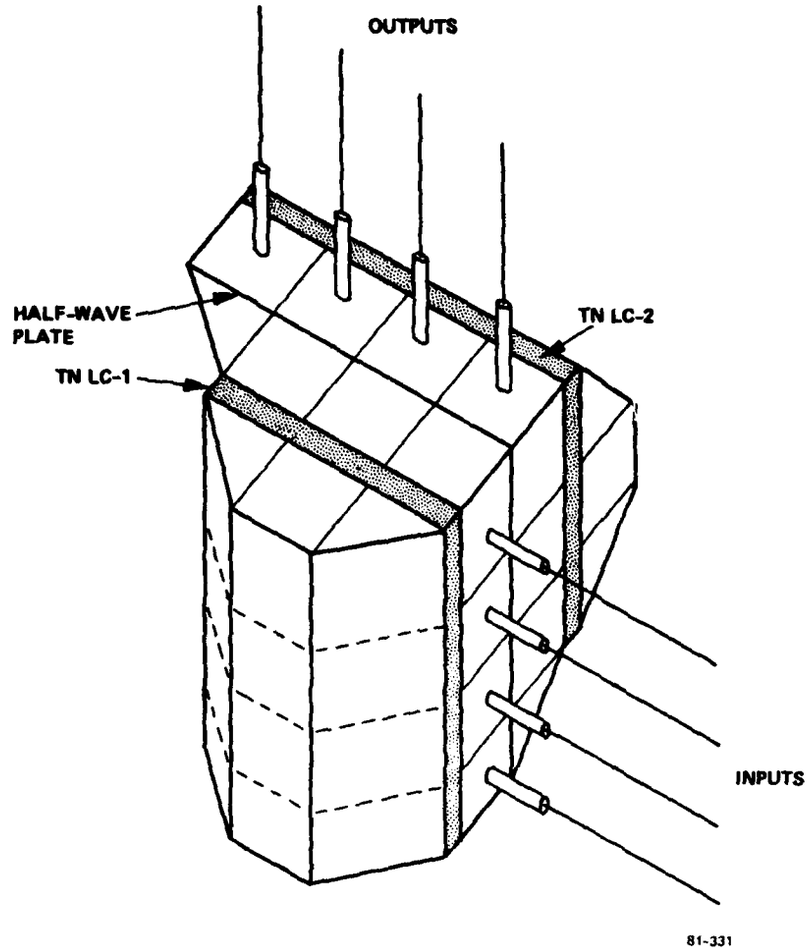

FIG. C-2 4 x 4 optical PBX controlled by two 3-volt LC layers.

between the two submatrices to convert s into p in 4 locations, and p into s in another 4 locations. We would anticipate the following performance for Fig. C-2: insertion loss of 4 dB on all paths, optical crosstalk of -40 dB at any output, control voltage of 3 V rms, and on/off response times of 10 to 100 ms. This PBX switch is a completely nonblocking optical network with 4! or 24 states. The only obvious disadvantages of this PBX are its cost and complexity. To save money, we could use "wide" components as in Fig. B-4 of QRS-2, but if this is not done, and if we assemble Fig. C-2 from "cubic" PBs, then we require 8x the number of parts in Fig. B-3, namely 32 PBs and 24 prisms.

APPENDIX D

IN-PLANE 4 x 4 MATRIX SWITCHES

This Appendix describes some simple matrix structures that have a limited number of states. Two designs are given here for a low-voltage 4 x 4 PBX that is simpler than Fig. C-2 but that has higher levels of crosstalk. Each 3 V matrix is contained within one plane, unlike the dual-array matrix.

Figure D-1 is a new strucutre for a 4 x 4 opto-matrix that is comprised of four 2 x 2 subswitches. A single liquid-crystal layer (90°-twisted orientation) controls the matrix and its ITO electrodes have eight independent segments. This is a 2-polarization switch, thus the matrix has low insertion loss. Unfortunately, Fig. D-1 is a "blocking" optical network that has only 16 distinct states out of the 24 that are desired for a 4 x 4 PBX.

We can, however, get a nonblocking network with a more elaborate version of Fig. D-1. We have designed a 3-stage Clos-type network comprised of six 2 x 2 switches optically interconnected, including two optical crossovers. Figure D-2 presents this new design for a 4 x 4 opto-matrix that has all 24 configurations of a "true" PBX. Both polarizations are switched, and the single LC layer has 12 control areas.

The problem with both Figs. D-1 and D-2 is that the expected optical crosstalk level is -20 dB at any output port, rather than -40 dB as in the dual-array structure of Fig. C-2. The Fig. D-1 and D-2 switches are essentially "permutation networks" comprised of 2 x 2 reversing switches. There is a full-strength crosstalk contribution at the last stage of the network, so the crosstalk performance is equivalent to that of a single-stage network.

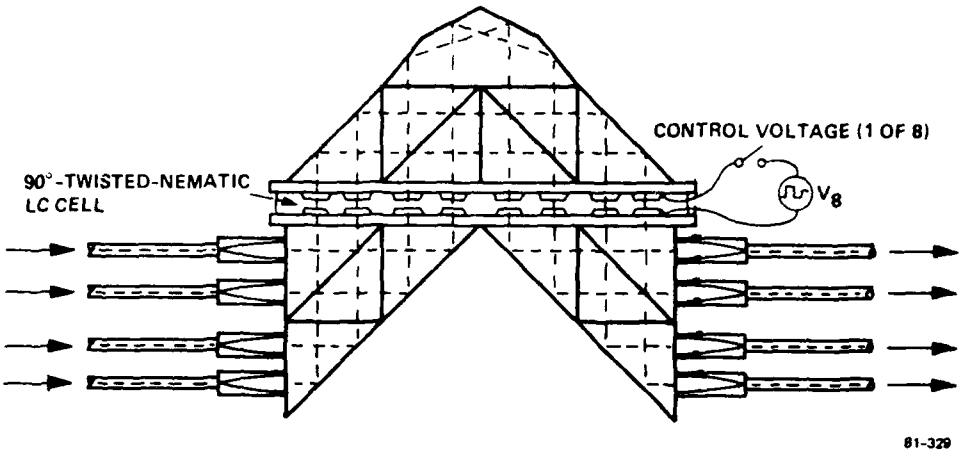

FIG. D-1 Planar 4 x 4 optical matrix switch actuated by one LC layer with eight regions. Switch has 16 states.

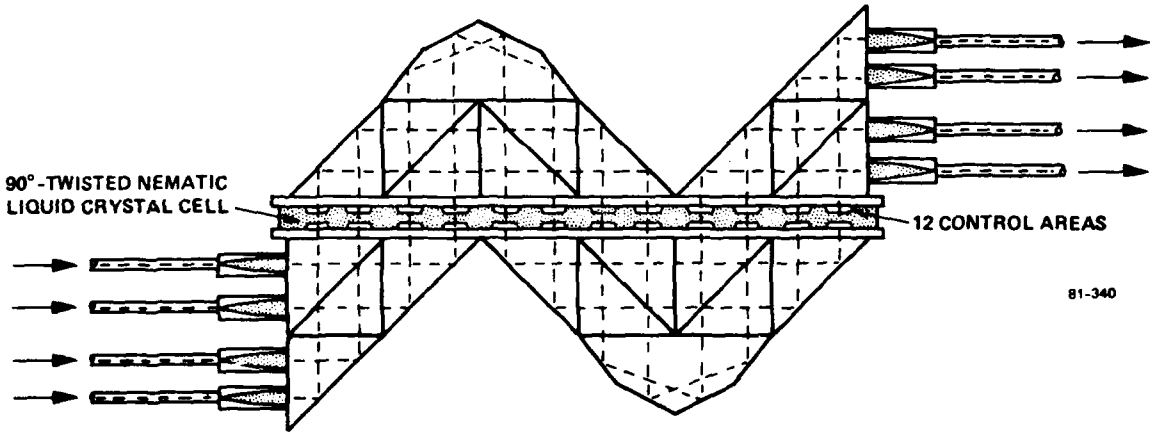

FIG. D-2 Planar 4 x 4 optical matrix switch actuated by one LC layer with twelve regions. Switch has 24 states.

APPENDIX E

4 x 4 AND 8 x 8 STAR COUPLERS

After delving into the properties of polarizing beamsplitters for the above switches, we found that PBs could be used to "mix" unpolarized light beams. Therefore, we determined that star couplers could be constructed from PBs.

This Appendix presents new designs for 4 x 4 and 8 x 8 star couplers that are an outgrowth of our switching work. The N x N stars are "beam" devices that required 2N Selfoc lenses (N-in, N-out) to collimate the fiberlight beams within the PB arrays. These couplers are in-plane structures because all the light beams lie in one plane.

Recall that a transmissive star coupler is a fiber-optic component that takes an optical signal from any one of its inputs and distributes that energy equally over all the outputs, an 1/N division. The basic concept in this Appendix stems from the s + p mixing property of a 2 x 2 transmissive star coupler made from one PB and two prisms in the manner shown in Fig. E-1 Here, two independent p-polarized beams, labeled a and b (upper diagram) are incident. They are transmitted (b,a) as shown. For s-input-polarization, the transmitted beams are (a,b). If the input light contains equal amounts of s- and p-light (as does a multimode fiber) then 50% of a will be superimposed upon (mixed with) 50% of b at each output port, as shown in the bottom diagram.

The extension of this idea to a 4 x 4 star is shown in Fig. E-2. Starting with the upper diagram, we see that doubling the unpolarized inputs (side-by-side) to four in Fig. E-2 namely a, b, c, d, leads to the two mixings (a + b) and (c + d). However, the output polarization of a is orthogonal to that of b; and c-out is orthogonal to d-out. Therefore, before proceeding further, we must "scramble" the output polarizations of a + b, and of c + d.

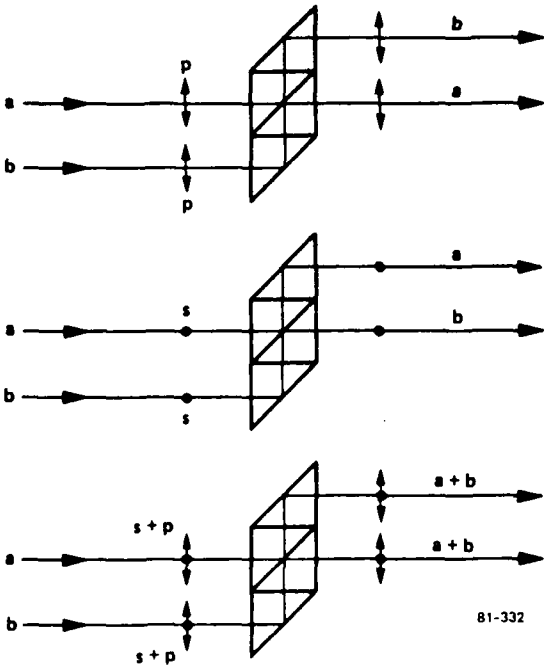

FIG. E-1 2 x 2 star coupler based on polarizing beamsplitter. Concept is to combine transmitted p-light with reflected s-light.

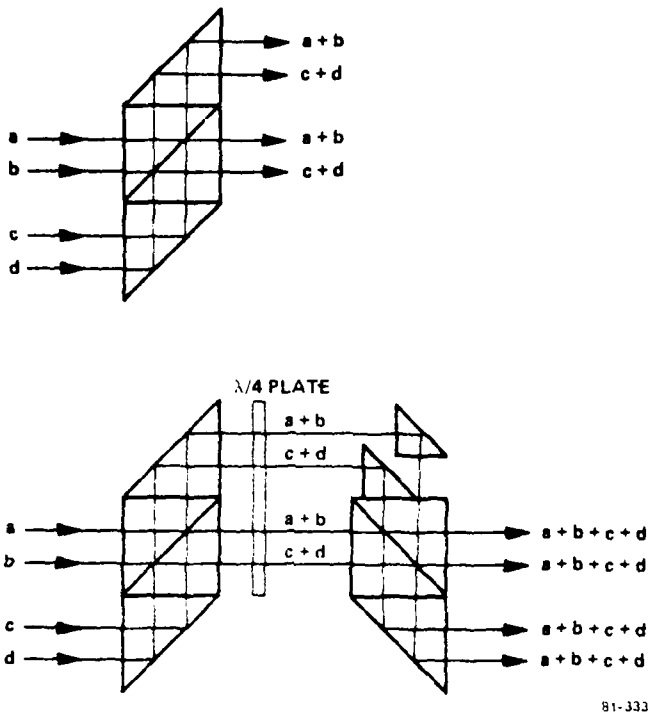

FIG. E-2 4 x 4 star coupler (lower diagram) based on two PB stages and one retardation plate. Upper diagram shows initial mixing of beam in first PB.

The scrambling technique we have found is to convert the linearly polarized a-light to circularly polarized light, with the same linear-circular process for b, c, and d. This is done by inserting a quarter-wave plate with fast/slow axes at 45° to the s- and p-vibration planes. Having obtained circular polarization, each beam will now impinge, in effect, as 50%-s + 50%-p on the next mixing stage, thereby insuring proper mixing of the stage-1 outputs.

The second mixing of ½(a + b) with ½(c + d) is done with two small transfer prisms (half the size of the other right-angle prisms) plus a PB in the second stage, as is shown in Fig. E-2 (lower) the side-view diagram of the complete transmissive star coupler which has ¼(a + b + c + d) at all four outputs. (This structure can be made more compact as indicated below).

It is a straightforward procedure to extend these ideas to higher-order stars and we now present the 8 x 8 structure. Two things are required in going from the 4 x 4 to the 8 x 8; first, we inject eight independent (unpolarized) parallel beams into the Fig. E-1 structure rather than four (this can be done simply by shrinking the interbeam spacing), and second, we add a third "mixing" stage for combining second-stage outputs. Quarter-wave plates are now needed at the second- and third stage-inputs to create equal s/p intensity at each input (apart from the 90° time-phase differences). Figure E-3 shows an expanded view of the 8 x 8 star coupler. To combine ½(a + e) with ½(d + h), etc. [second stage], and ¼(a + e + d + h) with ¼(b + f + c + g), etc. [third stage] we need a special arrangement of the small transfer prisms, the array shown in Fig. E-3. The result is a uniform set of outputs 1/8(a + b + c + d + e + f + g + h). By changing the discrete transfer prisms to a pair of multi-faceted roof prisms, and by cementing all parts together with clear adhesive, we obtain the compact star coupler shown in Fig. E-4 with the lo grinrod lenses that are required for multimode fiber coupling. (A similar structure holds for the 4 x 4).

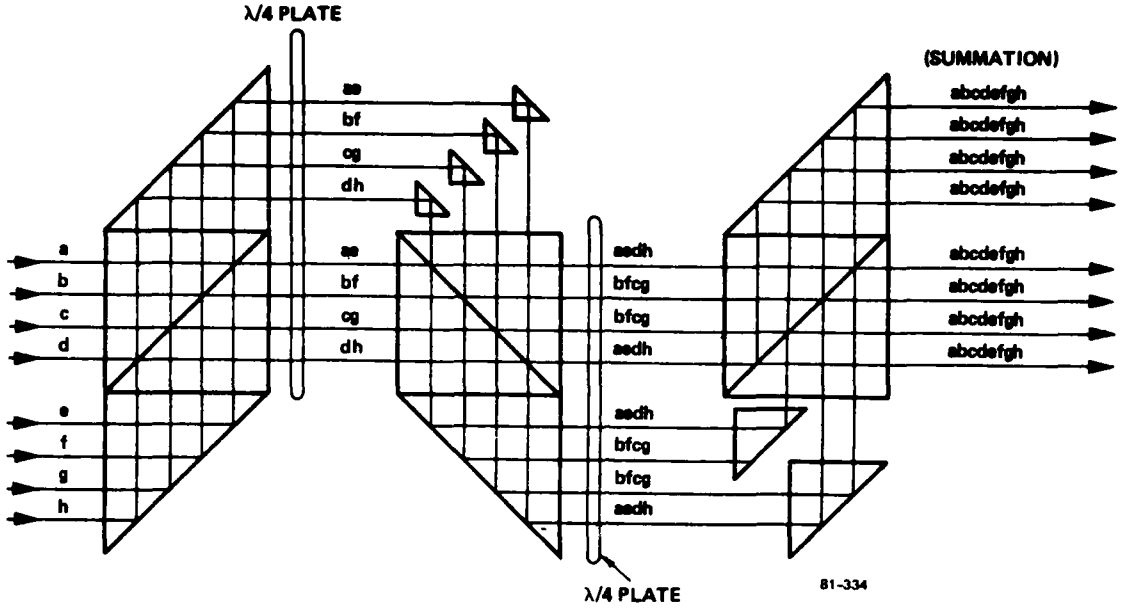

FIG. E-3 8 x 8 star coupler shown with optical components separated to clarify its operation.

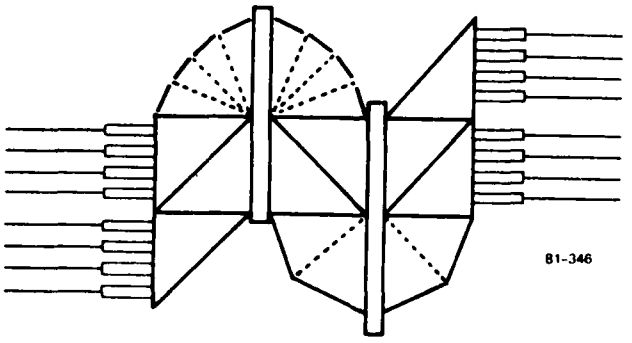

FIG. E-4 Proposed structure of 8 x 8 fiber-optic star coupler based on Fig. E-3.

With regard to performance, we expect the excess loss of these N x N stars to be just as low as obtained in the conventional fused-fiber approach. Uniform mode mixing and uniform output distribution are also expected. In addition, our 4 x 4 and 8 x 8 stars have three useful features: 1) by mounting each lens in a threaded socket, we can make chassis-mounted fiber connections to the coupler, 2) the coupler will work with differing fibers on each side of the star - different core sizes, different NAs, and 3) the coupler will work with plastic-clad fiber.

APPENDIX F

LOW-COST 2 x 2 SWITCH

In QSR-2 for this contract, we discussed 2 x 2 switches based on the design of Wagner and Cheng. The 2 x 2 is a relatively simple switch, yet quite important in data networks (where it is called an "active coupler"). The cost factors for such couplers must be brought under control in order to realize the promise of these optical switches.

In the 3-V 2 x 2, the most expensive items are the polarizing beamsplitters (PBs) and the graded-index rod lenses. By contrast, the liquid crystal cell is inexpensive and not very labor-intensive. Nor do the right-angle prisms cost much. With regard to lenses, the Nippon Sheet Glass Company is currently expending effort to reduce the Selfoc-lens cost, so the PBs presently remain as the most critical economic factor.

We have developed a design (starting from Wagner-Cheng) for a low-voltage 2 x 2 that requires only one PB for 2-polarization low-loss switching (insertion loss less than 2 dB). In so doing, the number of right-angle TIR prisms increases from two to three, but this is not a serious cost penalty.

We have devised a folded-path design that puts the 90°-twisted LC in a different location, namely, between two right-angle prisms whose surfaces have been coated (one surface, each prism) with transparent ITO electrodes. The prisms are spaced about 10 μm apart and have a slight overlap (out of plane) for electrical contact. Figure A16 shows this new low-cost design. The optical paths are shown by dashed lines. There are six TIR reflections that fold light into two parallel paths. The first TIR transfers light into the second "conjugate" path, and the s/p splitting and recombining occur at two locations on the same PB film. For this switch, the crosstalk is about -20 dB because this is a one-stage structure. We have also modified the Fig. F-1 design to make a compound 2 x 2 bypass switch.

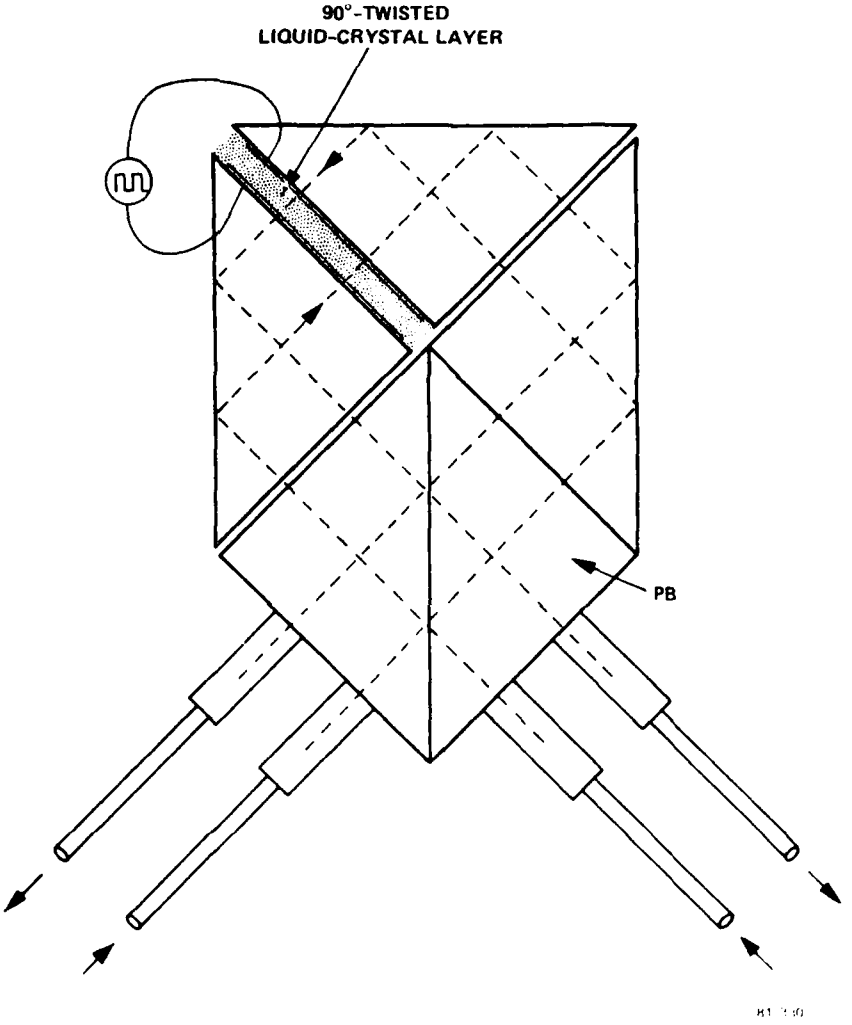

FIG. F-1 Low-cost design for 3-volt 2 x 2 optical switch using one PB.

MISSION
of
Rome Air Development Center

RADC plans and executes research, development, test and selected acquisition programs in support of Command, Control Communications and Intelligence (C^3I) activities. Technical and engineering support within areas of technical competence is provided to ESD Program Offices (POs) and other ESD elements. The principal technical mission areas are communications, electromagnetic guidance and control, surveillance of ground and aerospace objects, intelligence data collection and handling, information system technology, ionospheric propagation, solid state sciences, microwave physics and electronic reliability, maintainability and compatibility.

Printed by
United States Air Force
Hanscom AFB, Mass. 01731